Spring 5-20-2019

Applications of siRNA for Cancer Gene Therapy

Christopher Nicholas Cultrara
christopher.cultrara@student.shu.edu

Applications of siRNA for Cancer Gene Therapy

A thesis submitted to the Department of Chemistry and Biochemistry at Seton Hall University in partial fulfillment of the requirements for the degree of Doctor of Philosophy

By

Christopher Nicholas Cultrara

May 2019

Department of Chemistry and Biochemistry

Seton Hall University

South Orange, New Jersey, USA

DISSERTATION COMMITTEE APPROVALS

We certify that we have read this thesis and that in our opinion it is sufficient in scientific scope and quality as a dissertation for the degree of Doctor in Philosophy

APPROVED BY:

David Sabatino, Ph.D.

Advisor, Seton Hall University

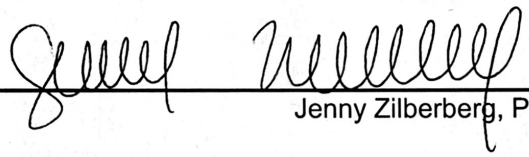

Jenny Zilberberg, Ph.D.

Co-mentor, Hackensack University Medical Center

Cecilia Marzabadi, Ph.D.

Reader, Member of Dissertation Committee, Seton Hall Universtiy

Stephen Kelty, Ph.D.

Chair Department of Chemistry and Biochemistry, Seton Hall University

Dedicated to my mother Renee and my father Nicholas for their unconditional love and support. Their motivation to consistently better myself and accomplish what is possible were the driving forces in completing this work and earning my Ph.D degree.

Abstract

Gene therapy is a potent and versatile nano-medicine strategy in the treatment of cancer. Of the many tools currently used in this application, short-interfering RNA (siRNA) are among the most commonly employed due to their ability to silence oncogenic mRNA with high precision and potentially induce cancer cell apoptosis through the RNA interference (RNAi) pathway. Our work revolves around silencing the Glucose-Regulated Proteins (GRPs) whose expressions are upregulated in cancerous tissues and are implicated in altering the proliferative, pro-survival, and anti-apoptotic pathways within these tumors.

Chapter 2 highlights a novel role that GRP78 has in cell-cell adhesion and its implication in tumors (multiple myeloma, MM and prostate cancer, PCa) that target the bone as a primary metastatic site. Using siRNA to silence GRP78, a concomitant downregulation of a mesenchymal cell-adhesion marker, N-cadherin, was observed in multiple myeloma and prostate cancer cell lines. Upon further investigation with an epithelial prostate cancer cell line, PC3, it was noted that the GRP78 silencing led to concomitant downregulation of E-cadherin and subsequent upregulation of TGF-β1 and Snail-2. Interestingly, TGF-β1 expression has been correlated with EMT and the upregulation of N-cadherin, suggesting that our findings indicate a novel function of GRP78 in which it can modulate the expression of adhesion molecules in a manner that supersedes the natural pathways that regulate their expression in PCa. Furthermore, the PC3 cells treated with GRP78 siRNA produced drastic changes in their morphology from their normal elongated shape to a more rounded shape which resulted in a reduction in their adhesion to an osteoblast (bone cell) monolayer in an N-cadherin dependent manner. These results help establish a novel correlation between GRP78 and N-cad in MM and PCa cells and present GRP78 as an ancillary regulator of markers associated with the EMT pathway andin the adhesion properties of PCa to the bone.

Chapter 3 discussed the application of a synthetic methodology that led to the production of linear, V-shape and Y-shape RNA templates, the latter two by the incorporation of a unique branchpoint ribouridine synthon. In this application, the RNA templates were used to hybridize complementary RNA strands that self-assembled into higher order nanostructure formulations. These formulations were designed to adopt genetically encoded shapes that resulted in siRNA hybrids that targeted multiple GRPs (GRP78, GRP94, GRP75). Moreover, they were capable of inducing synergistic knockdown of the GRPs in multiple tumor types (endometrial, breast, cervical) while being relatively inactive in a non-cancerous lung cell line. This established that the self-assembled siRNA nanostructures as a more potent anti-cancer gene therapy tool as compared to a cocktail of linear siRNAs, administered separately. Moreover, siRNA bioconjugates based on the V- and Y-shape RNA templates were designed to incorporate multi-functionality to the siRNA constructs and improve their scope of applications. A theranostic FITC-siRNA bioconjugate was synthesized and provided a unique opportunity to track cell uptake, localization, and mechanism of action. A self-assembly approach facilitated the incorporation of multi-FITC containing siRNAs, that resulted in greater sensitivity (up to 72 hours post transfection) relative to their singly labeled counterparts due to the enhanced signaling effect. Sense strand functionalization provided the most potent GRP KD effects (50-95%) which translated to the most significant cell death effects (20-95%) within a model PC3 PCa cell line. Furthermore, amphiphilic fatty acid- siRNA bioconjugates were generated to potentially improve the permeability of the siRNA across the cell membrane. The C16 (palmitic acid) and C18 (oleic acid) conjugated siRNAs were able to elicit GRP78 knockdown, albeit to a moderate extent (~30-40%). Sense strand functionalization and self-assembly to linear, V-, and Y-shape antisense templates afforded constructs containing a single, double, or triple palmitamide that also failed to improve GRP knockdown. Cellular uptake

studies performed by flow cytometry with a chimeric fluorophore –fatty acid siRNA bioconjugate revealed limited cell uptake, and/that rapidly dissipated within 24hrs post transfection. Furthermore, DLS and TEM analysis showed large aggregate particles with sizes upwards of 1 μm which we propose altogether inhibited cell uptake and RNAi activity.

Chapter 4 of this thesis illustrates a unique method for targeting cells for siRNA delivery. The cell targeting peptides (CTPs) function to target and bind to a cell surface receptor, in this case PSMA, found on the surface of PCa cells. Moreover, the incorporation of poly(cationic) cell penetrating peptides (CPPs), such as poly(arginine), can have the dual functionality of condensing siRNA by favorable electrostatic interactions and facilitating cell uptake within the target cell. A lead model peptide sequence, PSMA-1, was functionalized with short oligo(arginine) sequences (R_6 and R_9). The PSMA-1 peptide was able to effectively bind to $PSMA^+$ LNCaP cells with a limited amount of nonspecific binding to a $PSMA^-$ PC3 cell line. The R_6 variant was shown to efficiently complex and release siRNA according to a gel shift assay, yet no GRP78 KD was detecte mRNA and protein levels of expression within the PC3 or LNCaP cells. Flow cytometry revealed that the FITC-PSMA-1-R_9 peptide showed limited cell uptake when bound with siRNA. DLS and TEM analysis showed large particle sizes (1-2 μm), polydisperse particle distributions, negative surface charge densities and aggregation, all of which prevented cell uptake of the peptide:siRNA complexes when compared to siRNA complexed with a commercial transfection reagent. Together, this thesis will serve to highlight the biological evaluation of novel siRNA formulations for the study of GRP function in cancer.

KEYWORDS: siRNA, Glucose Regulated Proteins (GRPs), Prostate Cancer, N-cadherin, Adhesion, siRNA nanostructures, siRNA bioconjugates

ACKNOWLEDGEMENTS

Never did I believe I would be earning a Ph.D degree. Originally undecided in which direction I wanted to take my life, the Fall of 2011 introduced me to the world of chemistry and I never looked back. After completing an undergraduate degree in biochemistry and completing a short internship at Advanced Biotech I decided that I would further my passion for science by pursuing a graduate degree. Four years later, I can confidently state that it has been one of the most rewarding experiences. I've had the privilege of learning lessons that will serve me well in all facets of life.

I would like express my utmost gratitude to my Ph.D. advisor, Dr. David Sabatino, for accepting me into his research group and helping to mold me into the scientist I am today. Through the rollercoaster of emotions that comes with a graduate degree, he has been there to provide confidence, support, and most importantly, guidance to persevere and see this finished to the highest standard. I have been privileged to have you as a mentor and a friend and glad I've had the opportunity to complete my thesis work under your watch.

I would also like to extend my sincerest thank you to Dr. Jenny Zilberberg for serving as my co-mentor and for taking me under her wing and welcoming me into your research lab. When I asked to be a part of our collaboration, I never imagined it would lead to the relationship we've built and all the work we've been able to accomplish in only two short years. You've taught me to look at science from a much larger perspective and helped me to grow as an independent scientist. For that, I am ever thankful and am lucky to have had the opportunity to work with you.

I would also like thank the rest of my thesis committee : Dr. Nicholas Snow, Dr. James Hanson, and Dr. Cecilia Marzabadi. A special thank you to Dr. Marzabadi for reading and reviewing my dissertation. Your insights and knowledge have helped me to reach this point and complete my thesis work. I'd like to extend a thank you to the rest of the faculty in the Department of Chemistry and Biochemistry for all the fruitful interactions we've had over the years. You have constructively challenged me every step of the way and it has helped broaden my horizons. A special thank you also goes out to Ms. Maureen Grutt for everything she has done for me. This experience has been all the better because you have been a part of it.

I thank my friends and colleagues at Seton Hall. To Steve, Jeff, Mayur, Mariana, Niki, Sunil, Rachel, Gina, Nelson, Keith, Claudia, Andreih, and Adah, I extend a warm thank you for making my time here all the better. You've challenged and helped me and I consider you all as family. I am happy for the relationships we've built and I hope to keep them moving forward.

Lastly, and most importantly, I would like to thank my parents, my grandmother, the rest of my family, and my girlfriend Jessica for all of the love and support you've given me during this time. I cannot express my gratitude for all you've done for me and this has only been possible because of it.

Table of Contents

Chapter 3: Biological Activity of Higher-Order siRNA Nanostructures and their Bioconjugates

Chapter 5: Conclusions and Contributions to Knowledge

LIST OF FIGURES

LIST OF TABLES

LIST OF SCHEMES

ABBREVIATIONS AND SYMBOLS

P/S	Penicillin/streptomycin
©	Copyright
®	Registered
°C	Degrees Celsius
µg	Microgram
µL	Microliter
µM	Micromolar
µmol	Micromole
™	Trademark
1° mAb	Primary Monoclonal Antibody
2° mAb	Secondary Monoclonal Antibody
A	Adenosine
A.U.	Absorbance Units
AuNP	Gold Nanoparticles
Ago2	Argonaute 2
AHX	Amino-Hexanoic Acid
ATF-6	Activating Transcription Factor 6
Bax	Bcl-2-like Protein 4
BM	Bone Marrow
BCL-2	B-cell Lymphoma 2
BiP	Immunoglobulin Heavy Chain Binding Protein
BSA	Bovine Serum Albumin
BTZ	Bortezomib
C	Cytosine
Ca^{2+}	Calcium
cDNA	Complimentary DNA
CDH2	N-cadherin
CFDA	Carboxyfluorescein Diacetate Succinimidyl Ester
CHOP	DNA-Damage Inducible Transcript 3

cm-siRNA	Chemically Modified siRNA
CO_2	Carbon Dioxide
CPP	Cell Penetrating Peptide
CTP	Cell Targeting Peptide
DCM	Dichloromethane
DLS	Dynamic Light Scattering
DMEM	Dulbecco's Modified Eagle Medium
DMF	Dimethylformamide
DNA	Deoxyribonucleic Acid
DOPC	1,2-Dioleoyl-*sn*-Glycero-3-Phosphocholine
DOTAP	1,2-Dioleyl-3-trimethylammonium-propane
dsRNA	Double-Stranded Ribonucleic Acid
DTT	Dithiothreitol
e.g.	For example
E-cad	Epithelial Cadherin
EDTA	Ethylenediaminetetraacetic Acid
eGFP	Enhanced Green Fluorescent Protein
EGFR	Epidermal Growth Factor Receptor
EMT	Epithelial-Mesenchymal Transition
EPR	Enhanced Permeability and Retention Factor
ER	Endoplasmic Reticulum
ESI-MS	Electrospray Ionization Mass Spectrometry
F	Fluorine
FACS	Fluorescence Assisted Cell Sorting
FAK	Focal Adhesion Kinase
FAM	Carboxyfluorescein
FA-siRNA	Fatty Acid conjugated siRNA
FBS	Fetal Bovine Serum
FITC	Fluorescein Isothiocyanate
FL-siRNA	Fluorescently Labeled siRNA
G	Guanosine

GAPDH	Glyceraldehyde-3-phosphate Dehydrogenase
GRPs	Glucose Regulated Proteins
GRP75	Glucose Regulated Protein, 75 kilodaltons
GRP78	Glucose Regulated Protein, 78 kilodaltons
GRP94	Glucose Regulated Protein, 94 kilodaltons
H_2O	Water
HCTU	O-(1H-6-Chlorobenzotriazole-1-yl),1,1,3,3-tetramethyluronium hexafluorophosphate
HCS	High Content Screening
HfOB	Human Fetal Osteoblasts
HSPA5	Heat Shock Protein Family A
Hr	Hour
HRP	Horseradish Peroxidase
IGF-1	Insulin-Like Growth Factor 1
KD	Knockdown
LC/MS	Liquid Chromatography/ Mass Spectrometry
LDH	Lactate Dehydrogenase
LDS	Lithium Dodecasulfate
Lv	Levulinyl
M	Molar
m/z	Mass to Charge Ratio
Me	Methyl
MeCN	Acetonitrile
MEM	Minimum Essential Medium
MeOH	Methanol
Mg	Milligram
miRNA	Micro-RNA
mA	Milliamp
mL	Milliliter
mM	Millimolar
MM	Multiple Myeloma

mmol	Millimole
MMT	Monomethoxy Trityl
mRNA	Messenger RNA
MS	Mass Spectrometry
Mt-UPR	mitochondrial Unfolded Protein Response
NAb	Neutralizing Antibody
NaCl	Sodium Chloride
N-cad	N-cadherin
ncRNA	Non-coding RNA
ng	nanogram
NIR	Near Infrared
nm	Nanometer
nM	Nanomolar
nmol	nanomole
NMM	N-methymorpholine
OSB	Osteoblasts
PAGE	Polyacrylamide Gel Electrophoresis
PBS	Phosphate-Buffered Saline
PCa	Prostate Cancer
PEI	Polyethylenimine
PI	Propidium Iodide
Pim-1	Serine/Threonine Kinase
PKC-α	Protein Kinase C alpha
PKN3	Protein Kinase N3
PLK-1	Polo-like Kinase 1
PLGA	Poly Lactic-co-Glycolic Acid
PLL	Poly-L-Lysine
pM	Picomolar
pmol	Picomole
PSMA	Prostate Specific Membrane Antigen
PVDF	Polyvinylidene Fluoride

qRT-PCR	Quantitative Real-Time Polymerase Chain Reaction
RISC	RNA-Induced Silencing Complex
RNA	Ribonucleic Acid
RNAi	Ribonucleic Acid Interference
RP IP HPLC	Reverse-Phase Ion Pairing High Performance Liquid Chromatography
RPMI	Roswell Park Memorial Institute Medium
rU	Ribouridine
SDS-PAGE	Sodium Dodecasulfate Polyacrylamide Gel Electrophoresis
shRNA	Short-Hairpin RNA
siRNA	Short-Interfering RNA
ssRNA	Single Stranded RNA
T	Thymidine
TAE	Tris/Acetic Acid/EDTA
TBE	Tris/Borate/EDTA
TBST	Tris-Buffered Saline/ Tween-20
TEM	Transmission Electron Microscopy
TES	Triethylsilane
Tg	Thapsigargin
TGF-β	Transforming Growth Factor Beta
THF	Tetrahydrofuran
Tris	Tris(hydroxymethyl)aminomethane
U	Uridine
UPR	Unfolded Protein Response
UV-Vis	Ultraviolet- Visible Spectrophotometry
VEGF	Vascular Endothelial Growth Factor
Vs	Versus

Chapter 1: General Introduction into the Applications of siRNA in RNAi Based Gene Therapy

1.1 Discovery of RNAi

RNA interference (RNAi) is a potent biological process that serves as a regulator of gene expression by suppressing protein expression and degrading targeted mRNA. One of the first major examples of modern RNAi applications were pioneered by Andrew Fire, et al. when they demonstrated an effective and specific inhibition of the uncoordinated (*unc-22* and *unc-54*) genes in *C. elegans* muscle through the production of antisense RNA. In this application, DNA segments of the genes were placed in reverse orientation inside of plasmid vectors designed to produce RNA in body wall muscle. The constructs led to an observed a loss of wild-type motor function in test worms and an apparent loss of *unc-22* protein via immunoimaging. They further provided genetic evidence for an antisense mechanism, confirming that homology between an inverted region and the wild- type chromosome was necessary for the disruption of gene function.[1]

Guo and Kemphues further complemented Fire's findings on antisense RNA for their work on the *par-1* gene in *C. elegans*, a major protein involved in the worms' embryonic development. Upon injection of exogenous DNA constructs containing either the sense or antisense sequence of the *par-1* gene into *C. elegans*, they observed more than 50% of the embryos were terminated in both cases. While the results from the antisense vectors were consistent with an antisense inhibition mechanism complete with cell division patterns characteristic of *par-1* loss of function mutations, the sense vectors also induced unexplainable *par-1* phenotypic changes among the test worms' progeny. They summarized that, unlike the antisense constructs, the effects of the sense vectors seemed to be restricted to a putative translated region of the gene and may function on separate and unique mechanisms.[2]

Years later, Fire and Mellow set out to investigate the underlying mechanism of the interfering RNA. Building on previous work in *C. elegans*,[1] mixtures of RNA-producing DNA vectors containing the sense and antisense sequences for the *unc-22* and *unc-54* genes were injected into the worms. To their surprise, the expressing complementary RNA sequences elicited a far more potent loss in motor function in the worm's muscle compared to solely the antisense or sense sequences (100% for dsRNA vs 1-11% for ssRNA) and even at 120-fold lower doses of dsRNA, the same loss in function was observed (~30%) (Figure 1.1). From their investigation, they made three major claims about the observed RNA interference (RNAi) pathway: 1) targeting exon regions of the intended gene is essential as targeting intronic or promoter regions had little to no effect, 2) mRNA is the likely target for RNAi, and 3) the dsRNA-mediated interference could easily cross cellular boundaries. They concluded that this process likely exists as a mechanism used by organisms for physiological gene silencing and could extend into other invertebrates and vertebrates as well.[3] Fire and Mellow were awarded the Nobel Prize in Physiology or Medicine in 2006 for their discovery of the RNAi pathway.

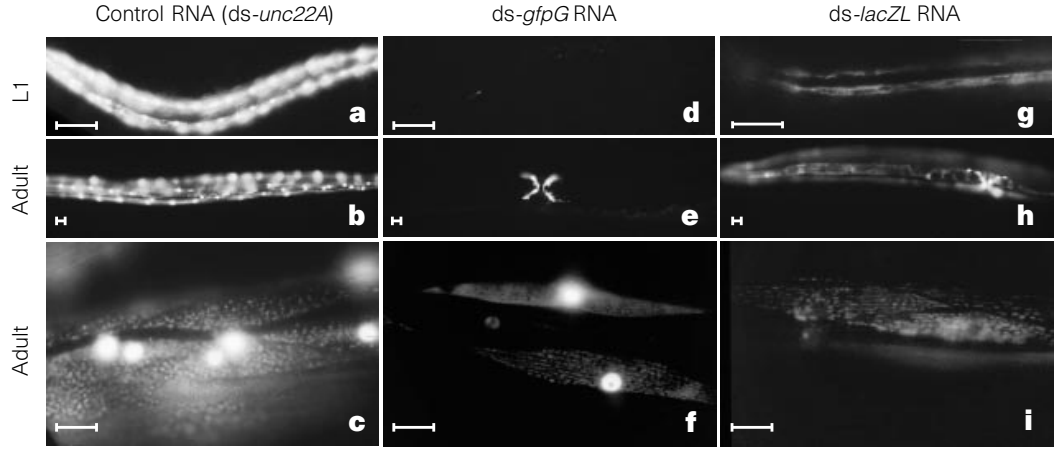

Figure 1.1 Phenotype responses in *C. elegans* after injection with dsRNA- producing DNA vectors. Fluorescent labeling of the muscle along the body cavity in wild-type (A-C) that is diminished after injection with dsRNA (G-I). Adapted from Fire, A.; Xu, S.; Montgomery, M. K.; Kostas, S. A.; Driver, S. E.; Mello, C. C., *Nature* **1998,** *391* (6669), 806-811.[3] with permission from Springer Nature.

1.2 siRNA Structure and Function in RNAi Pathway

There are numerous non-coding RNAs (ncRNAs) that have been established as important regulators of gene expression.[4,5] Prokaryotes use small antisense RNAs (asRNAs) to bind and inhibit the expression of target mRNA into functional proteins. Likewise, various small ncRNAs are active as inhibitors of gene regulation in eukaryotes, with the most prominent being microRNAs (miRNAs) and small interfering RNA (siRNAs) which can both activate the RNAi pathway[6-8].

While structurally and functionally similar, these two classes of small ncRNAs do have some unique characteristics. miRNAs are generally considered to evoke RNAi through an endogenous pathway, i.e synthesized within the cell. They are transcribed as long primary miRNA transcripts (pri-miRNA) which are partially cleaved by a microprocessor complex in the nucleus yielding a stem-loop pre-miRNA. This pre-miRNA is transported to the cytoplasm and further processed by a nuclease enzyme called Dicer into a small 19-25 nucleotide (nt) dsRNA consisting of an active strand and an inactive passenger strand (Figure 1.2).[9, 10]

While they can still be produced naturally by the enzymatic action of Dicer from long dsRNAs, siRNAs are generally considered to be exogenous RNAs (not synthesized within cells and introduced as external agents).[9,11] They are introduced into the cytoplasm of the cells via a cationic polymer formulation that can condense the siRNA into small, discrete particles and facilitate their transient permeability across the cell membrane.[12, 13] siRNAs are short dsRNAs ranging from ~20-25nt in length with a well-defined structure consisting of a phosphorylated 5'-end and a hydroxylated 3'-end typically containing a 2nt overhang. These small dsRNA also consist of an active guide strand and inactive passenger strand.[14, 15]

	siRNA	miRNA
Occurrence	Occurs naturally in plants and animals. It is currently unknown whether or not they occur naturally in mammals.	Occurs naturally in plants and animals.
Mean length	Approx. 21–22 nt	Approx. 19–25 nt
Complementarity t o target mRNA	100% perfect match; therefore, siRNAs knock down specific genes, with minor off-target exceptions.	Not exact; therefore, a single miRNA may target up to hundreds of mRNAs.
Biogenesis	Regulate the same genes that express them.	Expressed by genes whose purpose is to make miRNAs, but they regulate genes (mRNAs) other than the ones that expressed them.
Action	Cleave mRNA.	Inhibit or replace translation of mRNA.
Function	Act as gene silencing guardians in plants and animals that do not have antibody- or cell-mediated immunity.	Regulators (inhibitors) of genes (mRNAs)

Table 1.1 Structural and functional differences between siRNA and miRNA. Reprinted from Ahmadzada, T. R., G.; McKenzie, D. *Biophysical Reviews* **2018,** *10*, 69-86.[9] with permission from Springer Nature.

In particular, siRNA activates the RNAi pathway through a ribonucleoprotein effector complex known as RISC – RNA Induced Silencing Complex.[16] Once in the cytoplasm, the siRNA are incorporated into the RISC complex where Ago2, an Argonaute protein containing a ribonuclease, RNAse III type domain, identifies the active guide antisense strand of the siRNA duplex and degrades the passenger sense strand. [17-19] The loaded RISC complex uses the antisense RNA strand as a template to recruit and bind to complementary mRNA which is then rapidly degraded by the Ago2 protein at cleavage sites determined by the 5' end of the siRNA strand.[20, 21] Importantly, siRNA have near perfect complementarity to their target mRNA resulting in very specific knockdown of genes which is in stark contrast to miRNA which may target many mRNAs (Figure 1.2).[9] Cleavage of target mRNA by siRNA mediated RNAi prevents its translation into protein which may diminish cell function and viability. In this manner, the RNAi strategy can target nearly any gene, including silencing detrimental gene transcripts as a treatment option for a variety of genetic diseases.[22, 23] The modern advances in this field from its discovery by Fire and Mellow has

since evolved RNAi into a modern, precise, and efficient technology for screening and silencing targeted genes in a wide range of applications.

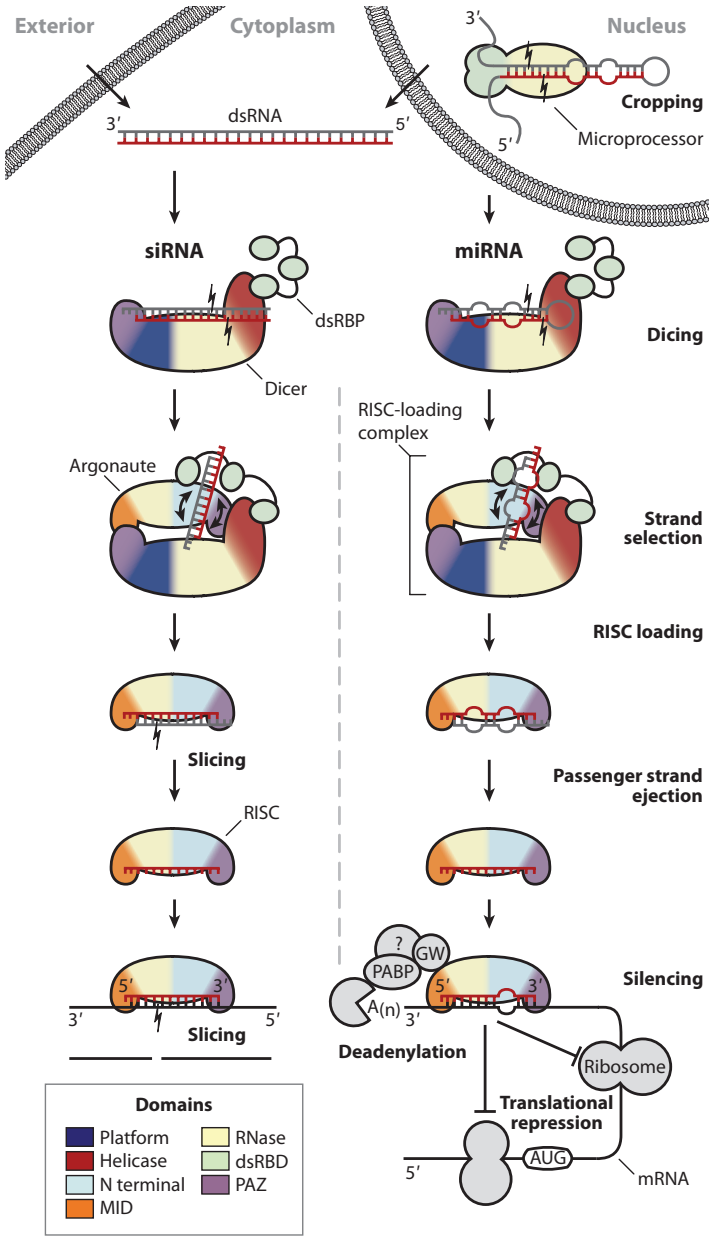

Figure 1.2. RNAi mechanism of action induced by siRNA or miRNA. Reprinted from Wilson, R.; Doudna, A., *Annu Rev Biophys* **2013,** *42*, 217-239.[16] with permission from Annual Reviews.

1.3 Applications of siRNA in Cancer Gene Therapy

The high efficiency and specificity of siRNA in silencing target genes have made them interesting and promising therapeutic candidates in the treatment of genetic disorders, including cancer. Genetic mutations are common throughout the tumor lifespan and may function as genetic markers for targeting and silencing the progression of the disease.[24] These tumor promoting genes, oncogenes, are defined as mutated genes related to tumor progression, can lead to altered protein function, amplification of specific gene products, deletions which alter the abundance of a particular protein, and alternate splicing leading to novel cancer proteins, oncoproteins.[25,26] However, not all of these mutations are direct causes of cancer, [27] rather, there is a small minority of mutations that act as "drivers" of tumor progressions that, once determined, offer a therapeutic regimen in the treatment of specific cancers (**Figure 1.3**).

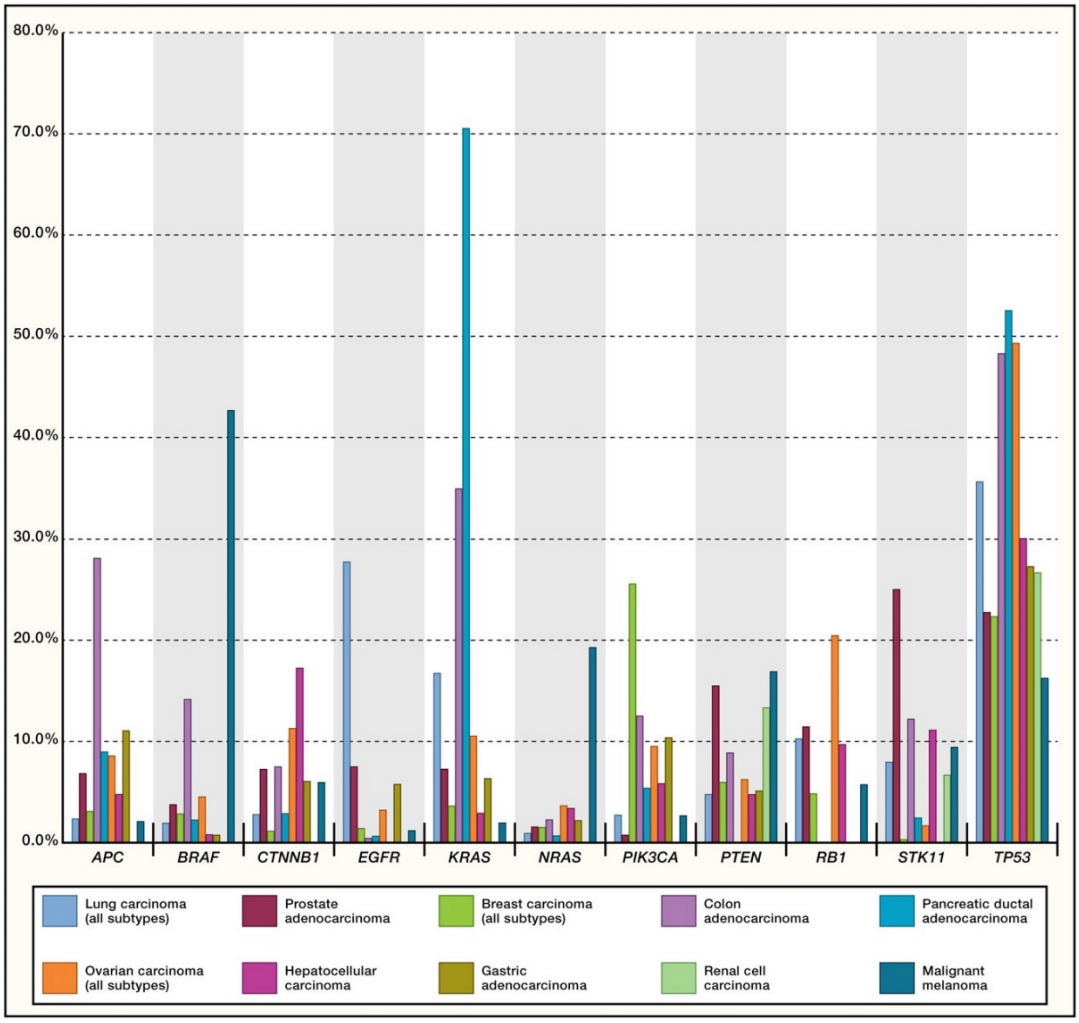

Figure 1.3. Frequency of mutations in selected genes of various cancers. Reprinted with permission from Elsevier: Dancey, J.; Bedard, P.; Onetto, N.; Hudson, T. *Cell* **2012,** *148*, 409-420.[24]

RNAi technologies have become a focal point, especially in the treatment of difficult oncoprotein targets which may not be targetable through conventional drug treatment approaches.[28] Furthermore, a major advantage of using RNAi technology is the ability to target multiple genes among various cellular pathways.[29] (**Table 1.2)**. This not only may lead to a practical therapy, but may also serve as a screening assay to identify important oncogene targets in specific cancer types.

Pathway	Target Gene
Cell Adhesion	Matrix metalloproteinase[30]
Apoptosis	Bax[31] Bcl-2[32, 33]
Angiogenesis	Focal Adhesion Kinase[34]
Signaling	H-Ras[32], K-ras[35] PLK-1[36] TGF-β[32] STAT3[37] EGFR[38, 39] PKC-α[32]
Cell-Cell Communication	VEGF[32]
Lipid Metabolism	Fatty Acid Synthase[40]

Table 1.2. siRNA gene targets in cancer. Adapted with permission from Springer Nature: Devi, G.R. *Cancer Gene Therapy.* **2006,** 13(9), 819-826.[41]

Despite the array of potential targets for siRNA in a cancer gene therapy approach, they are limited in their translation to clinical use by a few key obstacles. First, siRNAs are not intrinsically stable in the cellular cytosol and are rapidly degraded by resident nucleases. Secondly, siRNAs are not cell permeable and require chemical carriers to cross the plasma membrane of cells. These carriers, also referred to as transfection reagents are also affected by notable limitations, including delivery efficiency, uptake and release profiles and toxicity. Together, these limitations reduce the siRNA resident time at desired cellular target, thereby limiting their efficiency and potency often leading to higher dose concentrations, which increases the propensity for the siRNA to exhibit off-target side effects despite their high mRNA sequence specificity.[42]

1.4 Modified siRNA for Pre-Clinical and Clinical Applications

Native, non-modified siRNAs are at a clinical disadvantage due to their poor pharmacokinetic properties *in vitro* and *in vivo*. A majority of the main siRNA drugs in development now

incorporate a variety of chemical modifications that have been validated to increase siRNA stability and potency.[43] Solid phase oligonucleotide synthesis provides a unique site-specific approach for siRNA modification using modified RNA phosphoramidites that can influence biological activity, thermodynamic stability, and nuclease resistance.[44,45]

These chemically modified siRNAs (cm-siRNAs) typically fall into one of two broad categories: backbone modifications or base modifications. Backbone cm-siRNAs contain modifications either in the sugar ribose ring or along the phosphodiester bonds between the nucleosides. The most prevalent cm-siRNAs in this class often involve chemical substitutions at the 2'-OH in the ribose ring in order to confer oligonucleotide stability from degradation. These modifications include: 2'-O-Methyl (2'-OMe), 2'-deoxy, 2'-Fluro, 2'-aminoethyl, 2'-methoxyethyl, and 2'-methylene bridged Locked Nucleic Acids (LNA).[46-48] These 2'-OH modifications have been shown to moderately increase the stability of the cm-siRNAs without significantly affecting gene silencing.[48-50] Furthermore, site-selective incorporation and/or replacement of the phosphodiester backbone with phosphothioate or boranophosphonate linkages have also been promising modifications in increasing the stability and gene silencing activity of cm-siRNAs.[51] Interestingly, these modifications can also have positive effects on off-target gene silencing, as studies on 2'O-Me and LNA cm-siRNAs have shown that even a single incorporation increased the specificity of the siRNA activity.[52, 53]

Base modifications change the natural structure and affects base-pairing of the nucleobases adenine, cytosine, guanine, and more commonly, uracil (A, C, G, U). Therefore, they are less relevant in practical therapeutic applications. However, this class of cm-siRNAs have contributed to the basic understanding of the siRNA induced silencing method and off-target side effects.[54] These modifications include: 2'-uracil, hypoxanthine, pseudouridine, and dihydrouridine, which

when incorporated at selective positions in the sequence provide varying effects on siRNA hybrid stability and gene silencing activity.[55,56]

Despite the wide variety of modifications that can be made, the incorporation of too many changes can significantly reduce the efficiency of the siRNA.[57] This results in the careful design of cm-siRNAs with a balance between type, location and extent of modifications included within the sequence to maintain siRNA hybrid stability and gene silencing activity. The modern development of siRNA therapeutics includes more than 20 cm-siRNAs in different phases of clinical trials. For example, cm-siRNAs SPC2996 and EZN3042, targeting Bcl-2 and survivin, reached phase II and I for the treatment of leukemia and various solid tumors, respectively.[58-60]. Recently, a new database, siRNAmod, facilitated the identification of 128 unique modifications within nearly 5000 experimentally validated cm-siRNAs, in addition to descriptions of , their gene targets, and their silencing efficiency.[43] Tools like this will prove to be invaluable for the development of stable, potent, and safe siRNA based formulations that can effectively translate from the bench into the clinic.

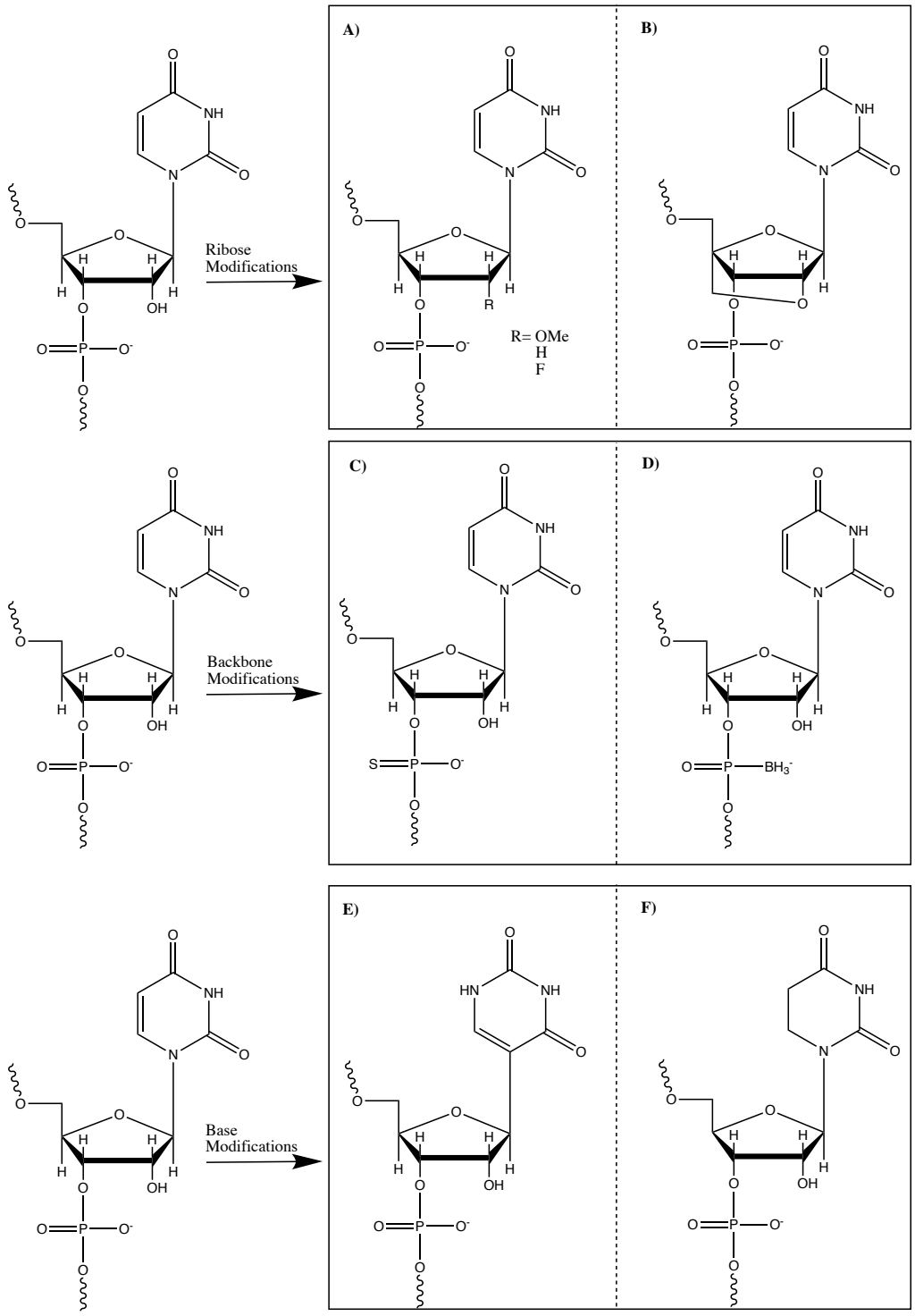

Figure 1.4. Common siRNA chemical modifications to increase potency and/or stability. A) 2' substitutions in the ribose ring. B) Locked Nucleic Acids (LNA). C) phosphothiorate linkage. D) phosphoboranate linkage. E) psuedouridine. F) Dihydrouridine Images were drawn in ChemBioDraw.

1.5 siRNA Cell Uptake, Trafficking, and Release for RNAi Activity

There are a number of cellular obstacles that delivery systems must overcome in order to promote efficient siRNA delivery and release. First, the delivery system must be amenable to a proper administration route. For example, oral ingestion is not preferred as many cancer target sites are not accessible through an oral route as well as intestinal stability and distribution across the epithelial gut wall into the circulatory system must be taken into consideration.[61] Therefore, intravenous injection (IV) or infusion injections are the most common methods, with IV having the added benefit of bypassing metabolism clearance from the liver and kidney.

The second obstacle is the vascular barrier. The delivery systems must condense siRNA into small, discrete nanoparticle formulations (≤ 80nm) in order to diffuse through the capillary vasculature found in the circulatory system and into solid tumors.[62] Nanocarrier delivery systems can take advantage of a phenomenon called the enhanced permeability and retention effect (EPR). In this mechanism, the access and accumulation of siRNA into target cellular areas, must fulfill the particle size requirement.[63] Furthermore, siRNA drugs are excreted through the kidneys which have a filtration barrier of roughly 8nm. Delivery systems which can condense the siRNA formulation to sizes less than 25nm can effectively address a large portion of this obstacle.[64,65] The sizes of the siRNA nanoparticle formulations are also important in mitigating their encapsulation and destruction by phagocytes. In this scenario, large size formulations (> 100nm) or aggregates formed from high lipophilicity or electrostatic interactions can lead to the siRNA elimination by phagocytosis.[66]

Thirdly, the delivery systems must be able to efficiently penetrate the cell plasma membrane and release the siRNA into the cytoplasm where it can activate the RISC complex. Both siRNA and the plasma membrane have an inherent negative charge due to the phosphodiester backbone

and integral phospholipids, respectively, that restricts transient diffusion across the membrane for siRNA. Many delivery formulations contain polycationic moieties to function as both a handle to condense and mask the siRNA, but also to enhance the interaction with the cell membrane. Typically, carrier mediated-endocytosis is the main mechanism for siRNA uptake into the cell and, preferably, should allow for the release of the siRNA before the late stage endosomes merge with lysosomes containing digestive enzymes that can lead to siRNA degradation.[67] Mechanistically, this can happen in one of two ways. Cationic moieties in the formulation can further increase the acidity by absorbing native protons and destabilizing the endosome membrane allowing for release. Likewise, once fused with the lysosome, they can act as a proton sponge and drastically change the osmotic pressure within the organelle until it ruptures leading to the release of the siRNA.[68]

Lastly, the delivery systems must limit an immune response upon administration. Specifically, they should not include any components that may be immunogenic, or invoke any unwanted or unseen side effects.[69,70] The mononuclear phagocyte system (MPS) is a branch of the immune system that relates to blood cell turnover and defense against microorganisms. As such, particularly large siRNA formulations as well as highly charged aggregates can incite the MPS to phagocytose the treatment before reaching its target.[66] While chemical modifications such as the 2'OMe nucleosides can help diminish immunogenicity on shorter (up to 23 nt) siRNA, care must be taken that the whole formulation remains stable, inert, and safe.

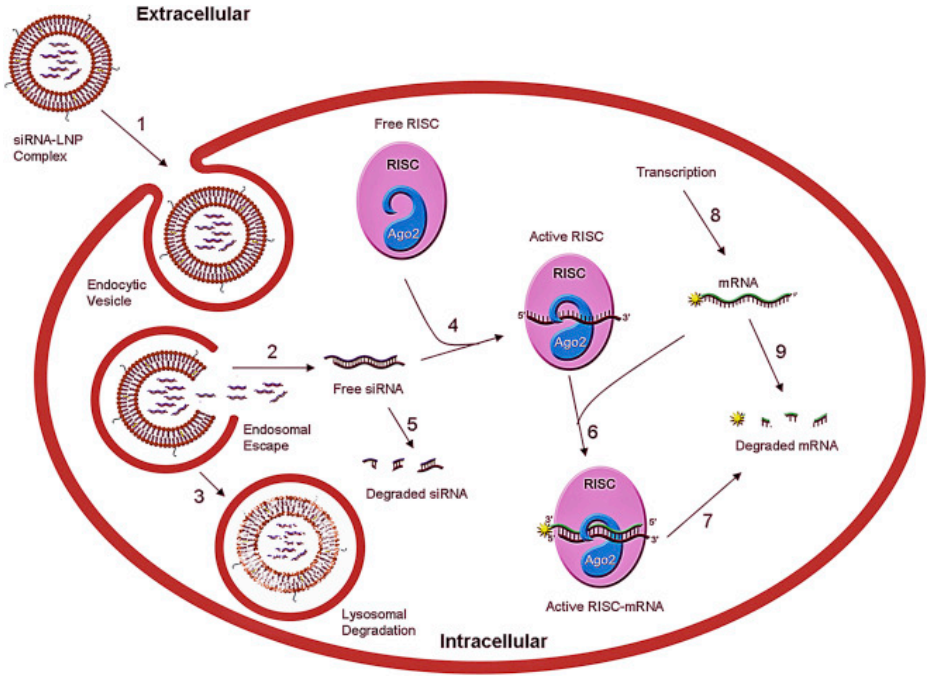

Figure 1.5 Graphical illustration of siRNA complexation by a nanoparticle carrier, entry into the cell, and subsequent endosomal release into the cytoplasm for RNAi activity. Image reprinted with permission granted by the Creative Common Attriubtion License: Mihaila, R.; et al. *Molecular Therapy: Nucleic Acids*. **2017**, 7.

1.6 siRNA Delivery Systems

Various delivery systems have been developed to safely and effectively introduce siRNA within their cell targets and circumvent the difficulties and limitations in administering siRNA based therapies. The use of nanoparticle formulations have revolutionized the field. They are sought after due to the tunable range of particle sizes that can be achieved, their inertness, their enhanced resident circulation time, their tunable stability and release profiles, and in some cases, their ability for multifunctionality.[62] They can be classified broadly into two categories: soft/organic or hard/inorganic. The organic nanoparticles are derived from both natural and synthetic sources and encompass liposomal, nanoemulsions, dendrimers, and polymer formulations. Liposomes a very common delivery agent and typically include amphiphilic and charged surfactants such as 1,2-Dioleoyl-*sn*-Glycero-3-Phosphocholine (DOPC) or 1,2-dioleoyl-

3-trimethylammonium-propane (DOTAP) to help with payload entrapment. These liposomal formulations are often cationic and can complex with the siRNA and easily interact with the cell surface.[72] However, they've been found to have a wide range of cytotoxic and immunostimulatory side effects which has limited their use over the years.[73,74] Regardless, these types of carriers have found their way into clinical applications with several FDA-approved formulations for the delivery of therapeutics including a chemotherapy drug, doxorubicin.[75] Moreover, a DOPC-based nanoliposome has been used in a Phase I clinical trial to deliver siRNA into solid tumors.[72] The inorganic nanoparticles are non-biodegradable and consist typically of metals, metal oxides, or hard carbon-based materials. One important example of this category is the loading of siRNA onto gold nanoparticles which have the added benefit of being inherently anti-angiogenic with anti-tumor properties.[62]

Polymer-based delivery systems, also known as polymeric nanoparticles, have gained recent traction due to their flexible and tunable properties including biodegradability, hardness, aqueous solubility, and functionality. For example, they can be designed for particular stability and release profiles which often involves a multimolecular scaffold including the incorporation of cationic, hydrophilic, and hydrophobic moieties.[78] These systems can also be bio-responsive, containing components that can assemble and release particles based on stimuli of the microenvironment which is especially important in the release of siRNA from their delivery formulation. The cationic components are commonly found as secondary and tertiary amines with polyethylenimine (PEI) being a model system that has been successfully used both *in vitro* and *in vivo*. Other commonly used polymer components include cyclodextrin, poly(D,L-lactide) (PLA), and poly(D,L-lactide-co-glycolide) (PLGA), all of which have been used to varying extents in murine models and clinical trials.[77]

Another important class of delivery systems are the targeted delivery systems. These formulations contain one moiety that is specific to a particular cell or tissue and will guide and internalize the siRNA to its target, typically by a receptor mediated endocytosis pathway. This has been found successful with ligands such as folate and transferrin conjugated covalently to the delivery system.[78, 79] Similarly, peptide-based delivery systems are bio-compatible formulations that can function to target and internalize siRNA within cells. Cell penetrating peptides (CPPs) have been shown to improve the delivery of siRNA across the cell membrane *in vitro* and *in vivo*.[80,81] Moreover, they exhibit minimal toxicity or immunostimulatory effects and can effectively form ionic complexes with siRNA along with their release intracellularly.[82,83] Similarly, cancer targeting peptides (CTPs) allow for the targeted delivery of siRNA by targeting a specific receptor on the cell surface similarly to folate targeting the folate receptor. However, compared to traditional ligands, CTPs can target a much wider range of receptors, so long as an appropriate peptide sequence can be found, commonly, through phage display.[84] CTPs have led to the development of potent anti-cancer bioconjugates with good pharmacokinetic properties and multi-functionalities. For example, RGD, is a short peptide that is known to bind to cell surface localized integrin receptors on solid tumor tissues and has been conjugated to fluorescent probes for *in vivo* imaging of mice[85]. Moreover, Leutinizing-hormone releasing hormone (LHRH) has been conjugated with the chemo-drug camptothecin and this resulted in accumulation specifically in a human ovarian carcinoma mouse xenograft with minimal dispersion in the surrounding tissues and amplification of the apoptotic effects of the drug at the tumor site.[86]. Taken together, CTPs and CPPs can be formulated with siRNA leading to a delivery system that is both efficient and specific. They provide a safe alternative to the conventional methods of siRNA delivery and circumvent many of the limitations associated with the non-selective forms of gene delivery.

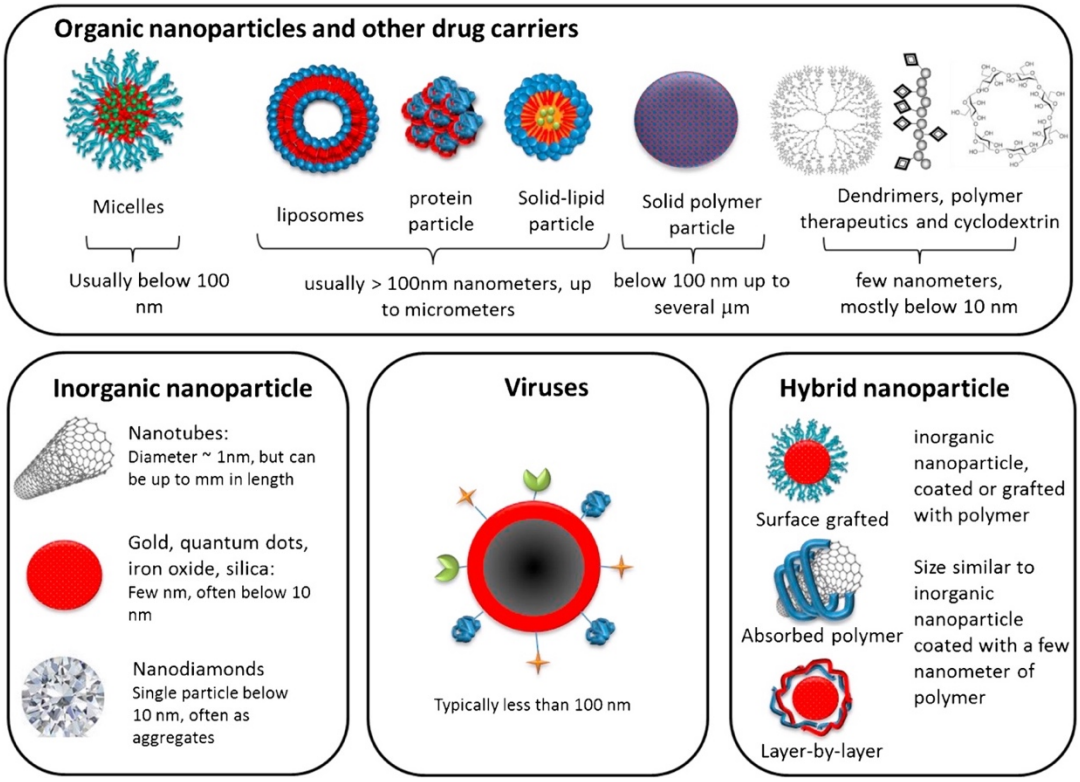

Figure 1.6. Various nanoparticle delivery system components for siRNA delivery. Image reprinted with permission from Elsevier: Young, S.W.S.; Stenzel, M.; Yang, J.L. *Crit. Rev. Oncol. Hematol.* **2016**. 98, 159-169.[87]

1.7 The Glucose Regulated Proteins – An Oncogenic Target

The glucose-regulated proteins (GRPs) are enzymes localized in the lumen of the endoplasmic reticulum (ER) or the mitochondria where they function mainly as chaperone proteins, guiding the folding and unfolding of newly synthesized proteins. This makes them intrinsically vital to proper cell function, homeostasis, proliferation, and survival. As such, they also serve as the main sensors for misfolded proteins and can trigger the unfolded protein response (UPR) under physiological or pathological cellular stress conditions. This pathway is then responsible for the mitigation of the stress or to signal for programmed cell death under prolonged stress conditions.[88] Moreover, non-ER bound GRPs, such as those localized on the mitochondria or on the cell surface, can function differently and also direct cell signaling.[89]

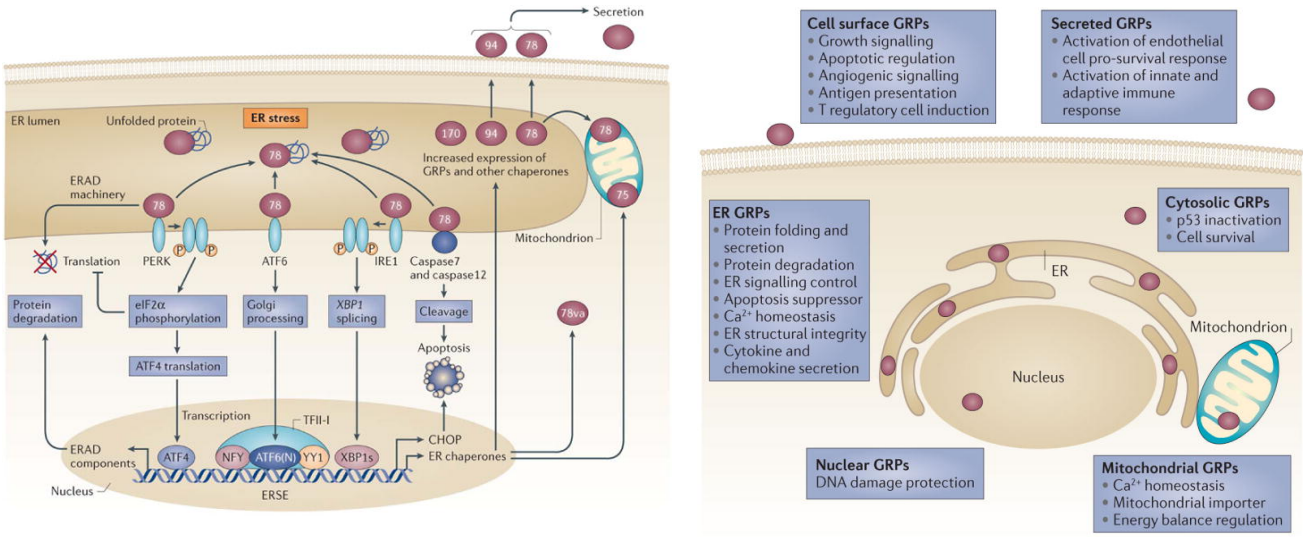

Figure 1.7 GRP localization and function. Images adapted with permission from Springer Nature: Lee, A.S. *Nat. Rev. Cancer* **2014**, *14*, 263-276.[88]

Of the various GRPs, the focus of this work is based on GRP78, GRP94, and GRP75. Glucose-regulated protein of 78kDa (GRP78), also referred as the immunoglobulin heavy chain binding protein (BiP), is a heat shock protein primarily localized in the ER where it serves as a master regulator of ER homeostasis and the UPR.[90] In its native state, GRP78 is bound to the ER transmembrane proteins PERK, ATF-6, and IRE-1 and prevents their activity in initiating the UPR. When exposed to cellular stress, GRP78 dissociates from these signal transducers which are then able to activate their signaling cascades in an effort to regain homeostasis.[91] ATF-6 is translocated to the golgi and cleaved into its active form that functions as a transcription factor to upregulate the expression of proteins such as the GRPs that enhance ER folding capabilities.[91,92] PERK, upon GRP78 dissociation, dimerizes and is phosphorylated into its active form that slows the rate of gene transcription to prevent the further accumulation of proteins until the stress has been reduced.[91,93] Similarly, IRE-1 activates and splices a short 26-base intron segment from the mRNA encoding for the X-box binding protein (XBP-1). This spliced protein then functions as a transcription factor to regulate the expression of ER chaperones and folding proteins.[91,94] In the

event that these branches of the UPR activated by GRP78 cannot return the cell to normal function, it then signals for apoptosis through the CHOP/Caspase signaling cascades.[89]

GRP78 upregulation is commonly associated with tumor cell progression, drug resistance, metastasis, and adhesion.[95-97] Silencing of GRP78 in the HepG2 liver carcinoma cell line resulted in a noticeable increase in tumor cell death (15%) with other studies showing that downregulation of GRP78 can inhibit tumor growth through the induction of apoptosis.[98-100] Oncogenic GRP78 expression is dysregulated and often translocated to the cell surface where it is associated with pathological stress typically related with the tumor microenvironment and signals for the survival and progression of the tumor.[101,102] Therefore, it serves as a viable gene therapy target by silencing its overexpression, minimizing cancer progression, and potentially regaining normal cell function.

Glucose-regulated protein of 94kDa, GRP94, is closely related to GRP78 in its function as an ER chaperone. Oncogenic GRP94 is similarly upregulated and helps to prevent apoptosis in cancer cells.[103] Moreover, its expression is often directly correlated with that of GRP78 and is involved in a compensation mechanism in which dysregulation of GRP78 induces the expression of GRP94 in order to maintain a high function chaperone activity for cancer cell proliferation. Silencing of GRP94 in patient multiple myeloma samples triggered apoptosis by inhibiting the *Wnt-survivn* pathway.[104,105] This implicates GRP94 as a promotor, with GRP78, of tumor survival and progression.

GRP75, also known as mortalin, is an interesting chaperone in that it is most closely associated with maintaining mitochondrial homeostasis through the mitochondrial UPR (mtUPR). Suppression of GRP75 has been shown to activate this version of the UPR, increase mitochondrial stress and fragmentation, reduce human mitochondrial mass *ex vivo*, and ultimately increase the rate of cellular apoptosis. Moreover, it has been found to interact with the well-known tumor

suppressor p53, altering its function and affecting the rate of cell apoptosis.[107] Together, these studies provide a solid ground of evidence highlighting the GRPs as good candidates for siRNA-based gene therapy mainly due to their overexpression and oncogenic activity.

Type of Cancer	GRP78	GRP94	GRP75
Bladder	+		
Brain	+		+
Breast	+	+	+
Colorectal	+	+	+
Endometrial	+		
Esophageal	+	+	
Gastric	+	+	
Head and Neck	+	+	
Leukemia	+		+
Liver	+	+	+
Lung	+	+	+
Melanoma	+		
Multiple myeloma	+	+	
Nasopharyngeal		+	
Oral	+	+	
Osteosarcoma		+	
Ovarian	+		+
Pancreatic	+	+	+
Prostate	+		
Renal	+		
Thyroid			

Table 1.3 Differential expression of the GRPs in a variety of cancer cell types. Reprinted with permission from Kozuch, S. PhD. Dissertation, Seton Hall University, 2018 who adapted it from Springer Nature: Lee, A.S. *Nat. Rev. Cancer* **2014**, *14*, 263-276.[88]

1.8 Thesis Objectives

This thesis highlights significant advances in the application of cm-siRNA, and the development of novel delivery strategies. The basis of our applications centers on the identification of the Glucose Regulated Protein, 78 kilodaltons (GRP78) as an important oncoprotein that is over-expressed and cell surface localized on a wide range of tumor cells. We have designed linear and higher order V- and Y- shape siRNAs targeting not only GRP78, but the other main resident GRP chaperones, GRP94 and GRP75, that have been found to be over-expressed in tumors and act as main executors of the unfolded protein response (UPR), a system that is related to endoplasmic reticulum (ER) stress. In the absence of normal GRP function under ER stress conditions, cellstypically undergo apoptotic responses triggering a series of cell death pathways. Thus, our main objective is to target and silence the GRPs in cancer, in order to synergistically activate tumor cell apoptosis as well as investigate the effect this silencing activity on other important biological pathways related to tumor survival and metastasis.

Chapter 2 describes relationship correlation in between GRP78 and the mesenchymal maker and adhesion protein N-cadherin (N-cad) in cancers that originate in or metastasize to the bone. Delivery of linear siRNAs against GRP78 into multiple myeloma (MM) and prostate cancer (PCa) cells resulted in concomitant knockdown of both GRP78 and N-cad protein expression levels. Further investigation resulted in drastic changes in the expression of proteins involved in the epithelial to mesenchymal (EMT) pathway and cellular adhesion in PCa cells. Moreover, GRP78 knockdown (GRP78 KD) reduced the adhesion of PCa to osteoblasts in a co-culture environment, likely implicating this important UPR chaperone in the metastasis of PCa to the bone (**Figure 1.9**).

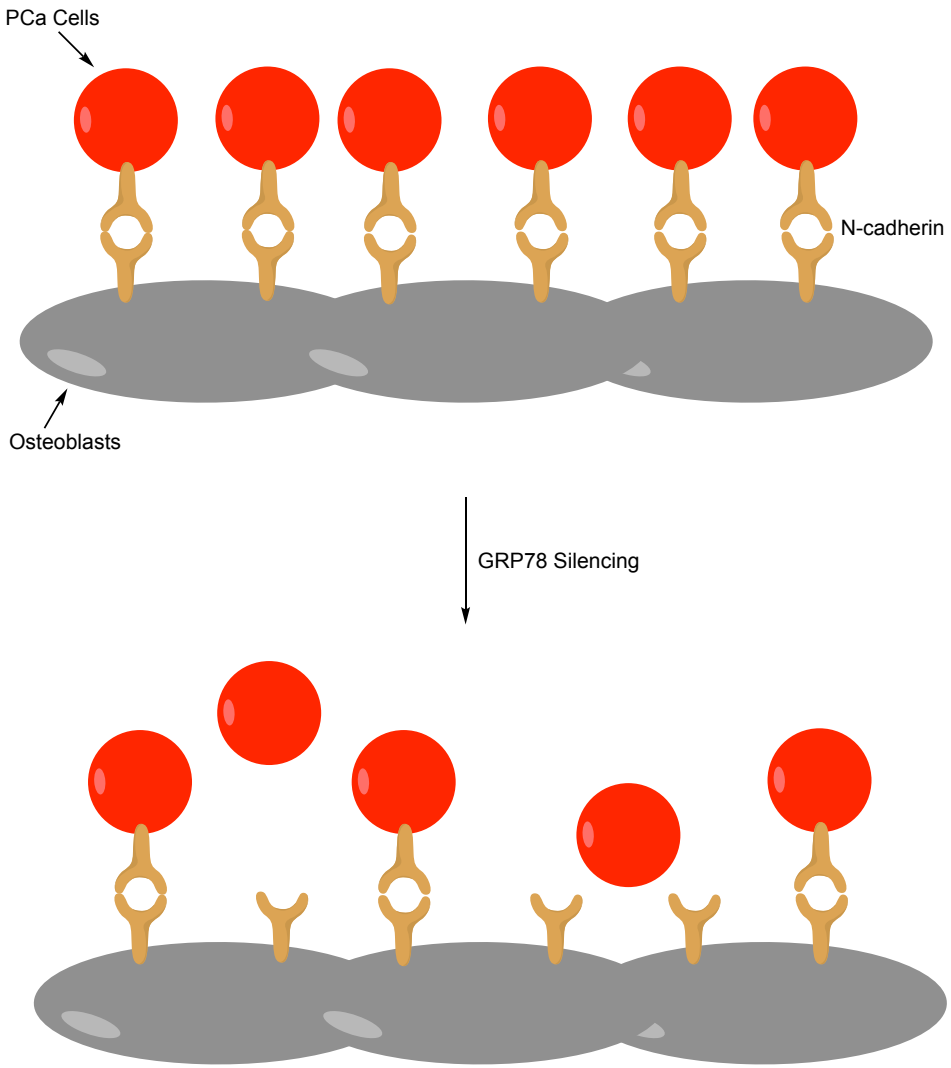

Figure 1.8 Graphical representation of the effect GRP78 silencing has on N-cad expression in PCa and its adhesion to osteoblasts. Drawn in Chemdraw.

Chapter 3 will focus on the evaluation of cm-siRNA resulting in the generation of V-, and Y-shape siRNAs that can simultaneously target and silence multiple oncogene targets. These multi-GRP silencing siRNAs have also been further functionalized by self-assembly and conjugation approaches for the generation of new cm-siRNA with improved structure-anti-cancer activity relationships. The higher order V- and Y-shape siRNAs self-assembled into discreet siRNA nanostructures adopting various sizes and shapes (**Figure 1.9a**) according to TEM and DLS measurements. These nanostructures targeted the above-mentioned resident GRPs in a small

panel of cancer cell lines. In the AN3CA endometrial cancer cells, the higher order siRNA nanostructures demonstrated a more potent and longer lasting silencing effect compared to the linear siRNA. Furthermore, a Y-shape siRNA construct targeting GRP78, GRP94, and GRP75 elicited significant GRP KD (50-95%) and synergistic tumor cell death (50-60%) in endometrial, cervical, and breast cancer cell lines. Conjugation approaches were next developed to include functionalized linear, V-, and Y-shape siRNAs with FITC and palmitamide, respectively functioning as theranostic probes or self-delivering agents (**Figure 1.9b**). The bioconjugates expanded the repertoire of functionally diverse cm-siRNAs while improving their applications in anti-cancer activity.

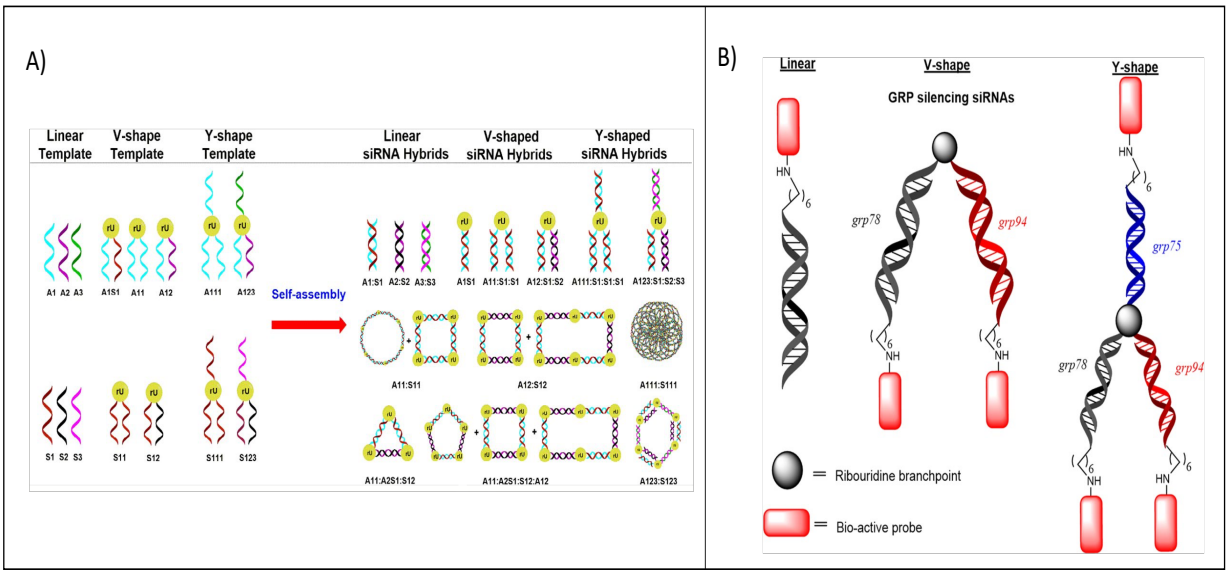

Fig 1.9 Graphical representation of linear, V-, and Y-shape siRNA constructs. A) Nanostructures derived from template guided self-assembly. B) Covalent bioconjugation strategy for introduction of fatty acid or fluorescent probes. Images adapted with permission from John Wiley and Sons: Cultrara, C.N.; Shah, S.; Kozuch, S.D.; Patel, M.R.; Sabatino, D. *Chem Biol Drug Des*. **2018.**[108]

Chapter 4 will discuss the generation of a CTP:siRNA formulations targeting the Prostate Specific Membrane Antigen (PSMA) receptor found on PCa cells. In this application, the lead CTP will be functionalized with a polyarginine sequence in order to effectively condense siRNA into small, discrete nanoparticle formulations that can internalize selectively within PSMA

expressing PCa cells. Once internalized, the multi-GRP targeting siRNAs are expected to trigger potent GRP silencing leading to apoptosis in PCa cells. In this manner, the bifunctional CTPs may function as effective and selective delivery systems for a wide range of siRNAs, including those adopting the higher-order V- and Y-shape nanostructures (Figure 1.11). As such the CTP:siRNA are anticipated to provide a tumor-targeting gene therapy strategy.

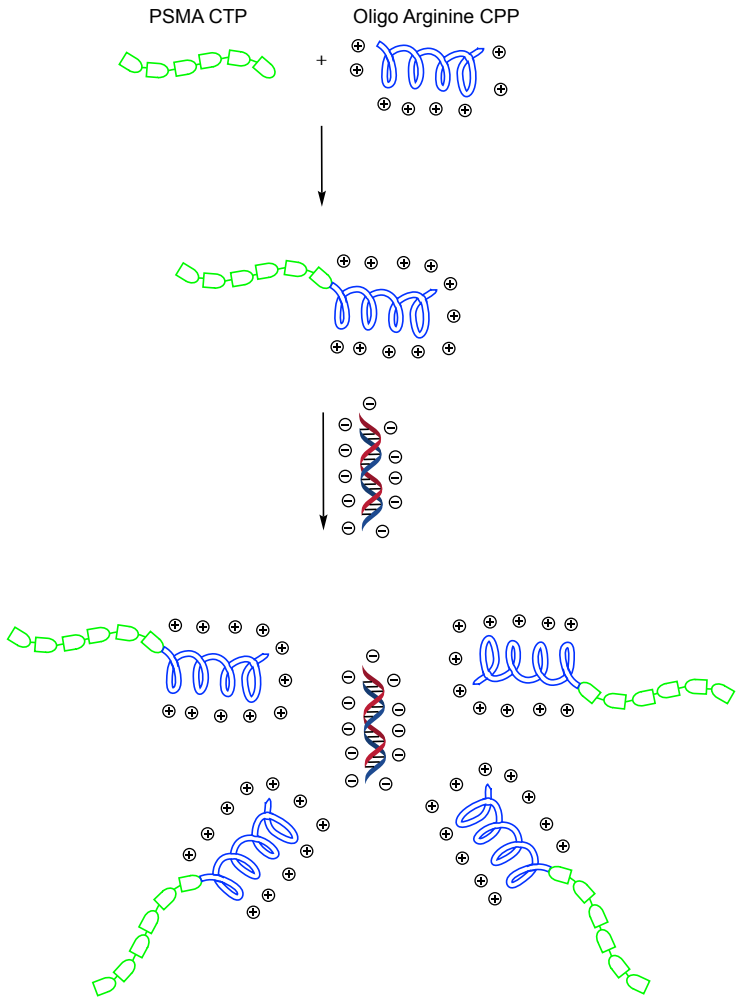

Figure 1.10 siRNA complex formation with novel PSMA targeting CTP/CPP hybrid. Drawn in ChemDraw.

References

1. Fire, A.; Albertson, D.; Harrison, S. W.; Moerman, D. G. *Development* **1991,** *113* (2), 503-514.
2. Guo, S.; Kemphues, K. J. *Cell* **1995,** *81* (4), 611-620.
3. Fire, A.; Xu, S.; Montgomery, M. K.; Kostas, S. A.; Driver, S. E.; Mello, C. C. *Nature* **1998,** *391* (6669), 806-811.
4. Mattick, J. S. *PLOS Genet* **2009,** *5*, e1000459.
5. Grosshans, H.; Filipowicz, W. *Nature* **2008,** *451*, 414-416.
6. Esteller, M. *Nat. Rev. Genet.* **2011,** *12*, 861-874.
7. Elbashir, S. M.; Harborth, J.; Lendeckel, W.; Yalcin, A.; Weber, K.; Tushcl, T. *Nature* **2001,** *411*, 494-498.
8. Hannon, G.; Rossi, J. *Nature* **2004,** *431*, 371-378.
9. Ahmadzada, T.; Reid, G.; McKenzie, D., *Biophys. Rev.* **2018,** *10*, 69-86.
10. Sioud, M., *Methods Mol. Biol.* **2015,** *1218*, 1-15.
11. Bernstein, E.; Caudy, A.; Hammond, S.; Hannon, G. *Nature* **2001,** *409*, 363-366.
12. Dalby, B.; Cates, S.; Harris, A.; Ohki, E.; Tilkins, M.; Price, P.; Ciccarone, V. *Methods* **2004,** *33*, 94-103.
13. Jensen, K.; Anderson, J.; Glass, E. *Vet. Immunol. Immunopathol.* **2014,** *158*, 224-232.
14. Zamore, P.; Tushcl, T.; Sharp, P.; Bartel, D. *Cell* **2000,** *101*, 25-33.
15. Vermeulen, A.; Behlen, L.; Reynolds, A.; Wolfson, A.; Marshall, W.; Karpilow, J.; Khnorova, A. *RNA* **2005,** *11* , 674-682.
16. Wilson, R.; Doudna, A. *Annu Rev Biophys* **2013,** *42*, 217-239.
17. Siomi, H.; Siomi, M. C. *Nature* **2009,** *457* , 396-404.
18. Preall, J.; He, Z.; Gorra, J.; Sontheimer, E. *Current Biology* **2006,** *16*, 530-535.
19. Gregory, R.; Chendrimada, T.; Cooch, N.; Shiekhattar, R. *Cell* **2005,** *123*, 631-640.
20. Elbashir, S. M.; Lendeckel, W.; Tushcl, T. *Genes Dev.* **2001,** *15*, 188-200.
21. Elbashir, S. M.; Martinez, J.; Patkaniowska, A.; Lendeckel, W.; Tuschl, T. *EMBO J.* **2001,** *20*, 6877-6888.
22. Agrawal, N.; Dasaradhi, P.; Mohmmed, A.; Malhorta, P.; Bhatnagar, R.; Mukherjee, S. *Microbiol. Mol. Biol. Rev.* **2003,** *67*, 657-685.
23. Rossi, J.; Kim, D. *Nature* **2007,** *8*, 173-184.
24. Dancey, J.; Bedard, P.; Onetto, N.; Hudson, T. *Cell* **2012,** *148*, 409-420.
25. Stratton, M. R. *Science* **2011,** *331*, 1553-1558.
26. Wong, K. M.; Hudson, T. J.; McPherson, J. D. *Annu. Rev. Genomics Hum. Genet.* **2011,** *12*, 407-430.
27. Pleasance, E. D.; Cheetham, R. K.; Stephens, P. J.; McBride, D. J.; Meynert, A.; Jones, D.; Lin, M. L.; Ordonez, G. R.; Bignell, G. R.; et al. *Nature* **2010,** *463*, 184-190.
28. Wu, S. Y.; Lopez-Berestein, G.; Calin, G. A.; Sood, A. K., *Sci. Transl. Med.* **2014,** *6*, 240ps7.
29. Burnett, J. C.; Rossi, J. J. *Chem Biol* **2012,** *19* , 60-71.
30. Sanceau, J.; Truchet, S.; Bauvois, B. *J Biol Chem* **2003,** *278*, 36537-36546.
31. Grzmil, M.; Thelen, P.; Hemmerlein, B.; Schweyer, S.; Voigt, S.; Mury, D.; Burfeind, P. *Am J Pathol* **2003,** *163*, 543-552.
32. Yin, J. Q.; Gao, J.; Shao, R.; Tian, W. N.; Wang, J.; Wan, Y. *Exp. Ther. Oncol.* **2003,** *3*, 194-204.

33. Futami, T.; Miyagishi, M.; Seki, M.; Taira, K. *Nucleic Acids Res. Suppl.* **2002,** *2*, 251-252.
34. Duxbury, M. S.; Ito, H.; Benoit, E.; Zinner, M. J.; Ashley, S. W.; Whang, E. E. *Biochem. Biophys. Res. Commun.* **2003,** *311*, 786-792.
35. Lois, C.; Refaeli, Y.; Qin, X. F.; Van Parijs, L. *Curr. Opin. Immunol.* **2001,** *13*, 496-504.
36. Spankuch-Schmitt, B.; Bereiter-Hahn, J.; Kaufmann, M.; Strebhardt, K. *J. Natl. Cancer Inst.* **2002,** *94* , 1863-1877.
37. Konnikova, L.; Kotecki, M.; Kruger, M. M.; Cochran, B. H. *BMC Cancer* **2003,** *3*, 23.
38. Nagy, P.; Arndt-Jovin, D. J.; Jovin, T. M. *Exp. Cell. Res.* **2003,** *285*, 39-49.
39. Zhang, M.; Zhang, X.; Bai, C. X.; Chen, J.; Wei, M. Q. *Acta. Pharmacol. Sin.* **2004,** *25*, 61-67.
40. De Schrijver, E.; Brusselmans, K.; Heyns, W.; Verhoeven, G.; Swinnen, J. V. *Cancer Res* **2003,** *63*, 3799-3804.
41. Devi, G. R. *Cancer Gene Therapy* **2006,** *13*, 819-826.
42. Bora, R. S.; Gupta, D.; Mukkur, T. K.; Saini, K. S. *Mol. Med. Rep.* **2012,** *6*, 9-15.
45. Lam, J. K.; Chow, M. Y.; Zhang, Y.; Leung, S. W. *Mol Ther Nucleic Acids* **2015,** *4*, e252.
46. Wang, J.; Lu, Z.; Wientjes, M. G.; Au, J. L. A. J. *AAPS* **2010,** *12* (4), 492-503.
47. Bakhtiyari, S.; Haghani, K.; Basati, G.; Karimfar, M. H. *Ther. Delivery* **2013,** *4* (1), 45-57.
48. Kanasty, R.; Dorkin, J. R.; Vegas, A.; Anderson, D. N. M., *12* (11), 967-77., *Nat. Mater* .**2013,** *12* (11), 967-977.
49. Tatiparti, K.; Sau, S.; Kashaw, S. K.; Iyer, A. K. *Nanomaterials* **2017,** *7* (4), 77.
50. Wang, J.; Mi, P.; Lin, G.; Xiang, Y.; Wang, J.; Liu, G.; Chen, X. *Advanced drug delivery reviews* **2016,** *104*, 44-60.
43. Ahmad Dar, S.; Thakur, A.; Qureshi, A.; Kumar, M. *Sci. Rep.* **2016,** *6* 20031.
44. Wilson, C.; Keefe, A. D. *Curr. Opin. Chem. Biol.* **2006,** *10*, 607-614.
45. Gaglione, M.; Messere, A. *Mini Rev. Med. Chem.* **2010,** *10*, 578-595.
46. Elmen, J. *et. al. Nucleic Acids Res* **2005,** *33*, 439-447.
47. Prakash, T. P. *et. al. J Med Chem* **2005,** *48*, 4247-4253.
48. Soutschek, J. *et. al*. *Nature* **2004,** *432*, 173-178.
48. Aboul-Fadi, T. *Current medicinal chemistry* **2005,** *12*, 2193-2214.
49. Chiu, Y. L.; Rana, T. M. *RNA* **2003,** *9*, 1034-1048.
50. Layzer, J. M. *et. al. RNA* **2004,** *10*, 766-771.
51. Detzer, A.; Sczakiel, G. *Curr. Top. Med. Chem.* **2009,** *9*, 1109-1116.
52. Jackson, A. L.; Burchard, J.; Leake, D.; Reynolds, A.; Schelter, J.; Guo, J.; Johnson, J. M.; Lim, L.; Karpilow, J.; Nichols, K.; Marshall, W.; Khvorova, A.; Linsley, P. S. *RNA* **2006,** *12*, 1197-1205.
53. Puri, N.; Wang, X.; Varma, R.; Burnett, C.; Beauchamp, L.; Batten, D. M.; Young, M.; Sule, V.; Latham, K.; Sendera, T.; Echeverri, C.; Sachse, C.; Magdaleno, S. *Nucleic Acids Symp Ser (Oxf)*. **2008**, *52*, 25-6
54. Peacock, H.; Kannan, A.; Beal, P. A.; Burrows, C. J., *J. Org. Chem.* **2011,** *76*, 7295-7300.
55. Somoza, A.; Silverman, A. P.; Miller, R. M.; Chelliserrykattil, J.; Kool, E. T. *Chemistry* **2008,** *14*, 7978-7987.
56. Sipa, K. *et. al. RNA* **2007,** *13*, 1301-1316.
57. Choung, S.; Kim, Y. J.; Kim, S.; Park, H. O.; Choi, Y. C. *Biochem. Biophys. Res. Commun.* **2006,** *342*, 919-927.

58. Lares, M. R.; Rossi, J. J.; Ouellet, D. L. *Trends Biotech.* **2010,** *28*, 570-579.
59. Dürig, J.; Dührsen, U.; Klein-Hitpass, L.; Worm, J.; Hansen, J. B.; Ørum, H.; Wissenbach, M. *Leukemia* **2011,** *25* , 638-647.
60. Raetz, E. A. *et. al*. *J Pediatr Hematol Oncol* **2014,** *36*, 458-463.
61. Haussecker, D. *J. Control Release* **2014,** *195*, 49-54.
62. Tatiparti, K.; Sau, S.; Kashaw, S. K.; Iyer, A. K. *Nanomaterials* **2017,** *7* (4), 77
63. Wang, J.; Mi, P.; Lin, G.; Xiang, Y.; Wang, J.; Liu, G.; Chen, X. *Advanced drug delivery reviews* **2016,** *104*, 44-60.
64. Jarad, G.; Miner, J. H. *Curr Opin Nephrol Hypertens* **2009,** *18*, 226-232.
65. Huang, Y.; Hong, J.; Zheng, S.; Ding, Y.; Guo, S.; Zhang, H.; Zhang, X.; Du, Q.; Liang, Z. *Mol. Ther.* **2011,** *19*, 381-385.
66. Moghimi, S. M.; Hunter, A. C.; Murray, J. C. *Pharmacol Rev* **2001,** *53*, 283-318.
67. Appelqvist, H.; Wäster, P.; Kågedal, K.; Öllinger, K. *J Mol Cell Biol.* **2013,** *5*, 214-226.
68. Sonawane, N. D.; Szoka, F. C.; Verkman, A. S., *J Biol Chem* **2003,** *278*, 44826-44831
69. Jackson, A. L.; Burchard, J.; Schelter, J.; Chau, B. N.; Cleary, M.; Lim, L.; Linsley, P. S. *RNA* **2006,** *12*, 1179-1187.
70. Judge, A. D.; Sood, V.; Shaw, J. R.; Fang, D.; McClintock, K.; MacLachlan, I. *Nature Biotechnol.* **2005,** *23*, 457-462.
71. Mihaila, R.; et al. *Molecular Threapy: Nucleic Acids*. **2017**, 7.
72. Ozpolat, B.; Sood, A.; Berestein-Lopez, G. *Adv Drug Deliv Rev*. **2014**, 66, 110-116
73. Dokka, S.; Toledo, D.; Shi, X.; Castranova, Y.; Rojanaskaul, Y. *Pharm Res*. **2000**, 17(5), 521
74. Spagnou, S.; Miller, M. *Biochemisty*. **2004**, 43, 13348-13356
75. Petros, R.A.; DeSimone, J.M. *Nat Rev Drug Discov*. **2010**, 9(8), 615-627
76. Semple, S. C.; Akinc, A.; Chen, J.; Sandhu, A. P.; Mui, B. L.; Cho, C. K.; Sah, D. W. Y.; Stebbing, D.; Crosley, E. J.; Yaworski, E.; *et. al, Nature Biotechnol.* **2010,** *28*, 172-176.
77. Wang, J.; Xu, C. *Asian Journal of Pharmaceutical Sciences*. **2015**, *10*, 1-12
78. Lee, D.J.; et al. *Bioconjug. Chem*. **2017**, 28(9), 2393-2409
79. Simoes, S.; Slepushkin, V.; Gaspar, R.; de Lima, M.C.; Duzgunes, N. *Gene Ther*. **1998**, 5, 955-964
80. El-Andaloussi, S.; Holm, T.; Langel, U., *Curr. Pharm. Des.* **2005,** *11*, 3597-3611.
81. Deshayes, D.; Morris, M. C.; Divita, G.; Heitz, F., *Cell Mol. Life* **2005,** *16*, 1839-1849.
82. Boisguérin, P.; Deshayes, S.; Gait, M. J.; O'Donovan, L.; Godfrey, C.; Betts, C. A.; Wood, M. J.; Lebleu, B. *Adv. Drug. Del. Rev.* **2015,** *87*, 52-67.
83. Lehto, T.; Kurrikoff, K.; Langel, U. *Expert Opin. Drug Disc.* **2012,** *9*, 823-836.
84. Kay, B. K.; Kasanov, J.; Yamabhai, M. *Methods* **2001,** *24*, 240-246.
85. Kwon, S.; Ke, Shi.; Houston, J.; Wang, W.; Wu, Q.; Li, C.; Sevick-Muraca, E. *Molecular Imaging*. **2005**, *4*(2), 75-78
86. Dharap, S. S.; Wang, Y.; Chandna, P.; Khandare, J. J.; Qiu, B.; Gunaseelan, S.; Sinko, P. J.; Stein, S.; Farmanfarmaian, A.; Minko, T. *PNAS* **2005,** *102* , 12962-12967.
87. Young, S.W.S.; Stenzel, M.; Yang, J.L. *Crit. Rev. Oncol. Hematol.* **2016**, *98*, 159-169.
88. Lee, A.S. *Nat. Rev. Cancer* **2014**, *14*, 263-276.
89. Wu, J.; Kaufman, R. J. *Cell Death Differ.* **2006** *13*, 374–384.
90. Lee, A.S. *Trends Biochem Sci.* **2001** *26*(8):504-510
91. Wang, M.; Wey, S.; Zhang, Y.; Ye, R.; Lee, A.S. *Antioxid Redox Signal*. **2009**, *11*(9), 2307-2316

92. Haze, K.; Yoshida, H.; Yanagi, H.; Yura, T.; Mori, K. *Mol Biol Cell*. **1999**,*10*(11):3787-3799.
93. Harding, H.P.; Zhang, Y.; Ron, D. *Nature*. **199,** *397*(6716),271-274.
94. Yoshida, H.; Matsui, T.; Yamamoto, A.; Okada, T.; Mori, K. *Cell.* **2001,** *107*(7):881-891.
95. Chang, Y.J.; Huang, Y.P.; Li, Z.L.; Chen, C.H. *PLoS One*. **2012,** 7(4):e35123
96. Mhaidat, N.M.; Alzoubi, K.H.; Almomani, N.; Khabour, O.F. *Cancer Biomark*. **2015,** *15*(2):197-203.
97. Zhang, L.; Li, Z.; Fan, Y.; Li, H.; Li, Z.; Li, Y. *Int J Biochem Cell Biol*. **2015,** 64,202-211.
98. Pi, L.; Li, X.; Song, Q.; Shen, Y.; Lu, X.; Di, B. *Oncol Lett*. **2014,** 7(3):685-692.
99. Suzuki, T.; Lu, J.; Zahed, M.; Kita, K.; Suzuki, N. *Arch. Biochem. Biophys*. **2007**, *468*, 1-14
100. Maina, A; Blackman, B.A.; Parronchi, C.J.; Morozko, E.; Bender, M.E.; Blake, A.D.; Sabatino, D. *Bioorg. Med. Chem. Lett*. **2013,** *23*, 5270-5274.
101. Gonzalez-Gronow M; Selim, M.A.; Papalas, J.; Pizzo, S.V. *Antioxid Redox Signal*. **2009** 11(9):2299-306.
102. Quinones, Q.J.; de Ridder, G.G.; Pizzo, S.V. *Histol Histopathol*. **2008** 23(11):1409-16.
103. Reddy, R.K.; Lu, J.; Lee, A.S. *J. Biol. Chem.* **1999** 274, 28476–28483.
104 Hua, Y. *et al. Clin. Cancer Res.* **2013,** *19*, 6242–6251.
105. Wadhwa, R. *et al. J. Biol. Chem.* **1998,** *273*, 29586–29591.
107. Wadhwa, R. *et al. Exp. Cell Res.* **2002,** *274*, 246–253.
108. Cultrara, C. N.; Shah, S.; Kozuch, S. D.; Patel, M. R.; Sabatino, D. *Chemical Biology and Drug Design* **2018**, 1-12.

Chapter 2: GRP78 Modulates Cell Adhesion Markers in Prostate Cancer and Multiple Myeloma Cell Lines[1]

2.1 Abstract

siRNA technologies have had a widespread impact in the treatment of various disorders, particularly in cancer. As such, siRNAs have been developed as gene therapeutic agents, and also in their ability to promote RNAi screening of various gene targets implicated in the translation of detrimental proteins involved in disease progression. This chapter will discuss the anti-cancer effects of an anti-GRP78 siRNA in prostate cancer (PCa) and multiple myeloma (MM) cell lines. Moreover, this study aims to define the functional role of GRP78 on drug treatment sensitivity, cell adhesion and metastatic spread to resident bone tissues in these important cancer types. Glucose regulated protein 78 (GRP78) is a resident chaperone of the endoplasmic reticulum and a master regulator of the unfolded protein response under physiological and pathological cell stress conditions. GRP78 is overexpressed in many cancers and is involved in the regulation of various signaling pathways including tumor initiation and proliferation, as well as adhesion, invasion and metastatic spread to secondary organs. GRP78 can also regulate cell survival and initiate apoptotic pathways to either prevent further damage caused by a particular stress or to alter a cell's responsiveness to anticancer drugs.

Tumors that reside or metastasize to the bone and bone marrow (BM) space can develop pro-survival signals through their direct adhesive interactions with stromal elements in the BM niche leading to drug treatment resistance. Here, we report a direct correlation between GRP78 and the adhesion molecule N-cadherin (N-cad), known to play a critical role in the adhesive interactions of MM and metastatic PCa within the bone microenvironment. N-cad mRNA and protein expression levels were evaluated upon silencing GRP78 in the MM.1S MM and the PC3 metastatic

PCa cell lines. Furthermore, we investigated the effects of GRP78 knockdown (KD) on PC3 cells including other epithelial-mesenchymal (EMT) transition markers, morphological changes and their adhesion properties to osteoblasts (OSB) cells. We found that GRP78 KD led to concomitant downregulation of N-cad at the protein levels of expression in both tumors types. In PC3 cells, GRP78 KD significantly decreased E-cadherin (E-cad) expression likely associated with the induction in TGF-β1 expression. Furthermore, GRP78 KD also triggered drastic changes in PC3 cells morphology and decreased their adhesion to OSB cells dependent, in part, to the reduced N-cad expression. This implicates GRP78 as a modulator of cell adhesion markers in MM and PCa which may lead to a clinical underscoring of GRP78 as a potential therapeutic target to reduce the adhesive nature of metastatic tumors to the bone niche.

2.2 Introduction

Tumor cells that reside or metastasize to the bone and BM can develop pro-survival interactions with stromal cells, including osteoblasts (OSB) at the endosteum, through adhesion molecules. Resistant malignant stem cells can remain moderately protected within the bone microenvironment during treatment and later re-initiate growth to from reoccurring tumors.[2-4] In particular, we have shown that N-cad is a necessary mediator of $CD138^+$ patient-derived multiple myeloma (MM) cells' adhesion to the endosteum, and that shRNA mediated down-regulation of N-cad in OSB decreased MM-OSB adhesive interactions, restricting the *ex vivo* survival of these tumor cells[5]. These adhesive interactions are considered to be major factors in which cancer cells remain "dormant" and escape the cytotoxic effects of therapeutic agents. This mechanism of drug resistance has been described in MM, as well as in disseminated/metastatic prostate cancer (PCa)

cancer.[6-8] Bone is a preferred site for PCa metastases, and currently no curative treatments exist once the tumor is established within this niche.[9-11]

The 78 kDa glucose-regulated protein (GRP78) is a chaperone protein that serves as the main sensor for misfolded proteins in the endoplasmic reticulum (ER) and triggers the unfolded protein response (UPR).[12] Moreover, GRP78 regulates intracellular signaling events associated with embryonic development, aging, pro-apoptotic/survival mechanisms, Ca^{2+} homeostasis and insulin/IGF-1 signal transduction.[12] GRP78 is expressed ubiquitously in all cell types and is located primarily in the endoplasmic reticulum where it chaperones protein folding activity. It can also be found in the mitochondria where it interacts with pro-survival and apoptotic executors and also at the cell surface where it initiates various cell signaling pathways, including those associated with oncogenic activity.[13] In cancer, GRP78 is commonly overexpressed and associated with tumor initiation, drug resistance, proliferation, adhesion and invasion to resident tissues resulting in metastatic spread.[13,14] GRP78 has also been found to be highly active in osteoblastic, androgen-independent prostate cancer[15] which suggests that it might play a pivotal role in the interaction of PCa cells with OSB. It was found to play a critical role in the adhesion and invasion of hepatocellular carcinoma[16] and MM[17] and can potentiate resistance against cytotoxic chemotherapy in PCa cells.[18] Furthermore, it is also overexpressed in a quiescent MM cell sub-population resistant to treatment.[19, 20] Of note, GRP78 has been correlated with the expression of EMT markers N-cad, E-cad and β-catenin, respectively in colon cancer and hepatocellular carcinoma.[16, 21, 22] While high levels of N-cad have been linked to poor prognosis of MM patients[23, 24] and to PCa metastasis in castration resistant models [25], no studies have examined the potential interplay between GRP78 and N-cad in MM and PCa for modulating tumor-bone adhesion. Similarly, GRP78 overexpression can affect the EMT signaling pathways related to Snail/Slug and

TGF-β/smad that are closely associated with metastasis of epithelial tumors.[16, 22] Classically, an EMT is associated with the upregulation of mesenchymal markers such as N-cad and vimentin along with parallel downregulation of the epithelial marker E-cad. [26, 27]

2.3 Chapter Objectives

This thesis chapter focuses on the use of GRP78 siRNA to investigate a novel correlation between GRP78 and N-cad in MM and PCa cells. N-cad expression has been shown to be directly proportional to GRP78 levels in hepatocellular carcinoma and colorectal cancer. [16, 22] Furthermore, circulating levels of N-cad have been linked to poor prognosis of MM patients,[23,24] while upregulation of this molecule was linked to PCa metastasis and castration resistance.[25] Together these findings served as basis for our hypothesis, implicating GRP78 and N-cad as important markers involved in tumor adhesion and metastasis of PCa with bone tissue. In order to investigate this purported correlation, an siRNA cocktail will be reverse transfected into MM and PCa cell lines in order to evaluate the relationship between GRP78 and related markers of cell adhesion and the EMT pathway. Quantitative analyses at the genetic and protein levels of expression will be evaluated by Real Time Polymerase Chain Reaction (RT-qPCR) and western blot, respectively. siRNA treatment will also be used in order to determine the functional role of GRP78 on PCa cells' morphology and adhesion to bone-derived OSB cells. Importantly, these results may contribute to a better understanding of the underlying survival properties conferred by cell-cell adhesion interactions, aiding in the development of more effective therapeutic strategies against cancers that interact with the bone niche.[10, 28-31] These results and data presented in this chapter are adapted with permission from the authored publication found in BMC Cancer : Cultrara, C. N.;

Kozuch, S. D.; Ramasundaram, P.; Heller, C. J.; Shah, S.; Beck, A. E.; Sabatino, D.; Zilberberg, J., *BMC Cancer* **2018,** *18* (1), 1263. doi: 10.1186/s12885-018-5178-8

2.4 Results and Discussion

2.4.1 GRP78 silencing leads to concomitant N-cad downregulation in MM.1S and PC3 cell lines

Initially, the basal GRP78 and N-cad levels were analyzed by western blot and revealed comparable expressions of these proteins in MM.1S and PC3 cancer cell lines (**Appendix fig. 1**). While GRP78 upregulation is well documented in many cancers,[15,19, 20] MM and PCa cells often display aberrant N-cad expressions.[24, 25, 32, 33] An optimized siRNA transfection protocol found suitable for suspension (MM.1S) and adherent (PC3) cell lines was used to assess the effects of GRP78 KD on the expression levels of N-cad. A commercial GRP78-silencing siRNA was transfected with the TransIT-X2® dynamic delivery system that is compatible with the transfection of suspension and adherent cells.[34] The suspension nature of MM.1S cells makes them inherently more difficult to transfect, therefore, we doubled the siRNA concentrations (to 100 nM) and used multiple GRP78 silencing siRNAs, in combination, to provide a more effective GRP78 KD in these cells. While this concentration was adequately tolerated (**Appendix Fig 2**), only a ~40% ($P<0.05$) decrease in GRP78 protein levels was achieved, compared with ~ 70% KD ($P<0.001$) in PC3 cells using only 50 nM of the same siRNA cocktail (**Fig. 1A**)..

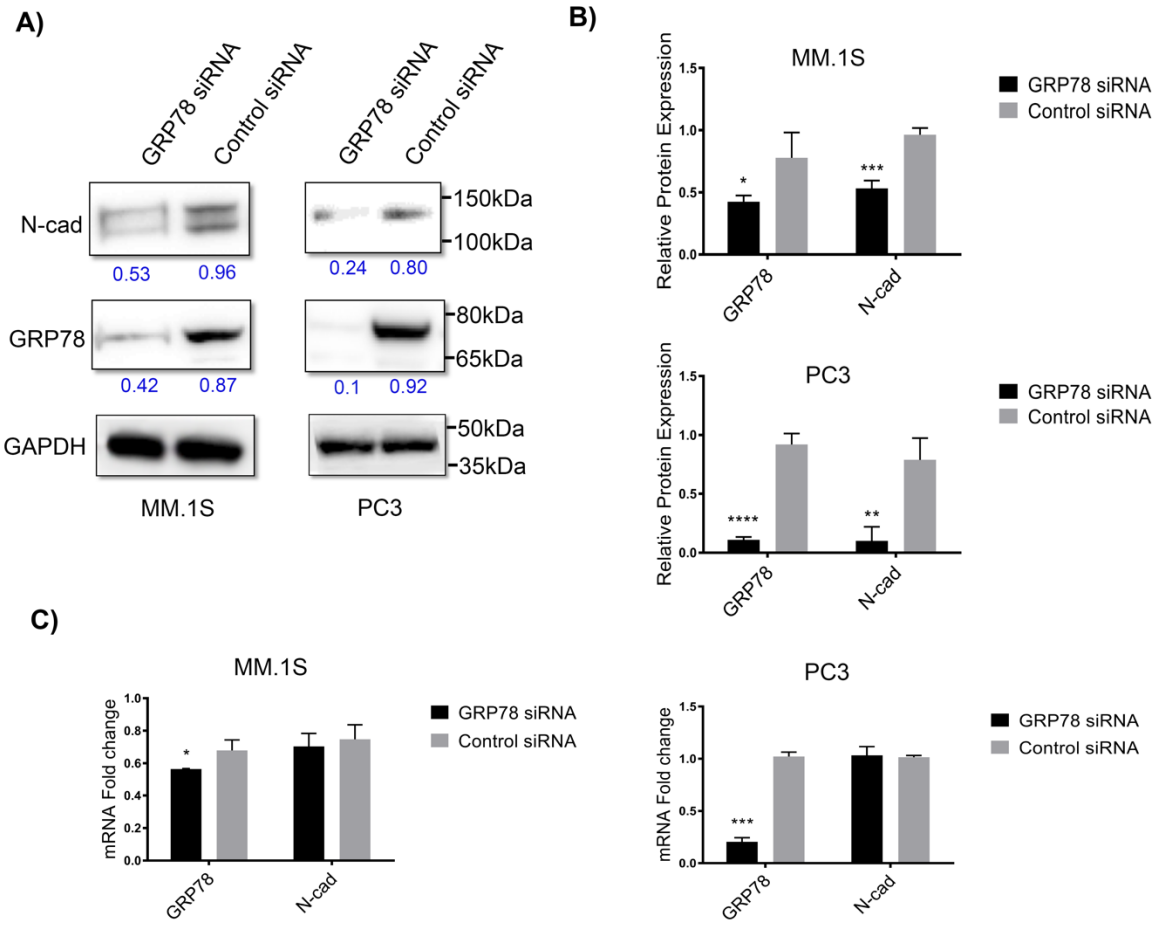

Figure 2.1 Relationship between GRP78 and N-cad in MM.1S and PC3 cells upon GRP78 KD. siRNA cocktail (100 nM and 50 nM) against GRP78 or a control siRNA were transfected into MM.1S and PC3 cells, respectively. Total mRNA and protein levels were analyzed at 48 hrs and 72 hrs, respectively. A) Western blots of endogenous GRP78 and N-cad protein expression after GRP78 silencing. B) Protein expression quantification. Target protein levels were normalized against the loading control GAPDH and compared with the control, non-targeting siRNA. Blot bands and quantitative values are presented as the mean ± SD and representative of 3 separate trials. Western blot analysis for MM.1S and PC3 cells were performed independently. *P<0.05 and ***P<0.001 in MM.1S cells and ****P<0.0001 and **P<0.01 in PC3 cells for GRP78 and N-cad, respectively. C) qRT-PCR analysis of relative mRNA levels for GRP78 and N-cad upon GRP78 silencing. Target mRNA levels are relative to the control siRNA and represented as the mean fold change ± SD of 3 separate trials. *P<0.05 in MM.1S cells and ***P <0.001in PC3 cells for GRP78.

Two other MM cell lines; MM.1R and RPMI 8226, were also transfected. Similarly, no significant knockdown of GRP78 was observed under optimized conditions (**Fig 2.2A**) likely due

to the known challenges of transfecting non-adherent MM cells.[35] Despite this difference in GRP78 KD efficiency, the MM.1S and PC3 cell lines exhibited significant decreases in N-cad protein levels although without changes in N-cad mRNA transcript levels (**Fig. 2.1B & C**), suggesting a preferential downregulation of N-cad translation over transcriptional modulation. Regardless, the decrease in N-cad protein expression level implies that a regulatory relationship between these two biomarkers exists in MM.1S and PC3 cells (**Fig 2.1**). Of note, only one of three MM cell lines (MM.1S) assayed showed appreciable GRP78 KD at high dose (100 nM) concentrations of siRNA. This demonstrates not only the difficulty of siRNA based gene silencing in MM, but also the dependence of MM on this important regulator of the ER/UPR system.[36] Alternatively, highly concentrated and long-lasting siRNA transfections (100 nM, 24-72hr) rendered further follow-up experiments unfeasible since the MM.1S cells were susceptible to apoptosis under these prolonged treatment conditions (**Fig 2.2B**)

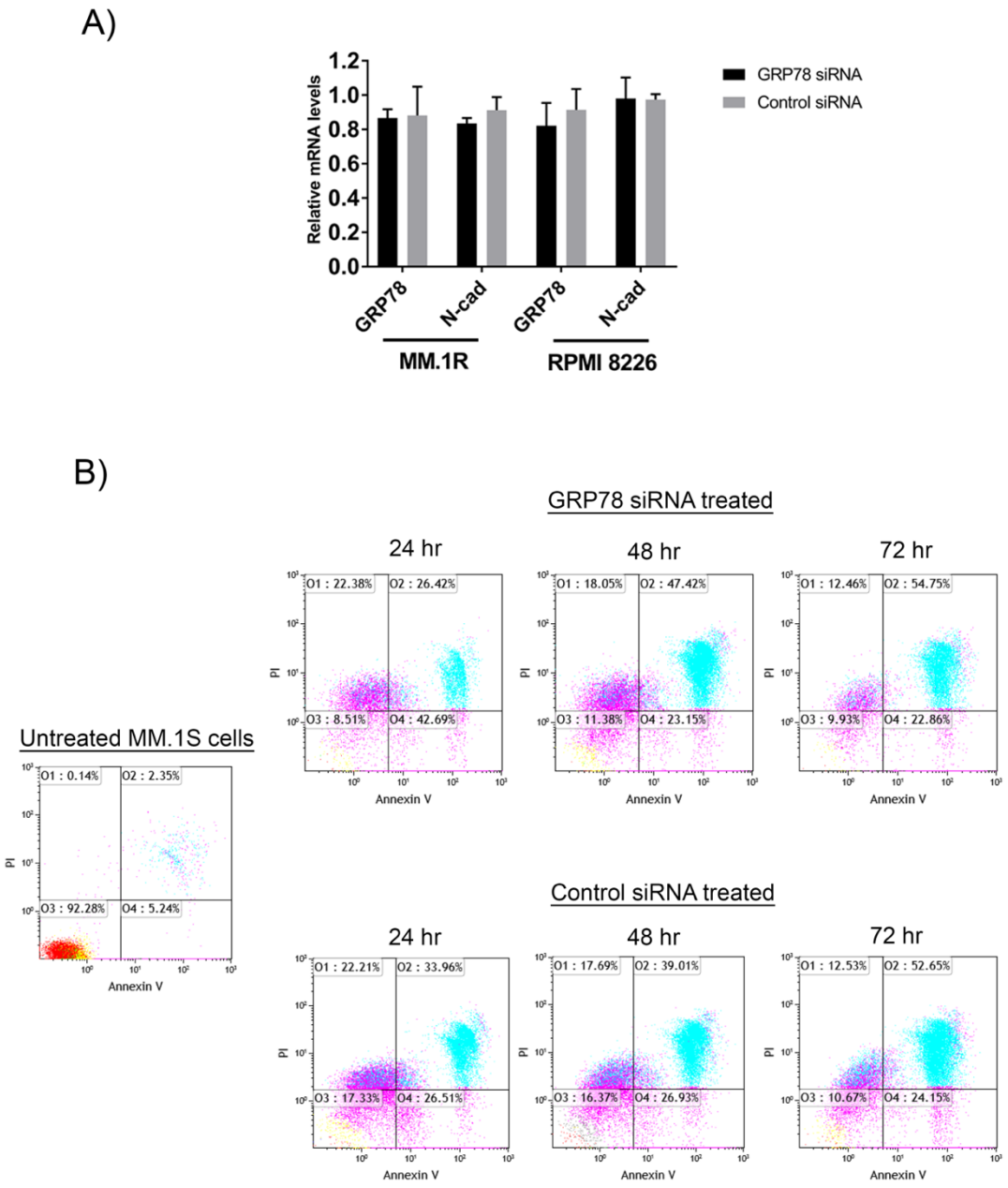

Figure 2.2 Viability assay of MM.1S cells after siRNA transfection. A) GRP78 silencing in MM.1R and RPMI 8226 MM cell lines. 100 nM siRNA cocktail against GRP78 or a control siRNA were transfected into each cell line. Total mRNA levels were analyzed at 48 h. qRT-PCR analysis of relative mRNA levels for GRP78 and N-cad upon GRP78 silencing. Target mRNA levels are relative to the control siRNA and represented as the mean fold change ± SD of 3 separate trials. B) Viability assay of MM.1S cells after siRNA transfection. 100 nM siRNA cocktail or a control siRNA were transfected into MM.1S cells and analyzed by flow cytometry over 72 hrs. Histograms are representative of 3 independent trials at each time point.

Moreover, the cancer cell lines studied (i.e., MM.1S and PC3 lines) did not manifest cell membrane bound GRP78 and have been shown in other reports to lack surface GRP78 under specified culture conditions.[37] Thus, our results likely indicate a role for cytosolic rather surface GRP78 on N-cad expression. However, surface expression of GRP78 has been observed in varying tumor cell lines and with ER stressors known to upregulate surface GRP78 expression allowing for potential future studies aimed at investigating the effects of exogenous GRP78 blocking antibodies on N-cad activity.[37] Likewise, additional methods[35] may be needed to fully characterize the functional relationship in between GRP78 and N-cad among multiple MM and PCa cell lines.

2.4.2 Oncomine cDNA Microarray analysis

We queried the Oncomine microarray repository to find any correlations in the expression profiles of HSPA5 (GRP78) and CDH2 (N-cad) in patient samples. Oncomine is a cancer microarray database and web-based data mining platform whose objective is to perform genome wide expression analysis and compare a cancer's target profile against that of healthy tissue. One major advantage of this platform is that the analysis can be set to clinically important limits such as membrane bound or known gene-drug target pairs which can help discover new therapy strategies.[38] All MM tumor tissue samples in these studies were accessed from BM aspirates from newly diagnosed patients. Patients in Dickens' et. al study received autologous transplantation following induction by either a cyclophosphamide, thalidomide and dexamethasone (CTD) chemotherapy regiment for younger fit participants or cyclophosphamide, vincristine sulfate, Adriamycin, and dexamethasone (CVAD) chemotherapy regimen for older, unfit participants, while no indication of treatment was presented for the Zhan and Agnelli cohorts. The analyzed PCa tumor tissue samples ranged in origin from patients with elevated PSA (>2.5ng/mL) but non-

confirmed cancer, prostatectomy samples, xenograft biopsies, primary organ tumor, and metastasized samples including bone, lymph node, and lung. Only one PCa trial indicated that patients had received no prior treatment. HSPA5 was overexpressed in 6/15 (40%) PCa studies (fold change ranging between 1.029-3.095, $P<0.05$) and 2/3 (66%) MM studies (fold change of 1.095 and 1.513, $P<0.05$). HSPA5 gene rank between 2-24% in PCa and was in the top 13% in the 2 MM studies with significant fold change. CDH2 was overexpressed in 1/17 PCa studies (fold change of 1.193, $P<0.05$) and a gene rank of 14%, and 2/4 MM studies (fold change of 1.094 and 3.411, $P<0.05$) and gene rank of 25% and 12% respectively. Results are summarized in **Tables 2.1** and **2.2.**

ONCOMINE cDNA microarray analysis summary for MM

Multiple Myeloma					
Study	**P-value**	**Fold Change**	**Tumor Tissue Samples**	**Healthy Tissue Samples**	**Gene Rank***
HSPA5					
Zhan	8.87E-06	1.513	74	37 (plasma)	top 13%
Dickens	1.15E-08	1.095	84	84 (leukocyte)	top 13%
CDH2					
Zhan	3.84E-06	3.411	74	37	top 12%
Agnelli	0.04	1.094	133	5	top 25%

Table 2.1 ONCOMINE was searched using the following filters: Gene: HSPA5 (GRP78) or CDH2 (N-cad), Analysis Type: Cancer vs. Normal Analysis, Cancer Type: prostate cancer or multiple myeloma. *Gene rank denotes the extent of significance out of all genes assayed; i.e. what percentage of genes whose upregulation has a more significant p-value as compared to the gene of interest

ONCOMINE cDNA microarray analysis summary for PCa

Prostate Carcinoma					
Study	**P-value**	**Fold Change**	**Tumor Tissue Samples**	**Healthy Tissue Samples**	**Gene Rank***
HSPA5					
Welsh	1.91E-07	1.958	25	9	top 2%
Singh	1.14E-04	3.095	52	50	top 4%
TCGA	1.12E-06	1.026	126	61	top 9%
	0.001	1.029	45	61	top 20%
Vanaja	0.004	1.586	27	8	top 15%
Taylor	0.013	1.169	131	29	top 17%
Grasso	0.029	1.158	59	28	top 24%
CDH2					
Arredouani	0.014	1.193	13	8	top 14%

Table 2.2 ONCOMINE was searched using the following filters: Gene: HSPA5 (GRP78) or CDH2 (N-cad), Analysis Type: Cancer vs. Normal Analysis, Cancer Type: prostate cancer or multiple myeloma. *Gene rank denotes the extent of significance out of all genes assayed; i.e. what percentage of genes whose upregulation has a more significant p-value as compared to the gene of interest.

For MM, the fold change was small likely because plasma cells and leukocytes (used as comparison samples) are secretory cells that also have high basal levels of the UPR markers.[39] CDH2 on the other hand was only significantly upregulated in one PCa study. That notwithstanding, a study describing the *de novo* expression of N-cad using two parameter immunofluorescence showed that this protein was expressed in high-grade human PCa, whereas no expression was found in normal prostatic tissue.[40] Likewise, circulating N-cad has also been associated with poor MM prognosis [23], supporting an underlying relationship between N-cad and GRP78 in the progression of both tumor types.

2.4.3 Effect of ER Stressors on GRP78 and N-cad expression in MM.1S

The UPR is highly upregulated in MM cells due to their secretory nature.[36,41,42] The lack of a strong transcriptional downregulation in the MM.1S cells prompted us to evaluate how the expression profiles of GRP78 and N-cad would be affected in the presence of acute drug challenge. The ER stress inducers Bortezomib (Btz) and thapsigargin (Tg); both of which are known to stimulate GRP78 expression and are used as current clinical treatments. Btz is a proteasome inhibitor that has been clinically approved for the treatment of MM while Tg is a Ca^{2+}-ATPase inhibitor that causes the accumulation of unfolded proteins. Both cause intense ER stress by either preventing protein turnover or sequestering inactive proteins destined for removal. This stress induces the expression of ER chaperones, like GRP78, and forces it into action to either remove the stress or enable apoptotic pathways. Due to this, we wanted to examine whether ER stress would sensitize MM.1S cells to siRNA transfection, leading to a more robust KD effect. Btz triggered the upregulation of GRP78 mRNA expression levels by ~3.0 fold ($P<0.01$) while Tg, led to a greater (~7.0-fold, $P<0.001$) increase in GRP78 mRNA transcript levels. Conversely, both ER stress inducers were found to downregulate N-cad mRNA expression levels. We performed a follow up transfection of BTZ treated MM.1S cells with GRP78-silencing siRNA (**Fig. 2.3B)** which interestingly resulted in GRP78 mRNA KD as well as concomitant N-cad mRNA KD.

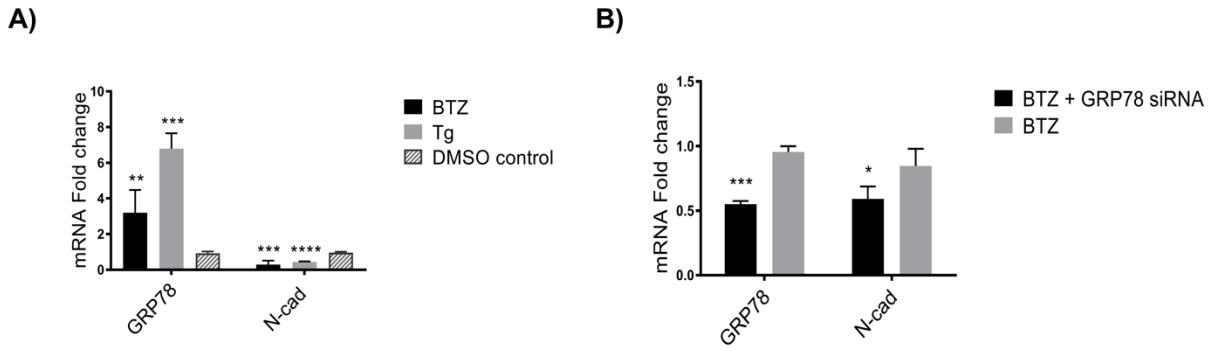

Figure 2.3 Effect of ER stress on GRP78 and N-cad mRNA levels in MM.1S cells. A) Effect of ER stress inducers on MM.1S cells. Cells were treated with 10 nM bortezomib (BTZ) or 1 nM thapsigargin (Tg). qRT-PCR analysis was performed after 18 h of consecutive treatment. **P<0.01 and ****P<0.001 for GRP78 with BTZ treatment and Tg treatment vs. vehicle control (DMSO), respectively. ****P<0.0001 for N-cad with both BTZ and Tg treatment vs. vehicle control (DMSO). B) GRP78 silencing after BTZ treatment. MM.1S cells were treated overnight with 10 nM BTZ followed by treatment with 100 nM siRNA cocktail against GRP78. qRT-PCR analysis was performed 48 hrs post-transfection. ***P<0.001 and P<0.05 for GRP78 and N-cad vs. BTZ only treatment, respectively. All target mRNA levels are represented as the mean fold change ± SD of 3 separate trials.

BTZ has been found to suppress the expression of N-cad [43] but little is known about the effects of Tg on this molecule. N-cad expression has been associated with intracellular Ca^{2+} flux, so inhibition of the ATPase-dependent Ca^{2+} flux by Tg may be correlated with its effects on N-cad transcription levels.[44] Nevertheless, when MM.1S cells were pre-treated with BTZ followed by GRP78 siRNA transfection, GRP78 KD caused an additional decrease in N-cad (**Fig 2.3B**) gene expression. Of note, siRNA treatment did not affect genetic levels of N-cad (**Fig 2.1C**) but the combination of ER stressors (i.e., drug treatments) and siRNA transfection did induce significant downregulation in N-cad mRNA levels, suggesting that ER stressors (such as that induced by BTZ) may sensitize MM cells to siRNA treatment. This strategy may be a potential clinically viable approach to facilitate the transfection of UPR dependent cancer cells.

2.4.4 GRP78 silencing has no significant effect on the expression of related GRPs in PC3 cells nor causes cytotoxicity.

In combination with GRP78, GRP94 and GRP75 are important ER chaperones and regulators of cell homeostasis.[45,46] Their overexpression has been linked to tumor progression, metastasis and survival in multiple cancer types.[45,46] Because GRPs work in concert and are closely related in function, we hypothesized that GRP78 KD could potentially have an associated effect on the client chaperones GRP94 and/or GRP75. To test this hypothesis, we measured mRNA and protein levels of GRP94 and 75 upon GRP78 KD in PC3 cells. Interestingly, GRP78 KD strongly increased GRP94 mRNA levels (~2.7-fold, $P<0.001$) but no changes were detected in GRP94 protein expression. GRP78 downregulation had no effect on the levels of GRP75 mRNA or protein expressions (**Fig. 2.5 A,B,C**)

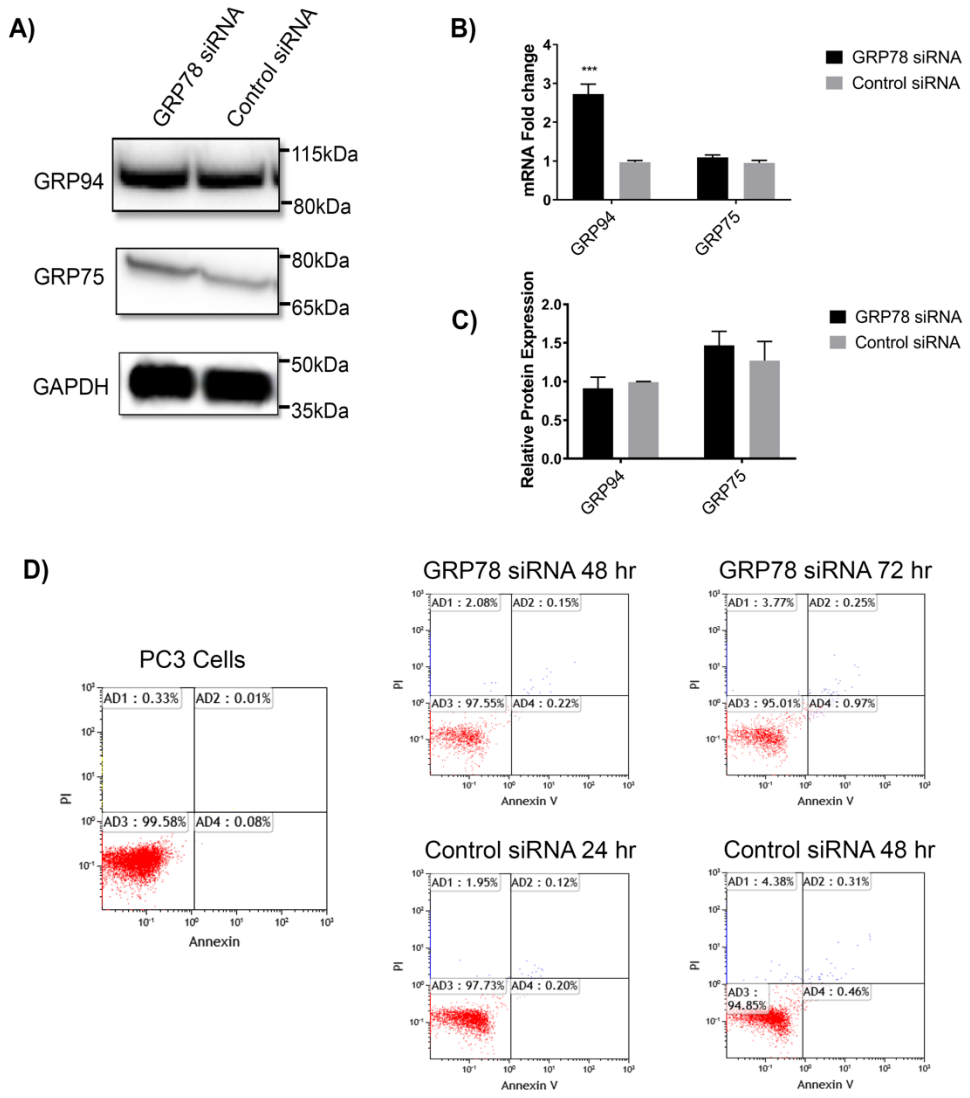

Figure 2.4. Effects of GRP78 silencing on GRP94 and GRP75 in PC3 cells. 50 nM siRNA cocktail against GRP78 or control siRNA were transfected into PC3 cells. Total mRNA and protein levels were analyzed at 48 h and 72 h, respectively. A) Western blot of GRP protein expression after GRP78 silencing. B) Protein expression analysis. Target protein levels were normalized against the loading control GAPDH and compared to control siRNA. Blot bands and quantitative values are presented as the mean ± SD and representative of 3 separate trials. C) qRT-PCR analysis of relative mRNA levels GRPs upon GRP78 silencing. Target mRNA levels are relative to the control siRNA and represented as the mean fold change ± SD of 3 separate trials. ***P <0.001 for GRP94. D) Viability assay PC3 cells after siRNA transfection. 50 nM siRNA cocktail or a control siRNA were transfected into PC3 cells and analyzed by flow cytometry at 48 and 72 hrs. Histograms are representative of 3 independent trials at each time point.

Work done in *C. elegans* has proven that a compensatory mechanism exists between nine different ER chaperones, of which GRP78 and GRP94 were included.[47] GRP94's activity is not replicative of GRP78 and tends to gain function when GRP78 is absent.[48] GRP78 knockdown, inactivation, or altering its cellular localization in mammalian cells have all be been reported to induce the expression of GRP94.[49-51] However, the reverse is not true as studies have shown GRP94 knockdown does not always induce the expression of GRP78 or other chaperones.[52] Interestingly, we observed this regulatory compensation by a strong transcriptional increase in GRP94 upon silencing of GRP78 in PC3. Yet, there was no increase in the protein expression suggesting that either 1) the cells had mitigated the stress caused by the initial knockdown and had no need for excess GRP94, or 2) the lack of GRP78 effectively suppressed the protein folding and no functional GRP94 was expressed despite the high transcriptional levels. Conversely, neither the transcript or protein expression levels of GRP75 were affected. Despite being an ER chaperone, GRP75 also functions as a crosstalk mediator between the ER and the mitochondria and its knockdown in neuroblastoma cells activated the mitochondrial stress response.[53] However, increased GRP75 expression has been shown to promote cytotoxicity in different cancer models. The lack of a compensatory reaction of GRP75 in response to our treatment also falls in line with the lack of cytotoxicity commonly observed in GRP78 suppressed cells. The PC3 model may not be as reliant on the ER chaperones or as sensitive to the effects of the UPR even over prolonged stress (i.e 72hrs). This prevents simple knockdown of the ER chaperones as an effective treatment strategy for PCa in terms of cell death, yet as shown, may have significant effects on other important pathways related to tumor progression. In fact, GRP94 knockout has been shown to disrupt cell adhesion of liver cells in mice.[54] Knockdown of multiple GRPs in combination may be a potentially potent way of increasing the therapeutic nature of this treatment.

2.4.5 GRP78 silencing has significant effects on the expression of EMT related markers in PC3 cells.

We next investigated the effects of GRP78 silencing on members of the EMT signaling pathway, in which N-cad is a major marker. The EMT of epithelial cells is partly characterized by elevated levels of N-cad, with concomitant suppression of E-cad, ultimately enabling a more migratory and invasive tumor phenotype.[55] GRP78 expression has been linked to cancer progression and metastasis in part through its effects on EMT markers in PCa.[56] Induction of GRP78 has been shown to trigger EMT in colorectal cancer cells, while GRP78 KD using shRNA reversed the EMT by suppressing N-cad and upregulating E-cad expression levels, referred to as a "cadherin switch." [22] However, using our GRP78-silencing approach, GRP78 KD in PC3 cells resulted in significant decreases of both N-cad and E-cad (**Fig. 2.1 & Fig. 2.5**) protein levels. In addition, we also investigated other EMT markers such as TGF-β and snail/slug. [27] We found a significant upregulation in TGF-β1 expression (~100%, $P<0.01$), suggesting a potential role for GRP78 as an important regulator of EMT markers in metastatic PCa. While not statistically significant, changes in β-Catenin and Snail-2 were also observed and may have important biological implications (**Fig. 2.5**). Once more, due to the inherent difficulties associated with transfection of suspension cells, MM cells were not used for this part of the study. The EMT process is controlled, in part, by the transcription factor Snail-2 which acts as a strong repressor of E-cad.[57,58] GRP78 KD induced Snail-2 expression (**Fig 2.5**) which may account for the downregulation of E-cad.

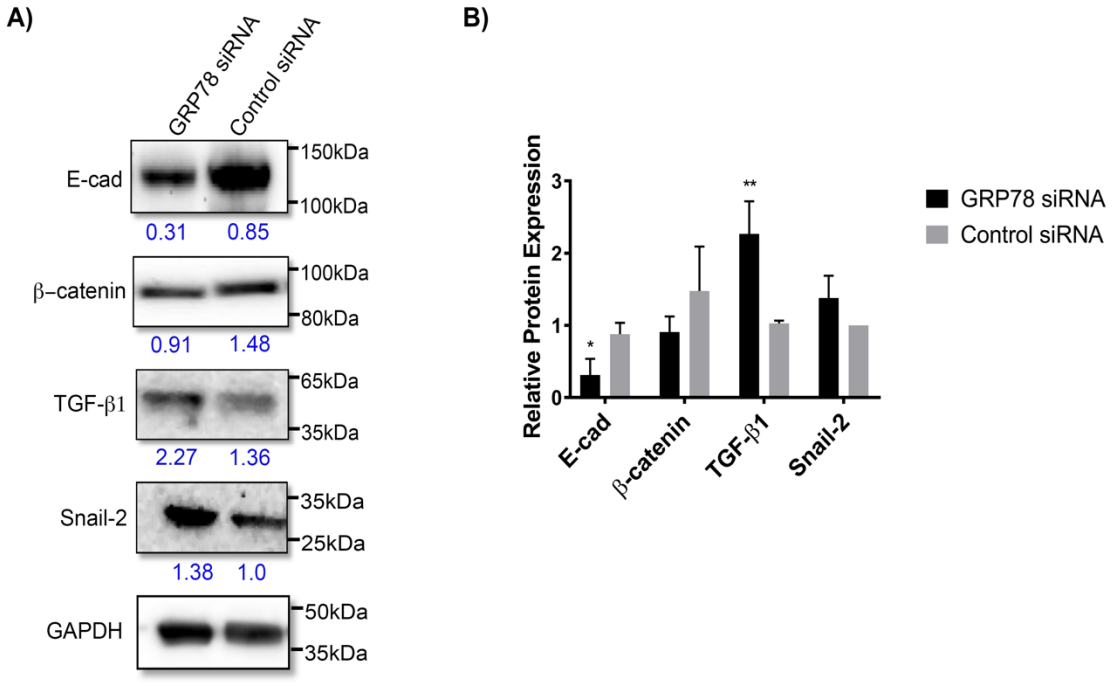

Figure 2.5 Analysis of markers related to EMT after GRP78 silencing. 50 nM siRNA cocktail against GRP78 or control siRNA were transfected into PC3 cells and total protein levels analyzed 72 hrs post-transfection. A) Western blot of EMT markers. B) Protein expression analysis. Target protein levels were normalized against the loading control GAPDH and compared to control siRNA. Blot bands and quantitative values are presented as the mean ± SD and representative of 3 separate trials. **P<0.01 for TGF-β1 and *P<0.05 for E-cad.

GRP78 overexpression, its localization to the cell surface, and its association with Cripto [59, 60] have been correlated with the activation of the TGF-β pathway. [61] TGF-β is a multifunctional cytokine which regulates prostate cell growth and epithelial cell proliferation.[62, 63] However, active TGF-β exists mainly as an extracellular matrix protein which can function both as a tumor suppressor or as a key player in promoting tumorigenesis in advanced cancers. [61-65] We showed that in PC3 cells, GRP78 KD induced a strong and significant increase in TGF-β1 protein expression; consistent with our findings, induction of Snail-2 expression has been credited to TGF-β associated pathways.[66] While we observed TGF-β1 upregulation and the expected downstream

effects that this molecule has on Snail-2 and E-cad, we found that GRP78 silencing decreased N-cad expression in PC3 cells. TGF-β1 upregulation is typically reported to be accompanied by N-cad upregulation,[22] hence our results suggest that N-cad expression is highly dependent on GRP78 in this cell line and its regulation via GRP78 KD may supersede the effects of TGF-β1; i.e., N-cad was downregulated in spite of the fact the TGF-β1 expression was significantly increased upon GRP78 KD. This may indicate a unique mechanism in which GRP78 KD can directly modulate the expression of certain adhesion and EMT molecules. We also showed that downregulation of GRP78 did not change the protein expression levels of other chaperone GRPs nor cause cytotoxicity in PCa. These results confirm that the observed effects on the EMT markers were GRP78-dependent and not the result of global changes in closely related chaperones that also maintain ER homeostasis.

2.4.6 GRP78 silencing changes the morphology of PC3 cells and reduces their adhesiveness to OSB

A co-culture assay with PC3 and hFOB 1.19 OSB cells was developed to test whether GRP78 silencing would translate into reduced adhesion to bone cells, due to the concomitant suppression of related adhesion and EMT markers. OSB were cultured to confluence in a 96-well plate. PC3 cells were initially transfected with GRP78 silencing siRNA and then cultured on top of the OSB monolayer. Parallel co-cultures were treated with the anti-N-cad mAb CG-4, known to neutralize its function.[67] Dramatic changes in morphology of the PC3 cells following GRP78 silencing were observed, indicated by a shift from a flatter, elongated shape to a rounded configuration. We also noticed a lower cell density in these wells 18 hrs after transfection. However, no significant changes in morphology were observed when cultures were incubated with an N-cad NAb **(Fig 2.6).**

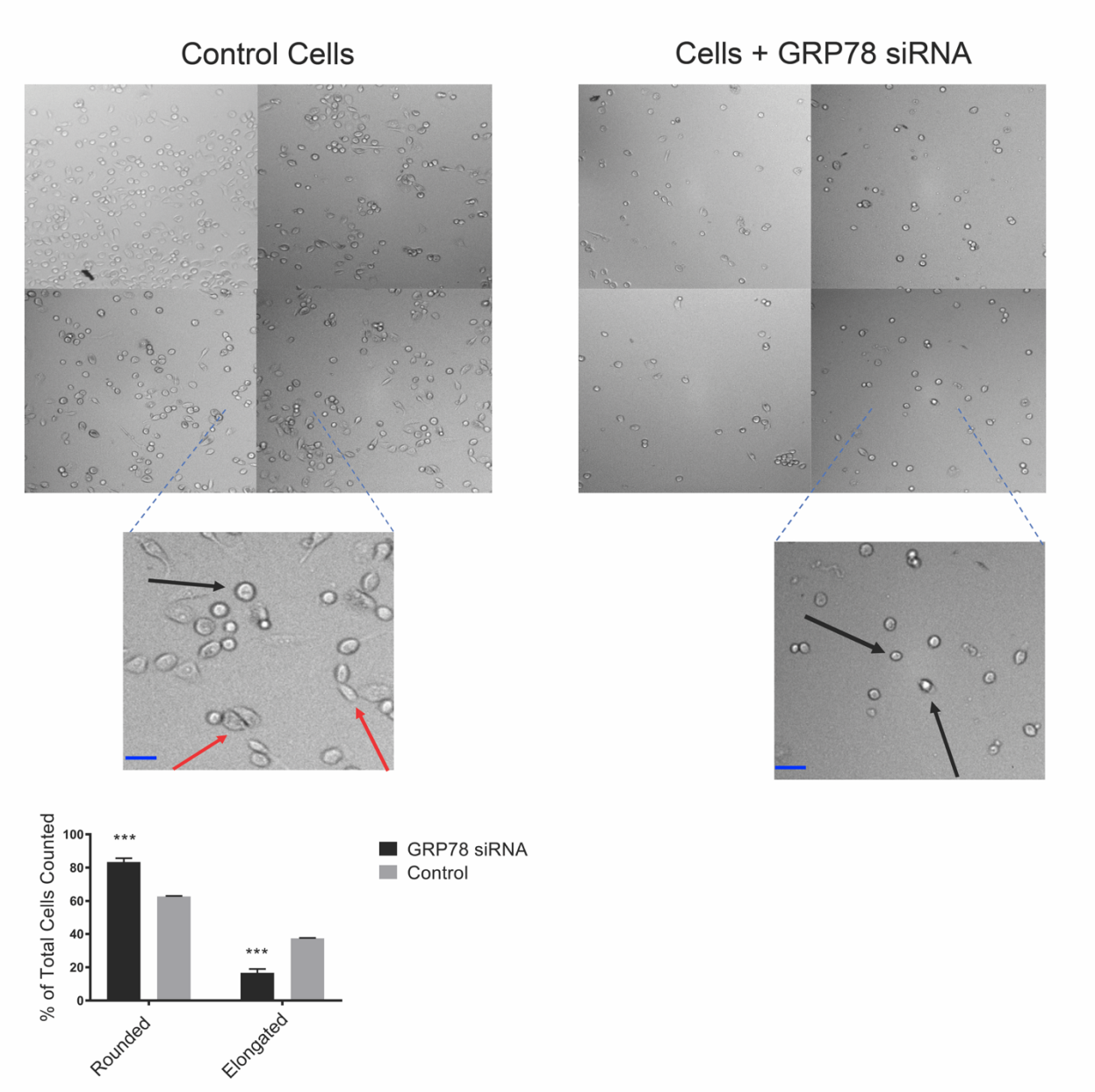

Figure 2.6 Morphological changes in PC3 cells after GRP78 KD. Cells were harvested 48 hrs post-transfection and re-seeded on a 24-well plate. Changes in morphology were analyzed 24 hrs after seeding. Bright-field microscope images (10x magnification) of cellular morphology containing 4 representative fields of view from 3 separate trials. Black arrows denote cells with rounded morphology and red arrows denote elongated cells. ***P< 0.001 compared to control (untreated) cells. Scale bar = 10 μm.

Importantly, transfected PC3 cells were found to be less adhesive to OSB, as determined by a small but significant increase (>10%) in the number of cells collected in the supernatant relative to the

untreated control wells. Likewise, the N-cad NAb treatment reduced the co-cultured PC3 adhesion to OSB by [~10%] (**Fig. 2.7B**). These data support a functional role for GRP78 and N-cad in mediating cell-cell adhesive interactions in between PCa and OSB cells. Ultimately, the cells were found to be less adherent to OSB, relative to untreated control cells, supporting the hypothesis that GRP78 KD and suppression of N-cad could significantly inhibit PCa cell-based adhesion to bone. In a comparable manner N-cad NAb treatment also diminished PCa adhesion to OSB (**Fig. 2.7**) highlighting the specific role N-cad plays in this phenomenon. That notwithstanding, other adhesion molecules have been reported to play a role in PCa-bone interaction,[68] potentially accounting for the only moderate decrease in PC3 adhesion to OSB in our assays.

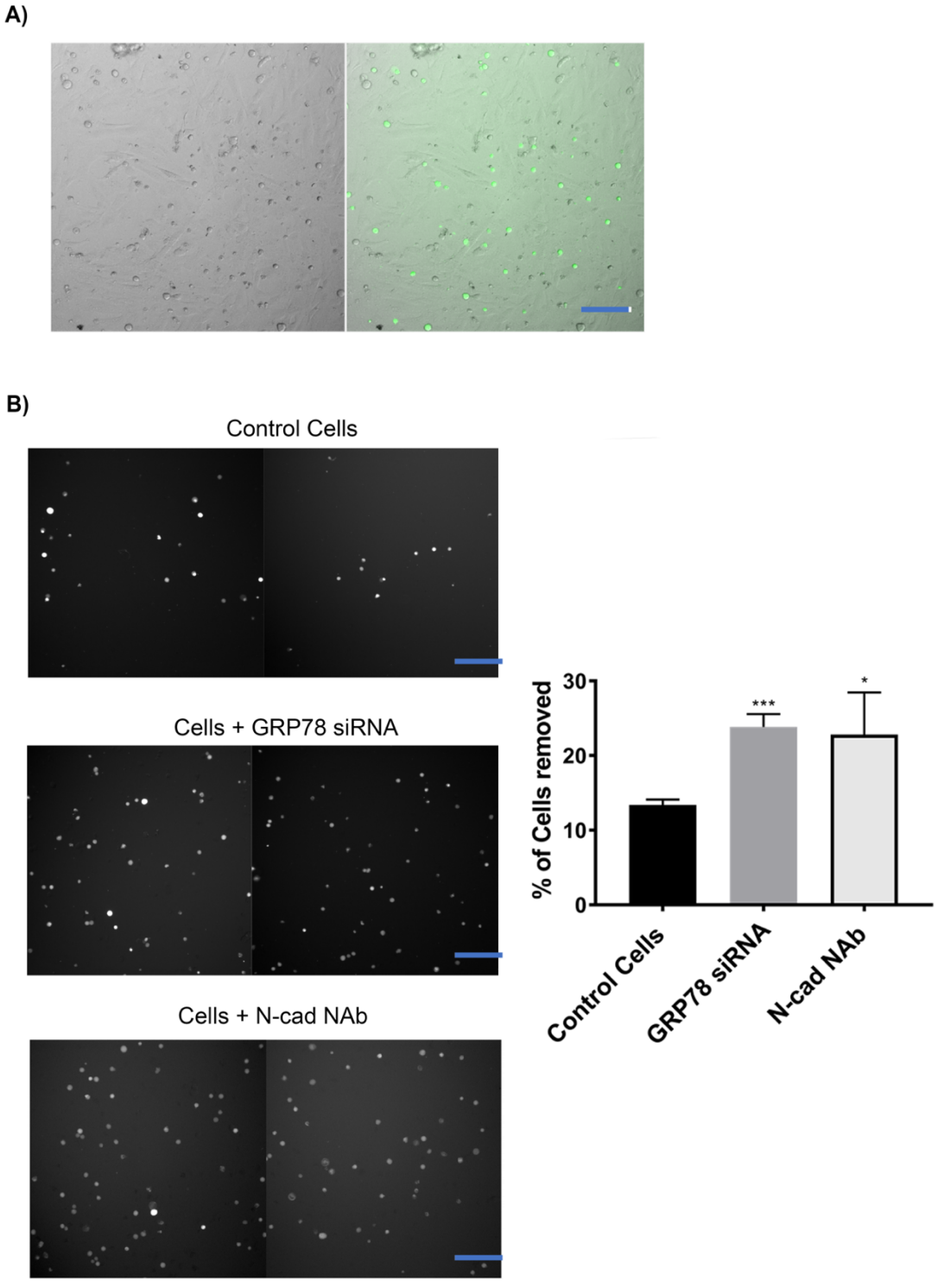

Figure 2.7 Functional changes in PC3 adherence to OSB after GRP78 KD or incubation with a N-cad NAb clone CG-4 (N-cad NAb). PC3 cells were fluorescently labeled and re-seeded into 96-well plates with confluent OSB 48 h post-transfection. Percentage of adhered cells was determined 24 hrs after co-culture. A) Representative image of PC3+OSB co-culture. Left = brightfield, right

= composite. B) Fluorescent images of labeled PC3 cells in supernatant after being removed from the co-culture and are representative of 3 independent trials. *P<0.05 and ***P< 0.001 compared to control (untreated) cells for the N-cad NAb or the GRP78 siRNA, respectively. Scale bar = 50 μm.

2.5 Conclusions

We have established a novel correlation between GRP78 and N-cad in MM and PCa cells and present GRP78 as an ancillary regulator of markers associated with the EMT pathway and its implications in the adhesion properties of PCa to the bone/BM niche. Our data suggest that downregulation of GRP78 may represent a suitable therapeutic intervention strategy for modulating tumor-microenvironment adhesive interactions leading to tumor progression and drug resistance. In summary, our results warrant additional investigations to further unravel the molecular interactions by which GRP78 asserts adhesion regulation, given its primary role as a master regulator of the UPR in the ER.

2.6 Methods and Materials

2.6.1 ONCOMINE Data Mining

The ONCOMINE repository (www.oncomine.com) is a repository of cDNA microarrays. [38] We searched ONCOMINE using the following filters: Gene: HSPA5 (GRP78) or CDH2 (N-cad), Analysis Type: Cancer vs. Normal Analysis, Cancer Type: prostate cancer or multiple myeloma. A summary table containing fold change and significance (P<0.05) for each comparison are presented as log2 median-centered intensity as reported by ONCOMINE.

2.6.2 Cell Culture

MM.1S (MM cell line, ATCC®CRL-2974), MM.1R (MM cell line, ATCC® CRL-2975), RPMI 8226 (ATCC® CCL-155), PC3 (bone metastatic PCa cell line, ATCC®-CRL-1435), and

hFOB 1.19 (OSB cell line, ATCC® CRL-11372) were purchased from ATCC. MM cell lines were cultured in high glucose RPMI-1640 medium supplemented with 15% fetal bovine serum (FBS), 2.5 mM of L-glutamine and 1% penicillin/streptomycin. PC3 cells were cultured in RPMI-1640 medium containing 10% FBS, 2.5mM of L-glutamine and 1% penicillin/streptomycin. Both cell lines were cultured at 37˚C in a humidified tissue culture incubator containing 5% CO_2. hFOB 1.19 cell medium consisted of 1:1 mixture of Ham's F12 Medium Dulbecco's Modified Eagle's Medium, with 2.5 mM L-glutamine, 10% FBS and 0.3 mg/ml G418 (Sigma-Aldrich). These cells were maintained and propagated at 33˚C and 5% CO_2 except during co-culture experiments which were conducted at 37˚C. All cell lines were checked periodically for mycoplasma using MycoAlert™ Mycoplasma Detection Kit (Lonza). Authentication of cell lines was performed by STR DNA profiling analysis conducted by the Molecular Resources Facility at Rutgers University. Cell populations were frozen after 3 passages from the time of initial receipt and growth and were discarded after 30 passages.

2.6.3 ER Stress Induction

For ER stress induction, MM.1S cells were seeded at a density of $7.5x10^5$- $1.0x10^6$ cells/well in a 24-well plate. Cells were treated for 18 hrs with 10 nM bortezomib (BTZ) (Caymen Chemicals), 1nM thapsigargin (Tg) (Sigma-Aldrich) or dimethyl sulfoxide (DMSO, Sigmal-Aldrich) as vehicle controls. Total RNA was isolated and subsequently analyzed via qRT-PCR.

2.6.4 siRNA Transfection

HSPA5 (GRP78) targeting siRNAs were purchased from Ambion (Carlsbad, USA). Two different siRNAs; *Silencer®* Select Pre-designed siRNA s6979 (5' UUC UGG ACG GGC UUC AUA Gtt 3') and s6980 (5' UCU AGU AUC AAU GCG CUC Ctt 3') targeting exons 6 and 8 of GRP78 mRNA, respectively, were tested. For control, the *Silencer®* select negative control No. 2 siRNA was used (Ambion). siRNA transfections were performed using a modified reverse transfection technique [69] using a cocktail containing equimolar quantities of each GRP78 siRNA to maximize silencing potential. The GRP78 siRNA cocktail (or siRNA control) was diluted in Opti-MEM reduced serum medium and incubated with the TransIT-X2 dynamic delivery system (Mirus Bio) according to the manufacturer's protocol. The siRNA-TransIT-X2 complexes were added to wells of either a 6- or 24- well plate upon which either MM or PC3 cells seeded in complete growth medium at a cell density of 7.5-9x10^5 cells/well (6 well plate) or 0.75-1x10^5 cells/well (24 well plate). GRP78 siRNA cocktail or control siRNA were used at a final concentration of 50 nM for PC3 and 100 nM for MM cell lines.

2.6.5 RNA Isolation and qRT-PCR

Total RNA was isolated following transfections (48 hrs) from TriZol (Ambion) preserved cells using a TriRNA Pure Kit (Geneaid), following the manufacturer's instructions. The collected RNA was quantitated on a Qubit 3.0 fluorimeter using the Qubit Broad Range (BR) assay kit (Thermo Fisher Scientific). RNA (200 ng) was reversed transcribed into cDNA using a high capacity cDNA kit (Applied Biosystems). RT-PCR was performed using pre-developed TaqMan™ gene expression primer-probes for GRP78 (assay ID Hs99999174_m1), N-cad (assay ID Hs00983056_m1), GRP94 (assay ID Hs00437665_g1), GRP75 (Hs00269818_m1), and GAPDH (Hs99999905_m1) and TaqMan™ fast advanced master mix. qPCR fast assay was

carried out on a StepOnePlus RT-PCR system (Applied Biosystems). Fold changes were calculated with the ΔΔCt method using GAPDH as endogenous control and the negative siRNA as the control sample.

2.6.6 Western Blot

Total protein was isolated from the cell cultures following transfection (72 hrs). Protein lysates were prepared by lysing the cells in ice-cold RIPA buffer (G-Biosciences) supplemented with a protease inhibitor cocktail (P2714, Millipore Sigma) which was diluted 1:10 as per the manufacturer's recommendations. Cell debris was removed by centrifugation at 16,000xg at 4°C and protein concentrations were determined using a Pierce™ BCA kit (Thermo Fisher Scientific). A sample (20-35 μg) of the supernatant protein was mixed with LDS buffer and DTT, incubated at 70 °C for 10 min and resolved on a 4-12% Bis-Tris PAGE gradient gel before being transferred to a PVDF membrane. Following transfer, the membrane was blocked in 5% skim milk for 1 h, washed and incubated at 4 °C overnight with a rabbit 1° mAb against human GRP78, GRP94, GRP75, N-cad, E-cad, TGF-β1, Slug, B-catenin or GAPDH (all purchased from Cell Signaling Technology) at a 1:1000 dilution. The membrane was subsequently washed and incubated with an anti-rabbit HRP-conjugated 2° Ab (Cell Signaling Technology) for 1 h at room temperature at 1:2000 dilution. The bands were visualized using a SignalFire™ ECL reagent (Cell signaling Technology) on a ProteinSimple FluorChem E imager. No changes in GAPDH band intensity between control siRNA and GRP78 siRNA were detected, therefore target protein bands were normalized against the loading control GAPDH.

2.6.7 Flow Cytometry and Cell Viability

Cell viability was assessed using an Annexin V/PI kit (Biolegend). Annexin V and PI were added to the cell samples post-transfection at 24, 48, and 72 hrs according the manufacturer's

recommendation, incubated for 15 min at room temperature in the dark, and followed by immediate analysis by flow cytometry (FC500 flow cytometer, Beckman Coulter). Data was processed with Kaluza® (Beckman Coulter) flow analysis software.

2.6.8 Cell Morphology Assay

For cell morphology analysis, PC3 cells were transfected with GRP78 siRNA and harvested 48 h later or treated overnight with 20ug/mL of a N-cad neutralizing monoclonal antibody, clone CG-4 (N-cad NAb, Sigma-Aldrich) prior to analysis. The cells were counted on Z2 Particle Counter and Size analyzer (Beckman Coulter) and re-seeded at cells/well in a standard 96 well plate and left to culture for an additional 18 h. The wells were subsequently washed and imaged under bright field on a Cell Insight CX5 high content screening instrument (Thermo Fisher Scientific). Images were analyzed using ImageJ software package (NIH). Fields of view (15 total, 5 each from 3 independent experiments) of control cells or cells treated with GRP78 siRNA were analyzed using the ImageJ software package (NIH). Cells with a clearly defined spherical and darker border (under bright field) were considered as rounded. Morphology was calculated as rounded: $N_{\text{rounded cells}}/N_{\text{total}}$ cells or elongated: $[N_{\text{total cells}}-N_{\text{rounded cells}}]/N_{\text{total cells}}$ and represented as a mean percentage ± SD.

2.6.9 Adhesion Assay

To determine the effects of GRP78 KD on PC3 cells adhesion to bone, PC3 cells were transfected with GRP78 siRNA and harvested 48 hrs later and cultured with hFOB 1.19 cells plated in a 96 -well plate until confluent. To track the PC3 cells in co-culture, transfected cells were labeled with the Vybrant CFDA SE (green) Cell Tracer Kit (5□M) (Thermo Fisher Scientific) counted on a Z2 particle counter and size analyzer (Beckman Coulter), and then seeded at 10,000 cells/well onto confluent OSB. For comparison, parallel co-cultures were treated overnight with

20 ug/mL of a N-cad NAb, clone CG-4 (Sigma-Aldrich). Number of fluorescently labeled cells [$N_{coculture}$] were counted by high content screening (Cell Insight CX5, Thermo Fisher Scientific) following an 18 hr co-incubation period. Supernatants were then transferred from co-culture wells into empty ones to determine the number of fluorescently labeled floating cells [$N_{supernatant}$]. Adherence was calculated as $\%N_{supernatant}/ N_{co\text{-}culture}$.

2.6.10 Statistical Analysis

All data was plotted and analyzed using the GraphPad Prism software, V 7.0d (La Jolla, CA). Each experiment was performed in triplicates (N=3). Data is represented as the mean ± SD. Comparisons between two groups were analyzed using unpaired student's *t*-tests. A probability (P) value of less than 0.05 was considered statistically significant.

2.7 References

1. Cultrara, C. N.; Kozuch, S. D.; Ramasundaram, P.; Heller, C. J.; Shah, S.; Beck, A. E.; Sabatino, D.; Zilberberg, J., *BMC Cancer* **2018,** *18* (1), 1263.
2. Brennan, S. K.; Matsui, W. *J Mol Med (Berl).***2009** *87* (11), 1079-1085.
3. Ghosh, N.; Matsui, W. *Cancer Lett.* **2009,** *277* (1), 1-7.
4. Morgenroth, A.; Vogg, A. T.; Zlatopolskiy, B. D.; Siluschek, M.; Oedekoven, C.; Mottaghy, F. M. *Mol. Cancer Ther.* **2014,** *13* (1), 144-153.
5. Zhang, W.; Gu, Y.; Sun, Q.; Siegel D., S.; Tolias, P.; Yang, Z.; Lee Y., W.; Zilberberg, J. *PLoS One* **2015**, 10(5):e0125995.
6. Neri, P.; Bahlis, N. J.*Curr Cancer Drug Targets* **2012,** *12* (7), 776-796.
7. Li, Z. W.; Dalton, W. S. *Blood Rev* **2006,** *20* (6), 333-342.
8. Damiano, J. S. *Curr. Cancer Drug Targets* **2002,** *2* (1), 37-43.
9. Hagberg Thulin, M.; Nilsson, M. E.; Thulin, P.; Ceraline, J.; Ohlsson, C.; Damber, J. E.; Welen, K. *Mol. Cell. Endocrinol* **2016,** *422*, 182-191.
10. Cui, Y. X.; Evans, B. A.; Jiang, W. G. *Anticancer Res.* **2016,** *36* (3), 1193-1201.
11. Shiozawa, Y.; Eber, M. R.; Berry, J. E.; Taichman, R. S. *BoneKEy Rep.* **2015,** *4*, 689.
12. Pfaffenbach, K. T.; Lee, A. S. *Curr Opin Cell Biol.* **2011,** *23* (2), 150-156.
13. Zhang, L. H.; Zhang, X. *J Cell Biochem.* **2010,** *110* (6), 1299-1305.
14. Abdel Malek, M. A.; Jagannathan, S.; Malek, E.; Sayed, D. M.; Elgammal, S. A.; Abd El-Azeem, H. G.; Thabet, N. M.; Driscoll, J. J. *Oncotarget.* **2015,** *6* (5), 3098-3110.
15. Mandelin, J.; Cardo-Vila, M.; Driessen, W. H.; Mathew, P.; Navone, N. M.; Lin, S. H.; Logothetis, C. J.; Rietz, A. C.; Dobroff, A. S.; Proneth, B.; Sidman, R. L.; Pasqualini, R.; Arap, W. *Proc. Natl. Acad. Sci. U S A.* **2015,** *112* (12), 3776-3781.

16. Zhang, X. X.; Li, H. D.; Zhao, S.; Zhao, L.; Song, H. J.; Wang, G.; Guo, Q. J.; Luan, Z. D.; Su, R. J. *BioMed Res Int.* **2013,** *2013*, 917296.
17. Hua, Y.; White-Gilbertson, S.; Kellner, J.; Rachidi, S.; Usmani, S. Z.; Chiosis, G.; Depinho, R.; Li, Z.; Liu, B. *Clin Cancer Res.* **2013.** *19* (22), 6242-51.
18. Zhang, Y.; Tseng, C. C.; Tsai, Y. L.; Fu, X.; Schiff, R.; Lee, A. S. *PloS One.* **2013.** *8* (11), e80071.
19. Jagannathan, S.; Abdel-Malek, M.A.; Malek, E.; Vad, N.; Latif, T.; Anderson K.C.; Driscoll, J.J. *Leukemia*. **2015**. 11(2), 2184-2191
20. Adomako, A.; Calvo, V.; Biran, N.; Osman, K.; Chari, A.; Paton, J. C.; Paton, A. W.; Moore, K.; Schewe, D. M.; Aguirre-Ghiso, J. A. *BMC cancer.* **2015,** *15*, 444.
21. Li, Z.; Wang, Y.; Wu, H.; Zhang, L.; Yang, P.; Li, Z. *Oncotarget* **2014,** *5* (14), 5369-5380.
22. Lichao Zhang, Z. L., Yongsheng Fan, Hanqing Li, Zhouyu Li, Yaoping Li. *Int J Biochem Cell Biol.* **2015,** *64*, 202-211.
23. Vandyke, K.; Chow, A. W.; Williams, S. A.; To, L. B.; Zannettino, A. C. *Br J Haematol.* **2013,** *161* (4), 499-507.
24. Ma, J.; Yu, Q. F.; Liu, X. Y.; Wang, C.; Zhang, Q. T.; Gan, S. L.; Chen, S. M.; Xie, X. S.; Liu, Y. F.; Liu, L. X.; Wan, D. M.; Sun, H. *J. Exp Hematol* **2015,** *23* (4), 1044-8.
25. Tanaka, H.; Kono, E.; Tran, C. P.; Miyazaki, H.; Yamashiro, J.; Shimomura, T.; Fazli, L.; Wada, R.; Huang, J.; Vessella, R. L.; An, J.; Horvath, S.; Gleave, M.; Rettig, M. B.; Wainberg, Z. A.; Reiter, R. E. *Nat Med.* **2010,** *16* (12), 1414-1420.
26. Busch, E. L.; Keku, T. O.; Richardson, D. B.; Cohen, S. M.; Eberhard, D. A.; Avery, C. L.; Sandler, R. S. *Clin Exp Metastasis.* **2016,** *33* (1), 53-62.
27. Heerboth, S.; Housman, G.; Leary, M.; Longacre, M.; Byler, S.; Lapinska, K.; Willbanks, A. *Clin Transl Med.* **2015,** *4*, 6.
28. Brook, N.; Brook, E.; Dharmarajan, A.; Dass, C. R.; Chan, A. *Int J Biochem Cell Biol* **2018,** *96*, 63-78.
29. Coughlin, T. R.; Romero-Moreno, R.; Mason, D. E.; Nystrom, L.; Boerckel, J. D.; Niebur, G.; Littlepage, L. E. *Curr Drug Targets* **2017,** *18* (11), 1281-1295.
30. Esposito, M.; Guise, T.; Kang, Y., *Cold Spring Harb Perspect Med.* **2018**, *8* (6), pii: a031252.
31. Pedersen, E. A.; Shiozawa, Y.; Pienta, K. J.; Taichman, R. S. *Asian J Andro.l* **2012,** *14* (3), 423-427.
32. Wang, M.; Ren, D.; Guo, W.; Huang, S.; Wang, Z.; Li, Q.; Du, H.; Song, L.; Peng, X. *Int J Oncol* **2016,** *48* (2), 595-606.
33. Shiirevnyamba, A.; Takahashi, T.; Shan, H.; Ogawa, H.; Yano, S.; Kanayama, H.; Izumi, K.; Uehara, H. *Br J Cancer* **2011,** *104* (3), 505-513.
34. Jones, A.; Kainz, D.; Khan, F.; Lee, C.; Carrithers, M.D. *J Biol Chem* **2014,** *289* (51), 35326-35340.
35. Steinbrunn, T.; Chatterjee, M.; Bargou, R.C.; Stümer, T.. *PLoS One* **2014,** *9* (6), e97443.
36. Vincenz, L.; Jager, R.; O'Dwyer, M.; Samali, A. *Mol Cancer Ther* **2013,** *12* (6), 831-843.
37. Misra, U.K.; Mowery, Y.; Kaczowka, S.; Pizzo, S.V. *Mol Cancer Ther* **2009,** *8* (5), 1350-1362.
38. Rhodes, D.R.; Yu, J.; Shanker, K.; Deshpande, N.; Varambally, R.; Ghosh, D.; Barrette, T.; Pandey, A.; Chinnaiyan, A.M. *Neoplasia* **2004,** *6* (1), 1-6.

39. Gass, J.N.; Gunn, K.E.; Sriburi, R.; Brewer J.W. *Trends Immunol.* **2004,** *25* (1), 17-24.
40. Tomita, K.; van Bokhoven, A.; van Leender, G.J.; Rujiter, E.T.; Jansen, C. F.; Bussemakers, M.J. *Cancer Res* **2000,** *60* (13), 3650-3654.
41. Nakamura, M. G., T. Okuno, Y. Tatetsu, H. Sonoki, T. Uneda, S. Mori, M. Mitsuya, H. Hata, H. *Leukemia & Lymphona* **2005,** *47* (3), 531-539.
42. Obeng, E. A.; Carlson, L.M.; Gutman, D.M.; Harrington, W.J. Jr.; Lee, K.P.; Boise, L.H. *Blood* **2006,** *107* (12), 4907-4916.
43. Bao, X.; Ren, T.; Huang, Y.; Ren, C.; Yang, K.; Zhang, H.; Guo, W. *Int J Oncol.* **2017,** *50* (2), 477-486.
44. Sheng, L.; Leshchyns'ka, I.; Sytnyk, V. *Cell Commun Signal.* **2013,** *11*, 94.
45. Zhu, G.; Lee, A. S. *J. Cell. Physiol.* **2015,** *230* (7), 1413-1420.
46. Lee, A. S. *Nat. Rev. Cancer.* **2014,** *14* (4), 263-276.
47. Kapulkin, V.; Hiester, B. G.; Link, C. D. *FEBS Lett.* **2005,** *579*, 3063-3068.
48. Dellto, D.; Dersh, D.; Argon, Y. *Semin. Cell. Dev Biol* **2010,** *21* (5), 479-485.
49. Maruri-Avidal, L.; Lopez, S.; Arias, C. F. *J. Virol.* **2008,** *82* (11), 5368-5380.
50. Wolfson, J. J.; May, K. L.; Thorpe, C. M.; Jandhyala, D. M.; Paton, J. C.; Paton, A. W. *Cell Microbiol* **2008,** *10* (9), 1775-1786.
51. Mimura, N.; Yuasa, S.; Soma, M.; Jin, H.; Kimura, K.; Goto, S.; Koseki H, Aoe T. *Mol. Cell. Bio.l* **2008,** *28* (1), 293-301.
52. Wanderling, S.; Simen, B.B.; Ostrovsky, O.; Ahmed, N.T.; Vogen, S.M.; Gidalevitz, T.; Argon, Y. *Mol. Biol. Cell*. **2007,** *18* (10), 3764-3775.
53. Honrath, B.; Metz, I.; Bendridi, N.; Rieusset, J.; Culmsee, C.; Dolga, A. M. *Cell Death Dis.* **2017,** *3*, 17076.
54. Chen, W.T.; et. al. *Hepatology*. **2014.,***59*(3), 947-957
55. Derksen, P.W.; et al. *Cancer Cell* **2006,** *10* (5), 437-439.
56. Zoni, E.; et al. *Oncogene* **2017,** *36*, 4739-4749.
57. Cano, A.; Perex-Moreno, A.M.; Rodrigo, I.; Locascio, A.; Blanoco, M.J.; del Barrio, M.G.; Portillo, F.; Nieto, M.A. *Nat Cell Biol.* **2000,** *2* (2), 76-83.
58. Ana Villarejo, A. Cortes.-Cabrera A., Molina-Oritz P., Portillo F., Cano A. *J Biol Chem.* **2013,** *289* (2), 930-941.
59. Klauzinska, M.; Bertolette, D.; Tippireddy, S.; Strizzi, L.; Gray, P. C.; Gonzales, M.; Duroux, M.; Ruvo, M.; Wechselberger, C.; Castro, N. P.; Rangel, M. C.; Foca, A.; Sandomenico, A.; Hendrix, M. J.; Salomon, D.; Cuttitta, F. *Connect. Tissue Res.* **2015,** *56* (5), 364-380.
60. de Castro, N. P.; Rangel, M. C.; Nagaoka, T.; Salomon, D. S.; Bianco, C. *Future Oncol.* **2010,** *6* (7), 1127-1142.
61. Gray, P. Vale, W. *FEBS letters* **2012,** *586* (14), 1836-1845.
62. Jones, E.; Pu, H.; Kyprianou, N. *Expert Opin Ther Targets* **2009,** *13* (2), 227-34.
63. Padua, D.; Massague, J. *Cell. Res.* **2009,** *19* (1), 89-102.
64. Fournier, P. G.; Juarez, P.; Jiang, G.; Clines, G. A.; Niewolna, M.; Kim, H. S.; Walton, H. W.; Peng, X. H.; Liu, Y.; Mohammad, K. S.; Wells, C. D.; Chirgwin, J. M.; Guise, T. A. *Cancer Cell* **2015,** *27* (6), 809-821.
65. Liu, X.; Ji, Q.; Deng, W.; Chai, N.; Feng, Y.; Zhou, L.; Sui, H.; Li, C.; Sun, X.; Li, Q. *Biomed Res Int.* **2017,** *2017*, 2613198.
66. Xu J., Lamouille S., Derynck R. *Cell Res* **2009,** *19* (2), 156-172.

67. Puch, S.; Armeanu, S.; Kibler, C.; Johnson, K.R.; Muller, C.A.; Wheelock, M.J.; Klein G. *J Cell Sci* **2001,** *114*, 1567-1577.
68. Huang, C.F.; Lira, C.; Chu, K.; bilen, M.A.; Lee, Y.C.; Ye, X.; Kim, S.M.; Ortiz, A.; Wu, F.L.; Logothetis, C. J.; Yu-Lee, L.Y.; Lin, S.H. *Cancer Res.* **2010**, *70* (11), 4580-4589.68.
69. Lu, Y., et al. *Oncogene* **2011,** *30* (45), 4567-4577.

Chapter 3: Biological Activity of Higher-Order siRNA Nanostructures and their Bioconjugates[1-4]

3.1 Abstract

The biological action of higher-order siRNA motifs and their bioconjugates have recently gained widespread attention in the development of new and improved gene therapeutics. In cancer gene therapy applications, these siRNA motifs target and silence important oncogene targets leading to potent cell death in a wide range of cancer models. In this study, we have developed an efficient method for the construction of higher-order RNA structures, including those adopting V-, and Y- and >-< shape RNA templates. Self-assembly of complementary RNA to the template strands led to higher-order siRNA nanostructures which produced a significant increase in the knockdown efficiency (50-95%) at low nanomolar concentrations (5 nM) of multiple oncogene targets simultaneously. In an effort to extend the repertoire of functionally diverse siRNAs, we have also developed bioconjugation strategies for incorporating bio-active probes such as fatty acid appendages and fluorescent reporters on to our V- and Y-shape templates allowing for the incorporation of up to three probes per molecule of siRNA. Our results indicate that introducing multiple fluorescent reporters significantly increased the *in vitro* limit of detection of the siRNA in a model prostate cancer (PCa) cell line with comparable knockdown efficiency to the control siRNA. Conversely, multiple fatty acid appendages yielded a mild silencing effect in the absence of a transfection reagent. Taken together, these results highlight the ability to generate higher-order siRNAs and their bioconjugates for exploring the influence of modified siRNA structure on anti-cancer activity.

3.2 Introduction

Among the many nucleic acids currently employed as gene therapy agents, short-interfering RNAs (siRNAs) are widely used as potent regulators of gene expression and for mitigating the progression of various diseases.[5-7] Structurally, siRNAs are short double stranded RNA duplexes composed of hybrid antisense (guide) and sense (passenger) strands which contain19-25 base pairs with nucleotide overhangs on the 3' ends.[8-10] These molecules trigger a regulatory system of genetic expression known as the RNA interference (RNAi) pathway. In the natural mechanism, long double stranded RNAs are cleaved into siRNAs by an RNAse III dependent endonuclease referred to as "Dicer". The siRNAs are then incorporated into the RNA Induced Silencing Complex (RISC), a multimeric protein complex with endonuclease activity mediated by the Argonaute (Ago) protein which uses the guide strand to target and cleave complementary mRNA, thus preventing protein translation.[11-14] Conversely, siRNA can be synthesized exogenously and then introduced into the cell target where it is immediately incorporated into RISC and leads to the degradation of mRNA transcripts.

In spite of their therapeutic promise, siRNAs are still plagued by poor pharmacokinetic properties,[15] including poor metabolic stability, off-target gene silencing and immunostimulatory effects. These effects increase toxicity, limits cell permeability and limits their duration of action which restricts their therapeutic potential and raises the need for more potent constructs. One approach to improve siRNA potency is to use an "siRNA cocktail" which incorporates multiple siRNAs that target the same or multiple mRNA sequences in one treatment. However, effectively delivering or expressing multiple siRNAs comes with a caveat, they are inherently more difficult to transfect and have shown limited *in vivo* applicability.[16] Alternatively, chemically derived siRNAs

can facilitate the incorporation of modifications and/or functional probes which can enable self-assembly into higher-order structures for improving RNAi activity.[17-19]

RNAi nanotechnology has led to the evolution of functional siRNA materials for a variety of applications, including the development of nanomedicines and nanoparticle formulations for gene therapy.[18,19] siRNA nanostructures have been formulated for silencing single or multiple gene targets. For example, a tripodal-interfering RNA (tiRNA) (**Figure 1, a**) and related supramolecular RNA nanostructures with polyethyleneimine (PEI) and galactose-functionalized PEI were self-assembled to promote silencing efficiency *in-vivo*.[17] The resultant siRNA nanoparticle produced an increase in stability and delivery efficiency while also accumulating in specific tissues (i.e. liver) leading to a much more robust and long-lived gene silencing effect. Likewise, DNA-RNA and RNA-RNA nano-cubes (**Figure 3.1, b**), the latter of which contained as many as six double-stranded dsRNA Dicer substrates, promoted the release of multiple siRNAs in breast cancer cells.[20] The siRNAs resulted in a significant increase in the duration of action due to the prolonged knockdown of enhanced green fluorescent protein, (eGFP) for up to twelve days. These nano-cube formulations have proven to be effective in biomedical studies as well. They induced potent suppression of the viral Gag proteins, p55 and p24, in HIV-1 pseudotyped with VSV-g 293T cells, which resulted in potent antiviral activity. These constructs were also found to be immunogenic, which ultimately limits their applicability due to the risk of toxic immunostimulatory responses. In another proof-of-concept study, the siRNA nanostructures composed of self-assembled three- and four-way junctions (**Figure 3.1, c**), triggered potent knockdown of multiple luciferase gene targets for up to five (5) days in HeLa cells.[21] Due to the impressive increases in the stability, potency, length of action, and flexible design, siRNA nanostructures have become an interesting tool of enhancing siRNA activity.

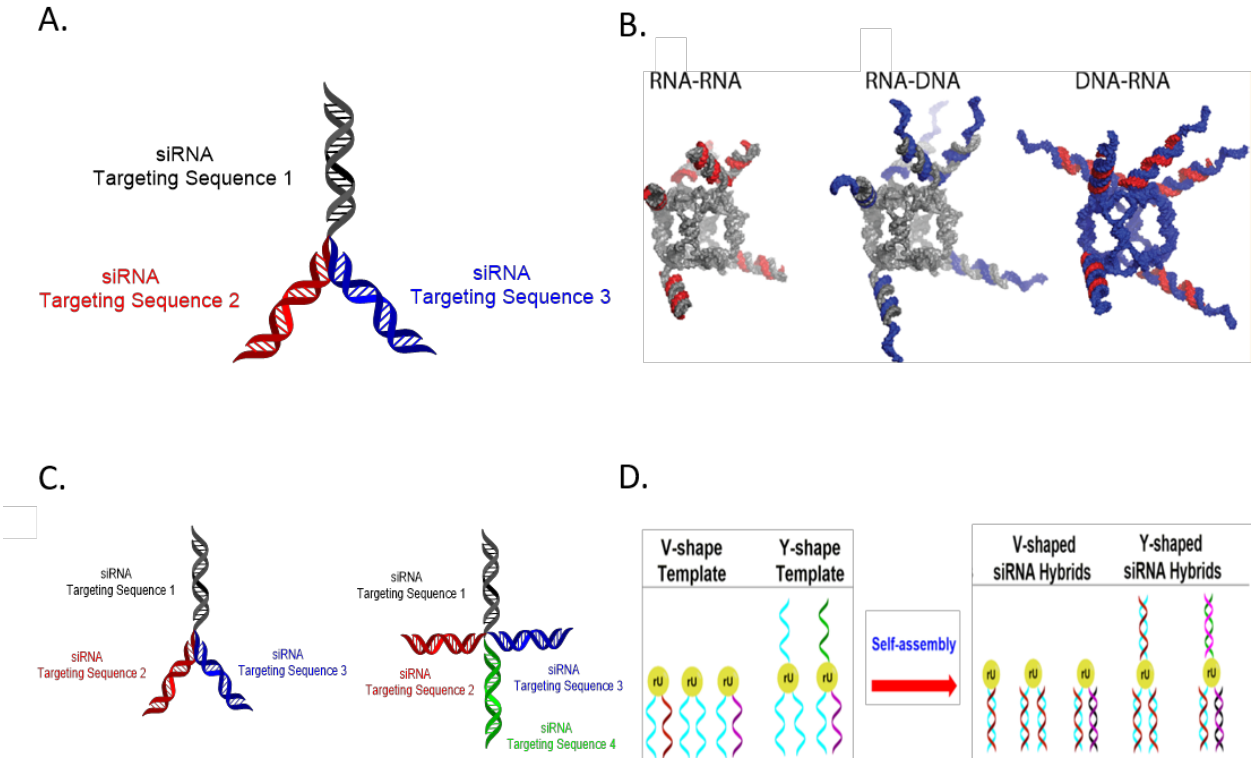

Figure 3.1. Schematic representations of siRNA self-assembly and nanotechnology. A) Design of a non-linear tripartite siRNA tripod based on the complementary base pairing of three independent siRNA sequences. B) Structural assembly of RNA and RNA-DNA "nanocubes" for delivery of up to six siRNAs after Dicer cleavage. C) Sequence dependent assembly of 3- and 4- way siRNA junctions. D) Design of V- and Y-shape siRNAs containing up to three siRNA sequences within the same molecular scaffold. Reprinted with permission from Wiley and Sons: Cultrara, C. N.; Shah, S.; Kozuch, S. D.; Patel, M. R.; Sabatino, D. *Chem. Bio. Drug Des.* **2018**, 1-12

Similar in action to nanostructure formulations, siRNA bioconjugates have shown the potential to improve the physicochemical and pharmacokinetic properties of siRNAs in preclinical and clinical studies.[22-24] The generation of amphiphilic siRNA with lipid-like moieties including fatty acids, steroids, or terpene derivatives have seen great use due to their inherent stability, longer duration of action, and improved penetration across cell membrane.[25-28] The appeal of these

lipophilic siRNAs are in their potential to act as self-delivering formulations through the interactions with lipoprotein particles, receptors, and transmembrane proteins embedded within the cell membrane.

Furthermore, the combination of therapy and diagnostics termed "theranostics" has led to the development of new and improved gene therapeutics for the diagnosis and treatment of cancers.[29] Specifically, siRNA bioconjugates containing reporter probes such as fluorophores, near-infrared (near IR) dyes and photosensitizers as well as those containing contrast agents and radiolabels (**Figure 3.2, B**) have been extensively used as theranostic agents in oncology.[30,31] These molecules have the capabilities of not only producing a therapeutic effect, but also allows for the mechanism of action to be studied. This is invaluable information when deducing new drug targets or determining the potential side effects when altering specific molecular pathways. However, most bioconjugates can only incorporate a single moiety and those covalent conjugations are limited to either the 3' or 5' end of the oligonucleotide. The latter can be problematic as both ends are important for siRNA incorporation into RISC and mRNA target recognition as well as being susceptible to RNA degradation by endogenous exonuclease. Therefore, new prototypes are still in demand to produce exceptionally efficient multi-functional siRNA conjugates.

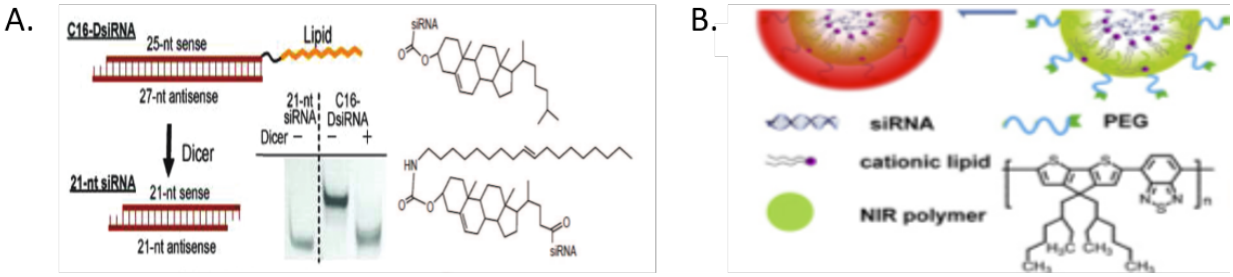

Figure 3.2. Representative examples of siRNA bioconjugates. A) lipid-siRNA bioconjugates. Figure adapted with permission from ref. 23, Kubo, T.; Yanaghara, K.; Sato, Y.; Nishimura, Y.; Kondo, S.; Seyama, T. *Bioconjugate Chem.* **2013,** *24*(12), 2045-2057. Copyright 2013, American

Chemical Society. B) Fluorescent-siRNA conjugated polymers used to image live cells. Figure adapted with permission from ref. 29, Liu, Y. Gunda, V.; Zhu, X.; Xu, X.; Wu, J.; Askhatova, D.; Farokhzad, O.C.; Parangi, S.; Shi, J. *Proc Natl Acad Sci U S A* **2016,** *113*(28), 7750-7755. Copyright 2016, National Academy of Sciences. Reprinted with permission from Wiley and Sons :Cultrara, C. N.; Shah, S.; Kozuch, S. D.; Patel, M. R.; Sabatino, D. *Chem. Bio. Drug Des.* **2018**, 1-12

3.3 Chapter Objectives

This thesis chapter builds on the work of Mayurbhai Patel, Ph.D., Stephen Kozuch, Ph.D., and Sunil Shah, M.Sc. which describes the self-assembly of a linear, V-shape, and Y-shape siRNA into novel nanostructures and further functionalization through bioconjugation. My contribution primarily involves siRNA formulation and biological testing in cell lines to evaluate the anti-cancer activity of the reported siRNA constructs.[1-4] Hybridization and self-assembly of complementary RNA strands using linear, V-shape and Y-shape RNA templates generated a library of siRNA nanostructures targeting the GRPs *in vitro*. Moreover, bioconjugation with an FITC fluorescent probe or with a variety of fatty acids led to the creation of new multi-functional V- and Y-shape siRNAs which can incorporate two or three moieties, respectively, to be tested for their unique structure-activity relationship in a model prostate cancer (PCa) cell line. Significantly, this work demonstrates the bio-activity of novel siRNA nanostructures, and their bioconjugates as potent multi-functional gene therapy tools in a variety of selected cancer cell lines. This work has been adapted and reprinted with permission from the following authored publications: Wiley and Sons: Cultrara, C. N.; Shah, S.; Kozuch, S. D.; Patel, M. R.; Sabatino, D. *Chem. Bio. Drug Des.* **2018**, 1-12. Copyright 2018, American Chemical Society. Kozuch, S. D.; Cultrara, C. N.; Beck, A. E.; Heller, C. J.; Shah, S.; Patel, M. R.; Zilberberg, J.; Sabatino, D. *ACS Omega* **2018,** *3*, 12975-12984. <https://pubs.acs.org/doi/10.1021/acsomega.8b01999>

Patel, M. R.; Kozuch, S. D.; Cultrara, C. N.; Yadav, R.; Huang, S.; Samuni, U.; Koren, J. I.; Chiosis, G.; Sabatino, D. *Nano Lett.* **2016**, *16*, 6099-6108. Shah, S.; Cultrara, C. N.; Kozuch, S. D.; Patel, M. R.; Ramos, J.; Samuni, U.; Zilberberg, J.; Sabatino, D. *Bioconj. Chem.* **2018,** *29*, 3638-3648. Copyright 2016, American Chemical Society

3.4 Results and Discussion

3.4.1. Self-Assembly of siRNA Nanostructures

Based on our previous work which produced linear, V and Y shape RNA templates using an orthogonally protected 5'-OLv 2'-OMMT rU phosphoramidite as branchpoint synthon,[32] we developed a self-assembly strategy for the generation of siRNA nanostructures targeting GRP 75, 78 and 94 (**Figure 3.3**). In our self-assembly approach, equimolar (200 pmol) quantities of purified linear, V- and Y-shape RNA templates along with their complementary RNA strands were used to form the siRNA hybrids and nanostructure formulations in annealing buffer (10 mM Tris, 50 mM NaCl, 1 mM EDTA, pH 7.5–8.0, 13-15 μL). Self-assembly into siRNA nanostructures which resembled circles, squares, rectangles, pentagons, hexagons and porous spheres were designed and detected using TEM imaging.[3] Furthermore, a native PAGE analyses confirmed the formation of more retained, self-assembled higher-order siRNA hybrids, whereas TEM and DLS provided additional structural information related to the varying geometric shapes and sizes (10-150 nm) of the observed self-assembled siRNA nanostructures.

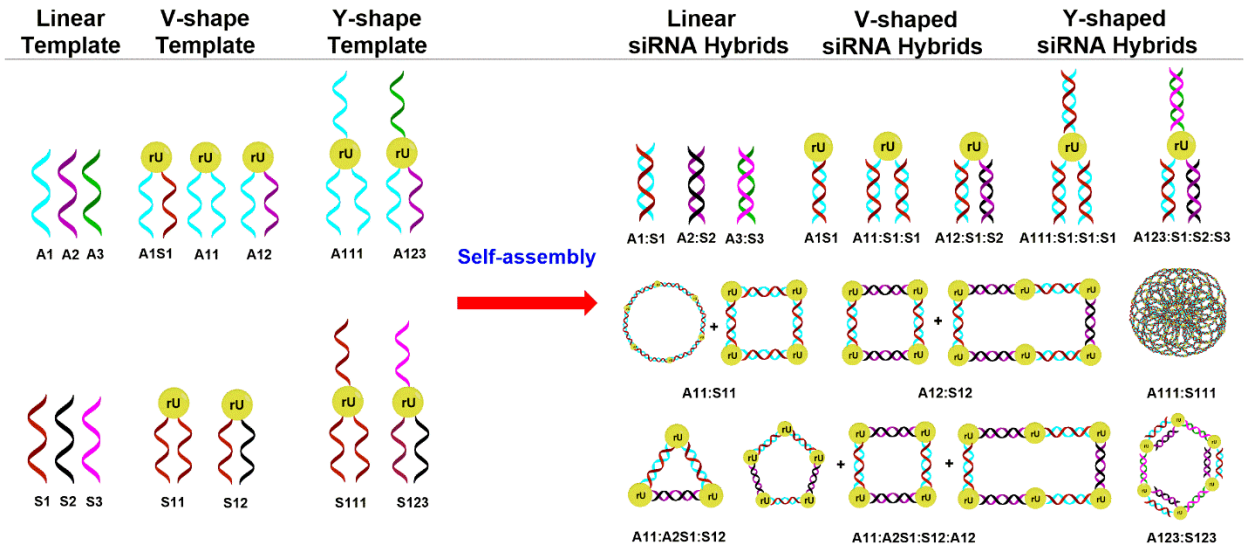

Figure 3.3 Design and self-assembly of siRNA nanostructures.

3.4.2. Activity siRNA Nanostructures in Various Cancer Cell Lines

The self-assembled siRNA hybrids (24 samples) were screened for their biological activity within the AN3CA human endometrial cancer cell line.[3] The RNAi screen investigated the influence of the siRNAs on the proliferative activity of the AN3CA cells. Among this library of siRNAs, a set of lead samples demonstrating the most potent anti-proliferative activity were evaluated for their RNAi activity. These samples demonstrated GRP78 KD and upregulation of cleaved PARP (cl-PARP), a marker of apoptosis (**Figure 3.4**).[33] Four lead siRNAs were selected, two V-shape (A12:S1:S:2, A12:S12) and two Y-shape (A123:S1:S2:S3, A123:S123) targeting GRP78 mRNA and transfected with the RNAiMAX™ transfection reagent.

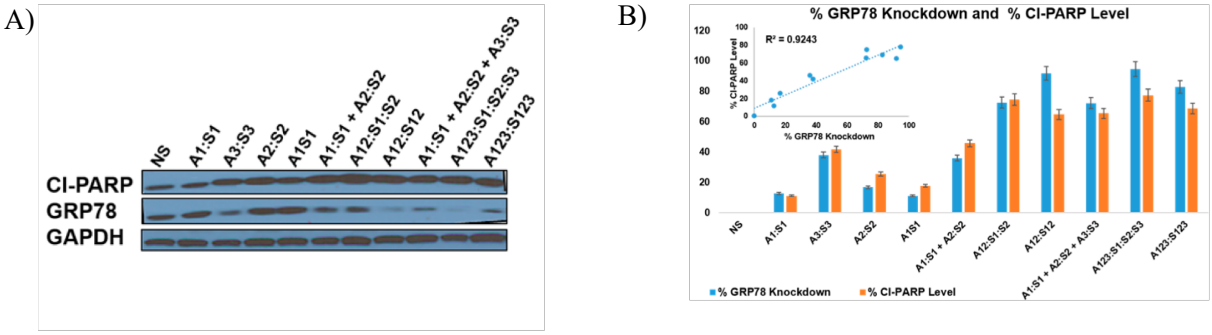

Figure 3.4 Biological evaluation of the V- and Y-shape siRNA targeting GRP78 in the AN3CA cell line. A) Western blot of the total GRP78 and Cl-PARP levels following siRNA transfections. The loading control, GAPDH, was used to normalize the detected bands for quantitative densitometry using NIH imager (ImageJ). (D) The percent GRP78 knockdown and the percent Cl-PARP levels were normalized according to the NS RNA control and quantitated following densitometry of the Western blot. The linear (r^2 = 0.9243) correlation diagram in between the percent GRP78 knockdown and the percent Cl-PARP levels is provided as an inset. All experiments were replicated in triplicate, with average values presented with their standard deviations about the mean. Statistical analyses produced error bars with acceptable variance ± SEM; N = 3; $p < 0.05$.

The V- and Y-shape siRNAs exhibited more potent GRP78 KD according to western blot when compared to the linear siRNA controls (>80% vs ~75%) (**Figure 3.4, A)**. Significantly, this result suggests that the higher order siRNA constructs are able to synergistically enhance the knockdown effect. Furthermore, the expression levels of Cl-PARP (cleaved 85-kDa protein poly(ADP-ribose) polymerase) were monitored as a molecular marker of apoptosis.[33] There is a direct correlation between GRP78 KD and upregulation of Cl-PARP, suggesting that downregulation of GRP78 results in cell apoptosis (**Figure 3.4, B**). Similarly, the V- and Y-shape siRNAs significantly increased the levels of Cl-PARP as compared to the linear controls (>65% vs 10-65%) implicating that the higher order siRNAs exhibit more potent, synergistic anti-cancer effects relative to the linear siRNA controls.

The lead V- and Y-shape siRNAs were then tested in the HeLa (ATCC CCL-2) cervical , MDA-MB-231 (ATCC HTB-26) breast cancer cell lines known to overexpress the GRPs[34,35] and a non-tumorigenic lung fibroblast cell line MRC5 (ATCC- CCL- 171) which was used as a control cell line with expressing basal GRP levels.[36] Moreover, the V- and Y-shape were re-designed to target multiple GRPs (GRP78, GRP94, GRP75). In this assay, a control non-specific siRNA (NS RNA), was tested against the control linear GRP siRNAs (78 + 94 + 75), and the lead Y-shape siRNA targeting all three GRPs (GRP757894) in combination. The siRNAs (5 nM) were transfected using RNAiMAX (7 μL) within the AN3CA, HeLa and MDA-MB-231 cancer cell lines and within the MRC5 normal human cell line as control. The RNAi activity of the siRNA samples was evaluated according to GRP KD and release of LDH as a measure of cell cytotoxicity (**Figure 3.5**).

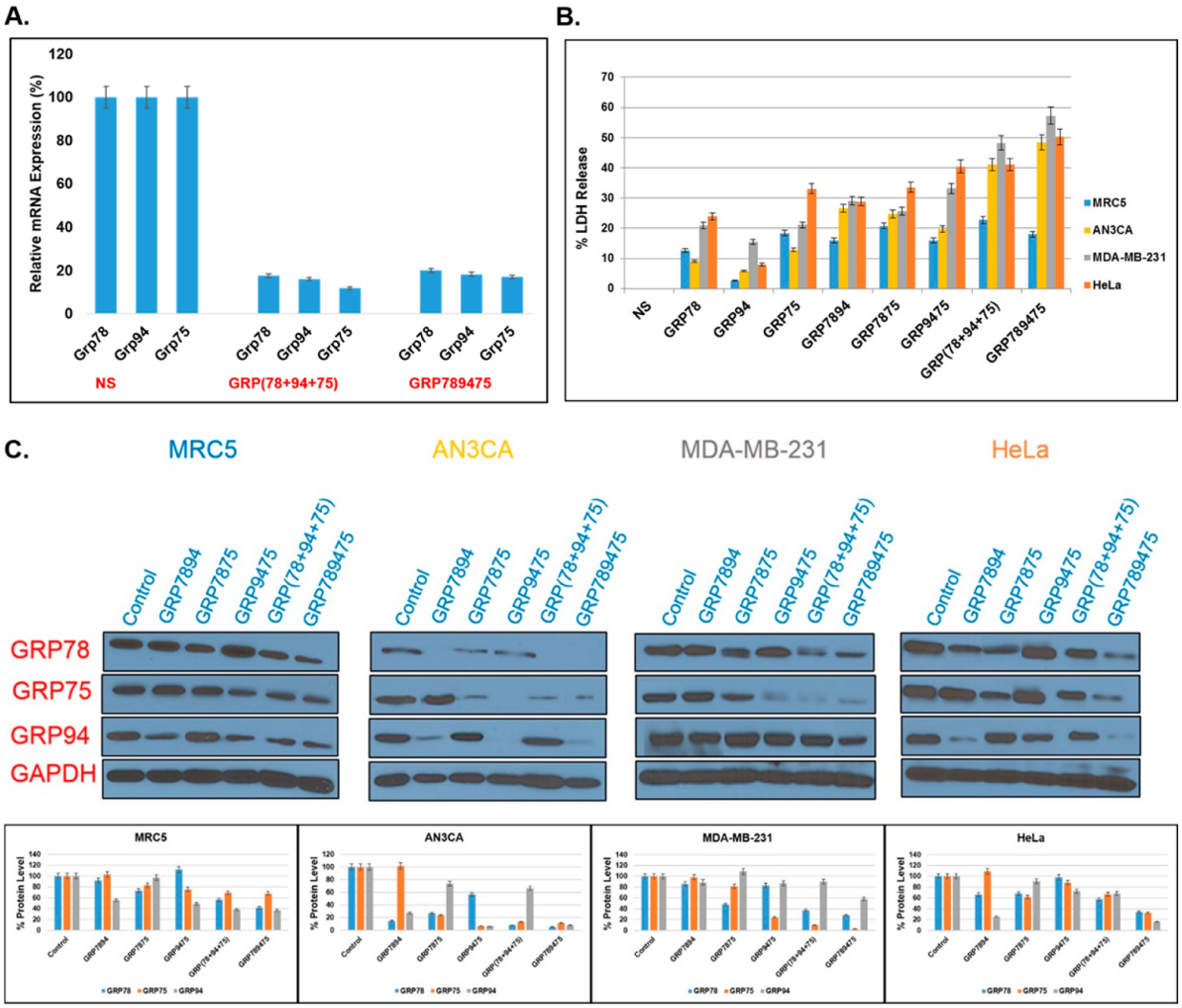

Figure 3.5 RNAi screening. (A) Grp mRNA levels detected by RT-PCR. HeLa cells were transfected with NS RNA, linear GRP (78 + 94 + 75), and Y-shape GRP(789475) siRNA (5 nM) using RNAiMAX (7 µL). Grp78, Grp94, Grp75, and GAPDH mRNA levels were normalized according to GAPDH and quantitated with respect to NS RNA. (B) LDH release assay. The percent LDH released was measured following transfections of all treated cell lines (MRC5, AN3CA, MDA-MB-231, and HeLa). The LDH levels were quantitated and normalized according to the NS RNA. (C) Western blots measuring GRP78, GRP94, and GRP75 (percent protein) levels following siRNA (5 nM) transfections in normal lung, MRC5, endometrial, AN3CA, breast, MDA-MB-231, and cervical HeLa cancer cells. The GRP78, GRP94, and GRP75 levels were normalized according to GAPDH and quantified with respect to the NS RNA. Data represents knockdown efficiency of V-shape siRNAs (GRP7894, GRP7875, and GRP9475), Y-shape siRNA (GRP789475), and the linear siRNAs (GRP78 + GRP94 + GRP75) added in combination. All experiments were replicated in triplicate, with average values presented with their standard

deviations about the mean. Statistical analyses produced error bars with acceptable variance ± SEM; N = 3; $p < 0.05$.

The knockdown efficiency of the siRNAs proved to vary among the cancer cell lines tested. The AN3CA cell line was the most sensitive to treatment yielding GRP silencing efficiencies of >85% for the Y-shape siRNA hybrid. Conversely, the HeLa and MDA-MB-231 lines showed variable levels of GRP knockdown. However, in general, the V- and Y-shape siRNAs exhibited a more potent GRP knockdown effect compared to the control linear siRNA targeting GRP 75, 78 and 94 as a cocktail mixture. This result validates the synergistic silencing effect of the siRNAs embedded within the same molecular scaffold as opposed to separate siRNAs (**Figure 3.5, C**). Interestingly in the AN3CA line, silencing of GRP94 and 75 with the V-shape siRNA hybrid had a separate silencing effect on GRP78 which was not the primary gene target. Moreover, silencing of GRP78 and 94 had little effect on GRP75 and these trends varied in the HeLa or MDA-MB-231 suggesting that the cell lines have a varying dependence on the GRPs. For example, there may be a compensation effect in the GRP expression levels to offset loss or downregulation of a related GRP.[37] Significantly, a modest KD effect of the GRPs was observed in the non-cancerous MRC5 cell line either with all of the siRNA samples, suggesting that the cancer cells are more sensitive to GRP activity. This trend was also extended to cell viability, in which the tumor cells exhibited a more pronounced cell death effect (as a result of LDH release) presumably due to GRP KD when compared to the control MRC5 cell line (**Figure 3.5, D**). Importantly, this result underscores the potential use of the multi-GRP silencing siRNAs in a selective cancer treatment strategy. This work also demonstrates the utility of higher order self-assembled siRNA constructs as potent gene therapy tools and probes to elucidate the role important oncoproteins on cancer cell biology.

3.4.3. Rational design of fluorescently labeled V- and Y-shape siRNAs

The linear, V- and Y-shape RNA templates were also applied to a simple bioconjugation strategy to tag a fluorescent reporter, fluorescein (FL), onto the 5' ends of the siRNA constructs (**Figure 3.6A**). Moreover, a self-assembly strategy was developed to hybridize complementary, linear FL-RNA strands with the linear, V- and Y-shape RNA templates to afford the multi-labeled siRNA constructs (**Figure 3.6B**). In this application, the incorporation of multi-fluorescent labels within a single molecular scaffold was hypothesized to increase signaling detection in cells in order to monitor siRNA cell biology.[2] Fluorescently labeled siRNAs are especially useful in studying cellular uptake, trafficking and localization in order to optimize siRNA KD efficiency. The latter forms the main objectives of the current study.

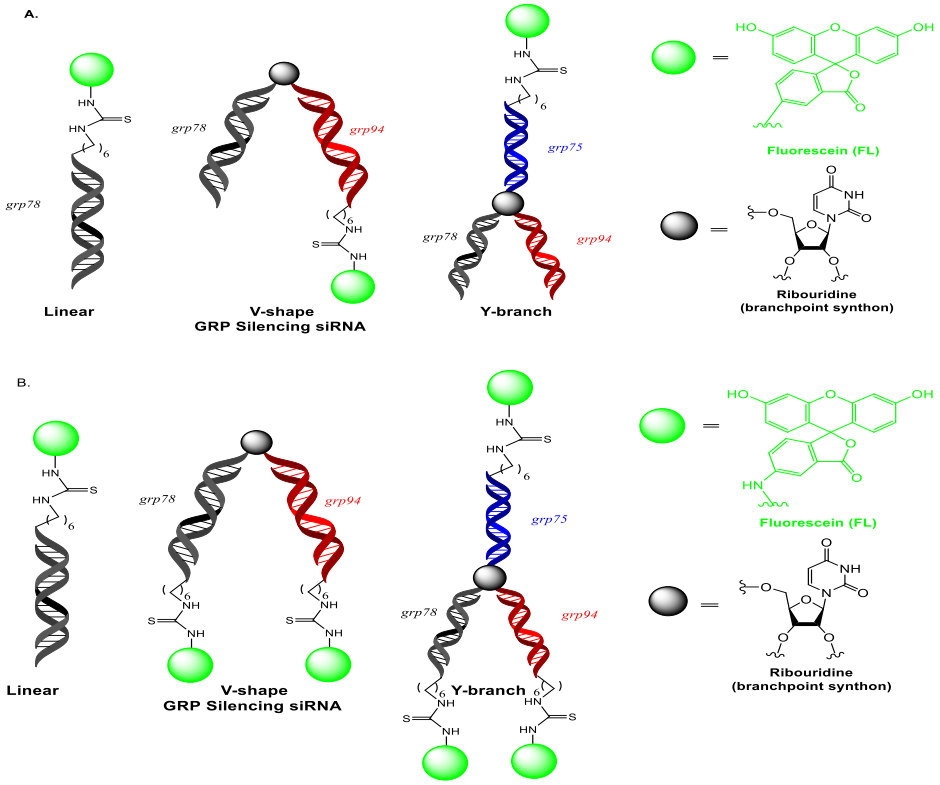

Figure 3.6 Design of fluorescently labeled linear, V-, and Y-shape siRNAs. A) Single probe bioconjugate or B) multi probe bioconjugate. Reprinted with permission from Kozuch, S. D.; Cultrara, C. N.; Beck, A. E.; Heller, C. J.; Shah, S.; Patel, M. R.; Zilberberg, J.; Sabatino, D. *ACS Omega* **2018,** *3*, 12975-12984. Copyright American Chemical Society 2018.

3.4.4. Internalization studies of the FL-siRNA bioconjugates

The FL-siRNA served as bifunctional probes, signaling the detection of siRNA activity in human cancer cells and mediating GRP KD post-transfection ultimately leading to potent anti-cancer effects. The V- and Y-shape siRNAs had been previously validated as lead constructs in our GRP silencing approach across a panel of cancer cell lines. In this application, the single and multi-labeled FL-siRNAs belonging to the linear, V- and Y-shape constructs were transfected in PC3 PCa cells using the Trans-IT X2 dynamic delivery system known to work efficiently in suspension and adherent cell lines.[38] High FL-siRNA doses (100 nM) of either a linear, V-, or Y-shape hybrid with a single FITC moiety was used to effectively track cell uptake within the PC3 cells at 3 and 20 hours by flow cytometry. Typically, transfection reagents rapidly shuttle siRNAs within cells during the first 4hrs. In our case, the FL-siRNAs showed a complete shift in fluorescence intensity in the flow histogram at 3 hours, which continued to persist up to the 20 hour time point (**Figure 3.7A**). This indicates rapid uptake and prolonged residency time of the siRNAs within the PC3 cells. Interestingly, when the cells were treated with a smaller 50 nM dose of FL-siRNA containing double (V-shape FL-siRNA) or triple (Y-shape FL-siRNA) FITC labels, the signal increases over time, hits a maximum at 4 hrs, and persists up until 72 hours (**Figure 3.7 B**). Therefore, by increasing the number of FITC molecules per siRNA construct, the ability to track robustly siRNA uptake in live cells over extended (72 hours) duration of time is significantly improved (**Figure 3.7**). Together, this data provides mechanistic insights into the cellular uptake of FL-siRNAs while validating their extended localization times (72 hours post-transfection) in PC3 cells.

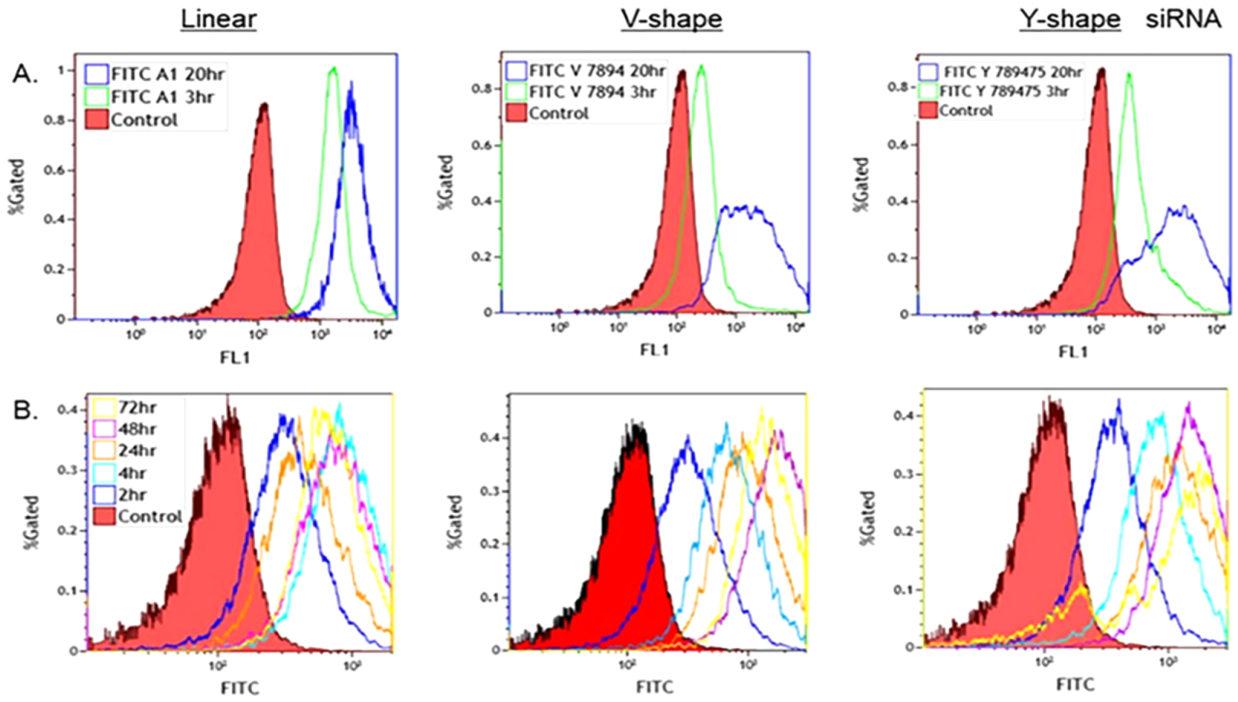

Figure 3.7 Uptake efficiency monitored by flow cytometry. A) 100nM dosage of a single-FITC linear, V-, and Y-shape hybrid and B) Time dependent study of a linear, V-, and Y-shape hybrid containing 1, 2, or 3 FITC labels, respectively, at a 50nM dosage. Images reprinted with permission from Kozuch, S. D.; Cultrara, C. N.; Beck, A. E.; Heller, C. J.; Shah, S.; Patel, M. R.; Zilberberg, J.; Sabatino, D. *ACS Omega* **2018,** *3*, 12975-12984. Copyright American Chemical Society 2018.

To validate the cell uptake activity detected by flow cytometry, fluorescence imaging of the cells was used to visualize cell uptake and residency time. The images (**Figure 3.7**) supported the flow cytometry data, indicating that at least 4hrs was needed to visualize the FL-siRNAs within the cells. Moreover, in all cases, the signal intensity increased with time and also as a function of the number of FITC labels incorporated within the FL-siRNA construct, with the tri-FITC labeled Y-shape siRNA providing the most vibrant and detailed images (**Figure 3.8 C**).

A

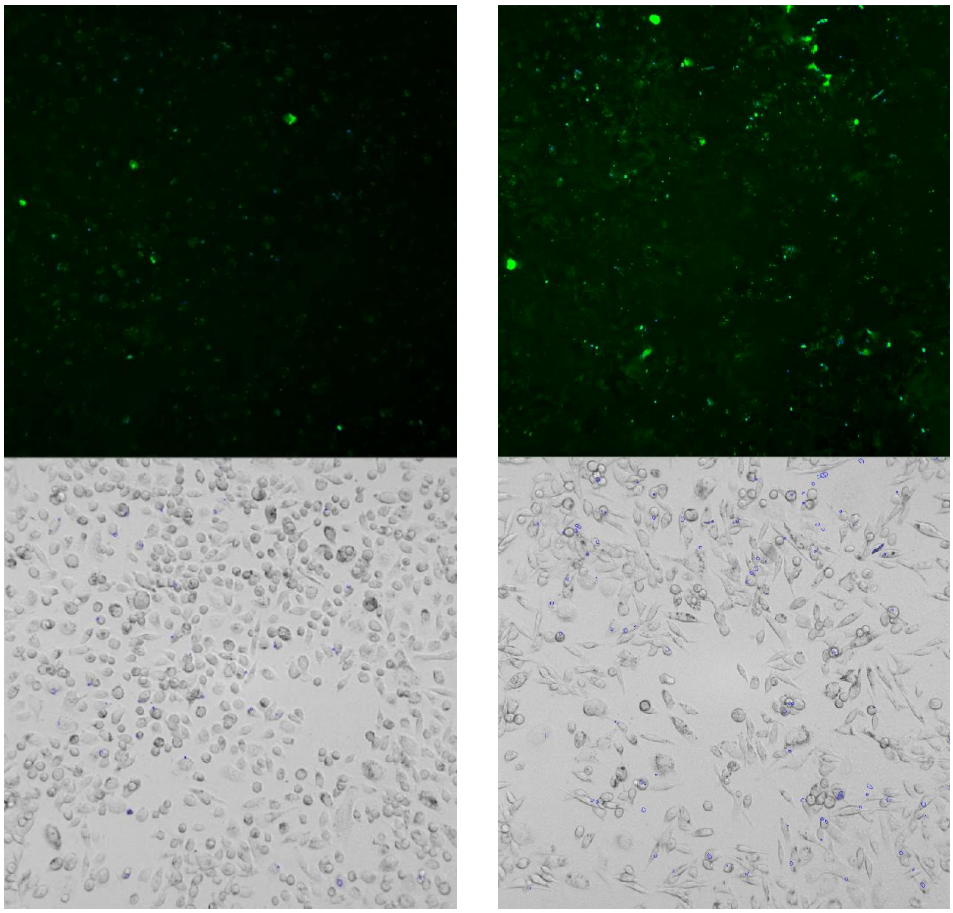

FL-linear siRNA

4 hours post transfection 24 hours post transfection

B

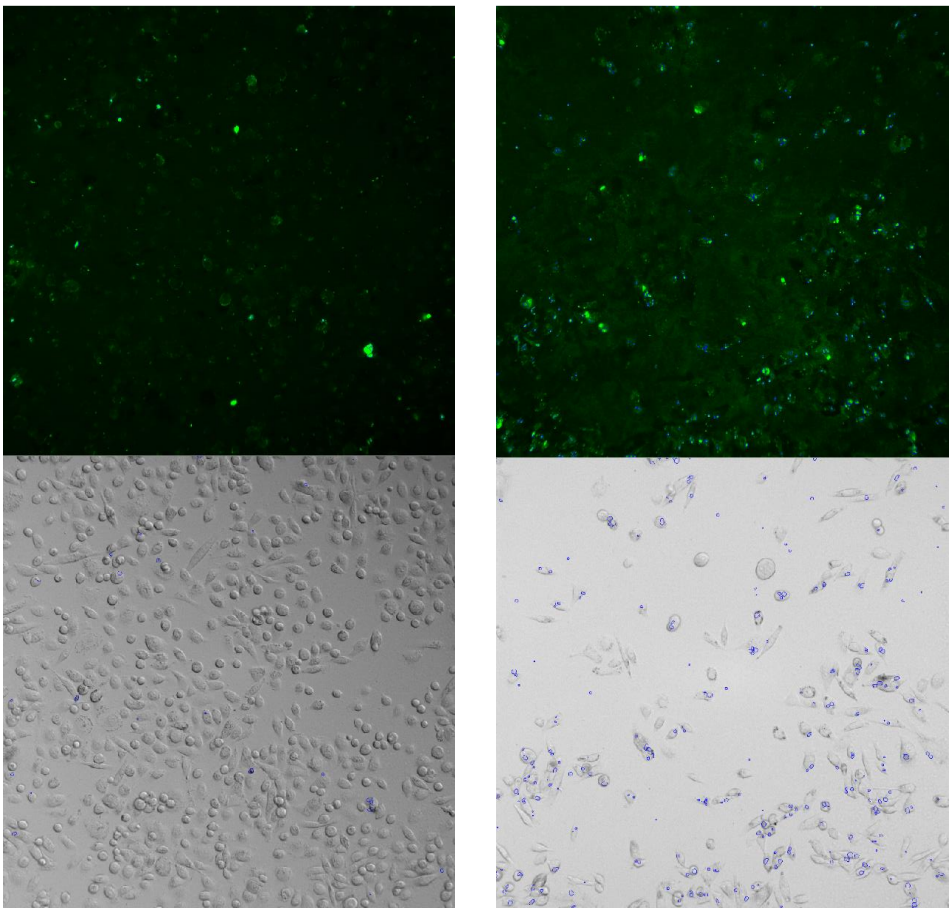

V-FL-siRNA

4 hours post transfection 24 hours post transfection

C

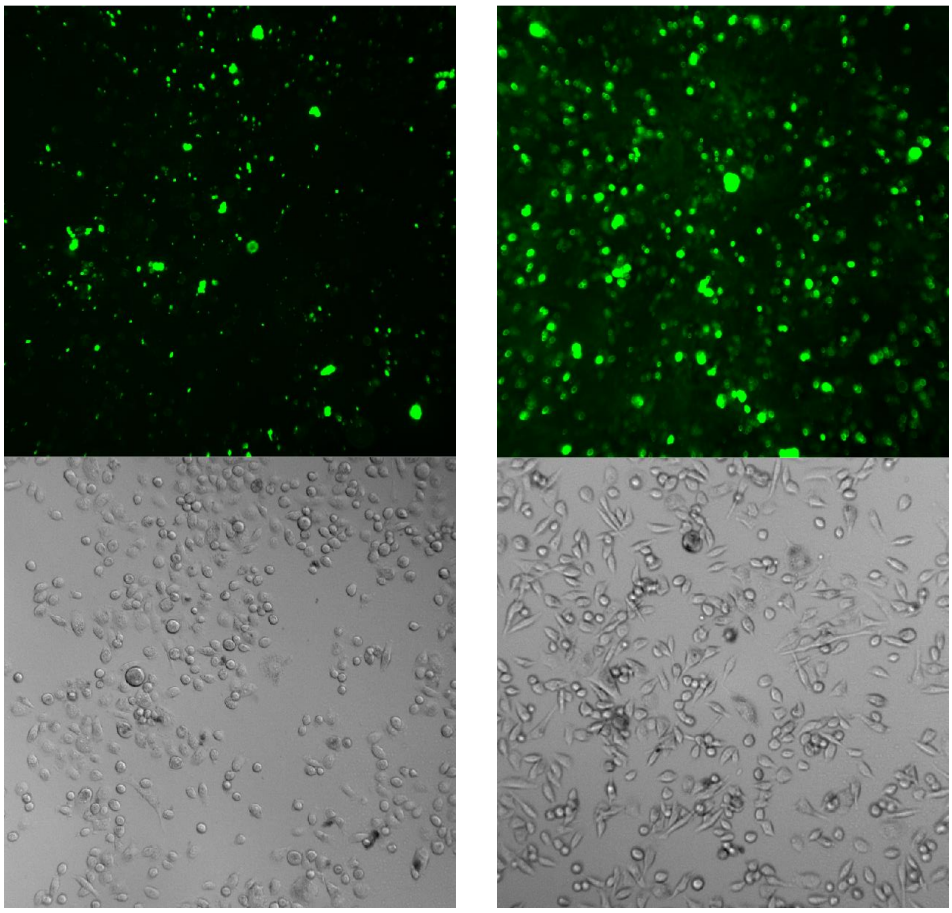

Y-FL-siRNA

4 hours post transfection 24 hours post transfection

Figure 3.8 Fluorescence microscopy of the FL-siRNA. 50 nM of A) FL-linear (1 FITC), B) FL-V-shape (2 FITC), and C) FL-Y-shape (3 FITC) were transfected into PC3 cells and imaged at 4hr and 24 h post transfection. Images reprinted with permission from Kozuch, S. D.; Cultrara, C. N.; Beck, A. E.; Heller, C. J.; Shah, S.; Patel, M. R.; Zilberberg, J.; Sabatino, D. *ACS Omega* **2018,** *3*, 12975-12984. Copyright American Chemical Society 2018.

3.4.5. Gene Knockdown Efficiency of the FL-siRNAs

With optimized transfection conditions in hand, the FL-siRNAs were assayed for their ability to track the knockdown effects of the target GRP (GRP78, GRP94, GRP75) mRNA transcripts. Briefly, the FL-siRNA (50 nM) were transfected into the PC3 cells and analyzed by qRT-PCR for 48hrs for mRNA silencing and by western blot at 72 hrs for protein knockdown.

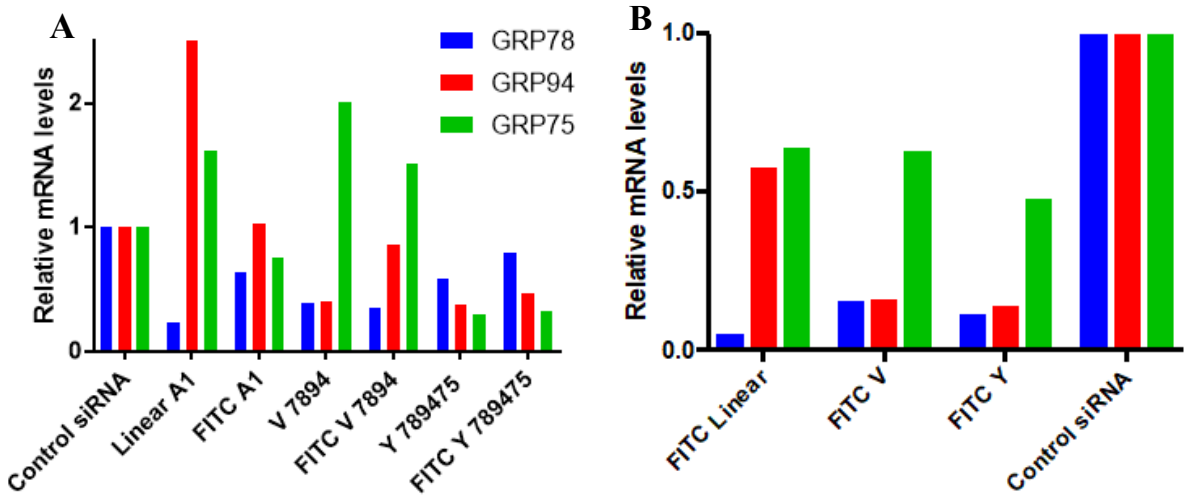

Figure 3.9 qRT-PCR analysis of GRP75, 78 and 94 mRNA knockdown. FL-siRNA (50 nM) samples were transfected into PC-3 cells and relative mRNA levels were normalized to a control, non-specific siRNA. (**A**) Total mRNA levels were analyzed 72 h post transfection for the antisense strand labeled FL-siRNA constructs. (**B**) Total mRNA levels were analyzed 48 h post transfection of the sense-strand labeled FL- siRNA constructs containing 1, 2 and 3 FITC probes (**B**).

An initial screen of the antisense (guide) labeled linear and V-shape siRNA showed a diminished silencing effect of the GRP transcript levels with the FL-siRNA (20-70%) compared to their naked controls (40-80%). The inability to acquire sufficient yields of pure FL-Y-shape siRNA (**Figure 3.6 A**) prevented it from being included in this assay. Instead, a single labeled sense (passenger) strand was hybridized to the antisense Y-shape RNA template (**Figure 3.6 B**) to self-assemble the Y-shape FL-siRNA construct. This sample triggered similar knockdown efficiencies when compared to the unlabeled Y-shape siRNA confirming that sense strand modification was more tolerant (with respect to anstisense strand modifiers) to RNAi activity in

PC3 cells (**Figure 3.9, A**). The reduced silencing effects of the FL-labeled linear and V-shape hybrids when compared to the unlabeled siRNAs can be partially attributed to the FITC conjugation at the 5' end of the sequence.[40] This position has been shown to play an important role in the incorporation of siRNA into RISC and mRNA processing in the RNAi pathway. Conversely, when the guide, antisense siRNA strands were left unmodified and the FITC label (single, double or triple FITCs for the linear, V-, and Y- shape siRNAs , respectively) was incorporated within the passenger, sense strands the knockdown efficiencies improved (55-95%) which were comparable to the control, unlabeled siTNA sequences (40-80%) (**Figure 3.9, B**). These siRNA constructs also proved to be most useful in the cellular uptake and imaging studies (**Figures 3.6** and **3.7**). As previously seen, silencing one or two GRPs can elicit an upregulation of the non-targeted one (i.e GRP94 when silencing GRP78 with the FL-linear and GRP75 when silencing GRP78 and GRP94 with the FL-V, **Figure 3.9, A**). However, this was not observed when treating the cells with the Y-shape hybrids suggesting the synergistic silencing of all three (3) targeted GRPs is maintained even with FITC labeling.

Based on the qRT-PCR results, we selected the Y-shape hybrid containing 3 FITC probes as our lead siRNA construct for further analysis. Similarly, the FL-Y-shape siRNA hybrid (50 nM) was transfected into the PC3 cells and analyzed for mRNA and protein knockdown. A significant knockdown of GRP78 and GRP94 mRNA (40-60%) was observed by qRT-PCR with little effect on GRP75. These mRNA knockdown effects translated differently at the protein level, with diminished levels of GRP78 and GRP75 (30-35%) observed with little effect on GRP94 (**Figure 3.10**). This is not uncommon as post-transcriptional regulation can alter the protein expression levels despite little to no changes observed at the mRNA level.[41] Furthermore, the expression

levels of the GRPs varies significantly among cell lines, further compounding the siRNA KD effects.

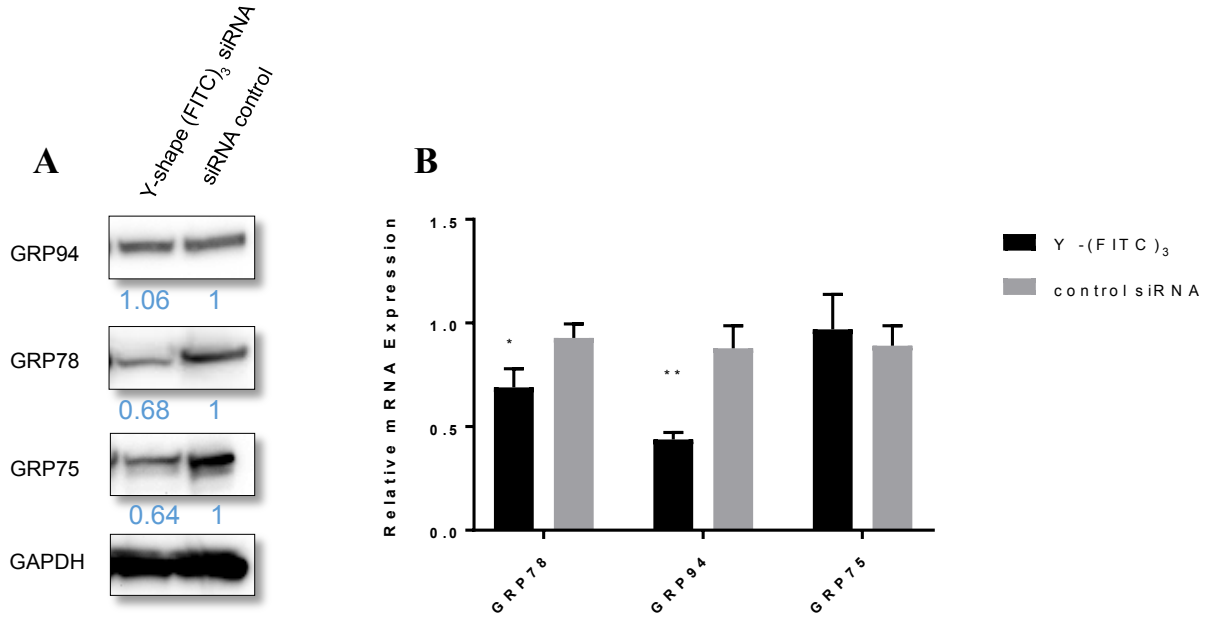

Figure 3.10 Protein and mRNA knockdown levels of GRP75, 78 and 94 determined by Western Blot (**A**), and RT-PCR (**B**). *P< 0.05 in PC-3 and **P<0.01.

3.4.6. Cell Viability after treatment with the FL-siRNAs

Given the observed GRPs silencing effects of the FL-siRNAs, their cytotoxicity to the PC3 cells was next determined. In this assay, PC3 cells were stained with propidium iodide (PI), a fluorescent DNA intercalator that is not cell permeable in living, healthy cells and permeable in cells with compromised cellular and nuclear membranes.[42] The extent of cytotoxicity was measured by the release of PI fluorescence intensity (636 nm), 72 hrs post transfection. Brightfield microscopy showed populations of PC3 cells that were both adherent (live) and in suspension (dead). The PC3 cells are designated as an adherent epithelial cell line that grows and thrives when adhered to the culture plate and are generally considered compromised when detached and found in suspension. Flow cytometry revealed significant increases in the populations of dead cells in suspension over time, peaking at 48 hrs (**Figure 3.11**). At 72 hrs, the cells still adhered to the

culture plate appeared to have recovered and the viability returned to a comparable level observed within the first 24hrs. Conversely, the percentage of compromised cells was maintained at high levels in the supernatant suggesting that the FL-siRNAs were capable of eliciting cancer cell death upon GRP KD. In this assay, the FL-labeled Y-shape siRNA construct yielded the most potent cell death effects following synergistic GRP (GRP75, 78 and 94) knockdown.

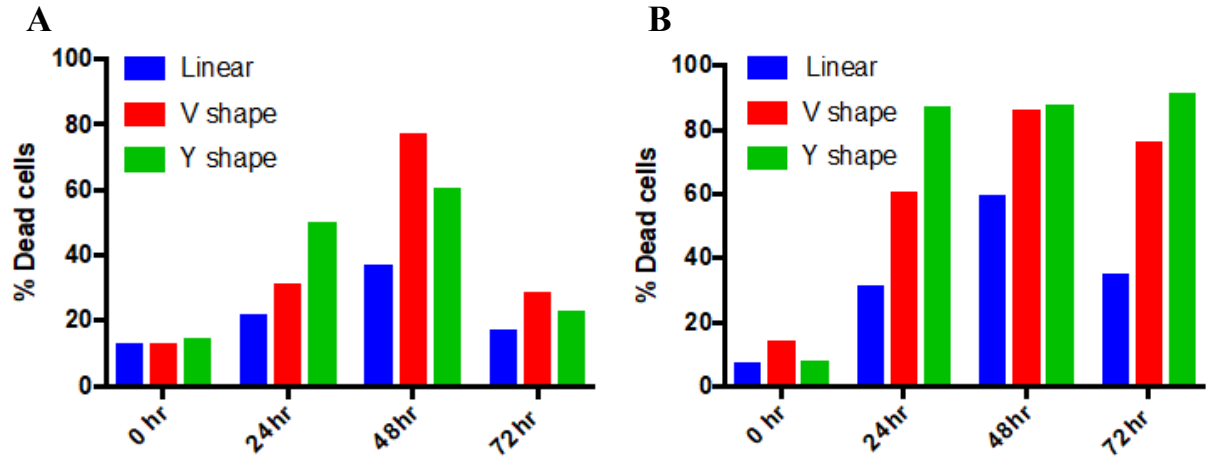

Figure 3.11 Cell viability determined using PI on flow cytometry, adhered cells (**A**) and supernatant cells (**B**).

3.4.7 Rational Design of Fatty Acid Labeled siRNA Bioconjugates.

In this related application, fatty acid conjugated siRNAs were designed to address the lack of cell permeability associated to siRNAs. The hydrophilicity and net anionic charge of RNA prevents its passive diffusion across the cell membrane and requires the use of a transfection vector or reagent to facilitate cell uptake.[43] In spite of their promise in preclinical and clinical siRNA applications, these reagents are limited in utility due to their cytotoxicity, immunogenicity, and variable efficiency based on the cell type being studied.[44, 45] Previous work has shown that the bioconjugation of fatty acids and related lipid moieties can improve siRNA metabolic stability as well as facilitate passive diffusion across cell membranes in the absence of a transfection

Reagent.[25-27] To build on this, we designed a simple strategy to expand the scope of fatty acid-siRNA (FA-siRNA) bioconjugation with its application to the higher order V-, and Y-shape RNA templates.

In this application, a fatty acid conjugation strategy was adapted for the incorporation of lengthy (C18) and shorter chain (C12) saturated {lauric acid (12:0), palmitic acid (16:0), stearic acid (18:0)} and unsaturated {oelic acid (18:1), linoleic acid (18:2), and linolenic acid (18:3)} fatty acids.[4] Moreover, the development of a self-assembly strategy was designed, in order to functionalize the 5'-terminus of the sense RNA strand with palmitamide followed by hybridization with the complementary RNA template strand (**Scheme 3.1**). In this manner, self-assembled linear, V-shape, and Y-shape siRNAs respectively containing a single, double and triple palmitamides were designed and developed to investigate the effect of fatty acid conjugation on siRNA cell permeability and RNAi activity in PC-3 cells.

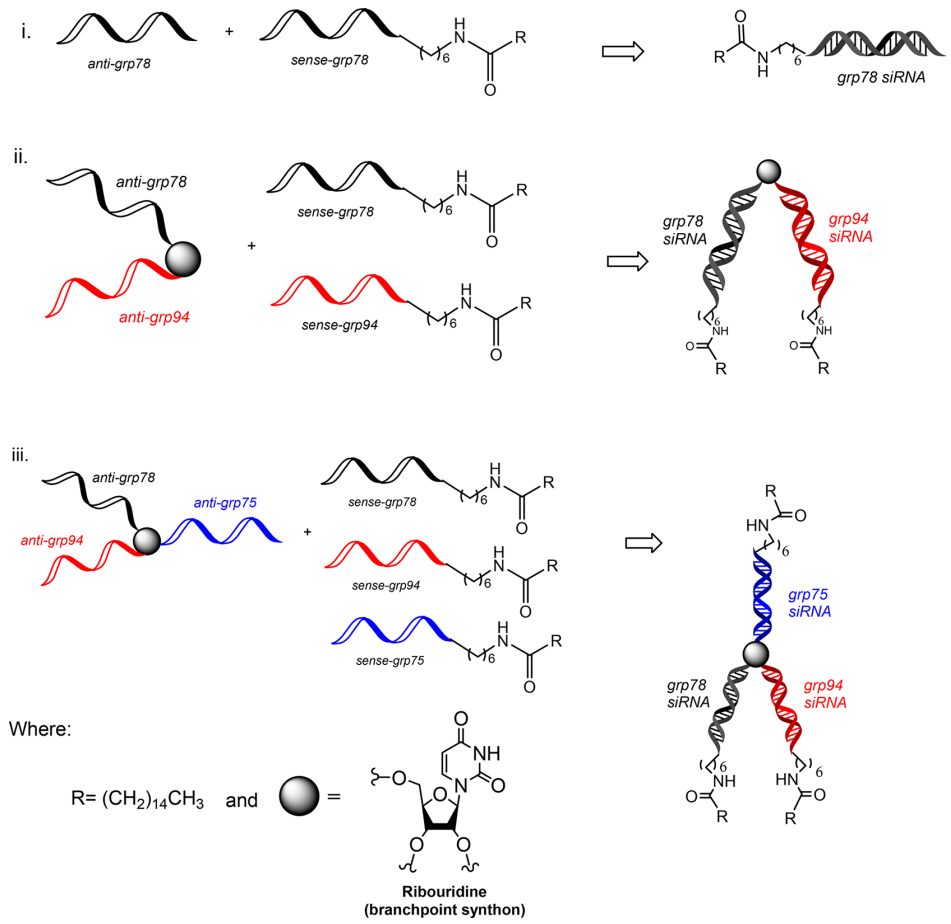

Scheme 3.3. Self-assembly of the linear, V-, and Y-shape siRNA templates to generate hybrids containing 1, 2, or 3 fatty acid moieties, respectively.

3.4.8. GRP Knockdown Efficiency of the FA-siRNAs

The linear and V-shape guide strand labeled FA-siRNA hybrids and a Y-shape hybrid containing a single FA molecule to maintain consistency across this assay (**Figure 3.12, B, C**) were transfected with the Trans-IT X2 dynamic delivery system (**Figure 3.12, A**) and directly (**Figure 3.12, B-D**) within PC-3 cells to determine the extent of GRP (GRP75, GRP78 and GRP94) knockdown efficacy at the mRNA levels of expression. In this assay, the FA-siRNAs incorporating a single (linear), double (V-shape) and triple (Y-shape) palmitamides were also screened to determine whether multiple FAs effect knockdown efficiency (**Figure 3.12, D**).

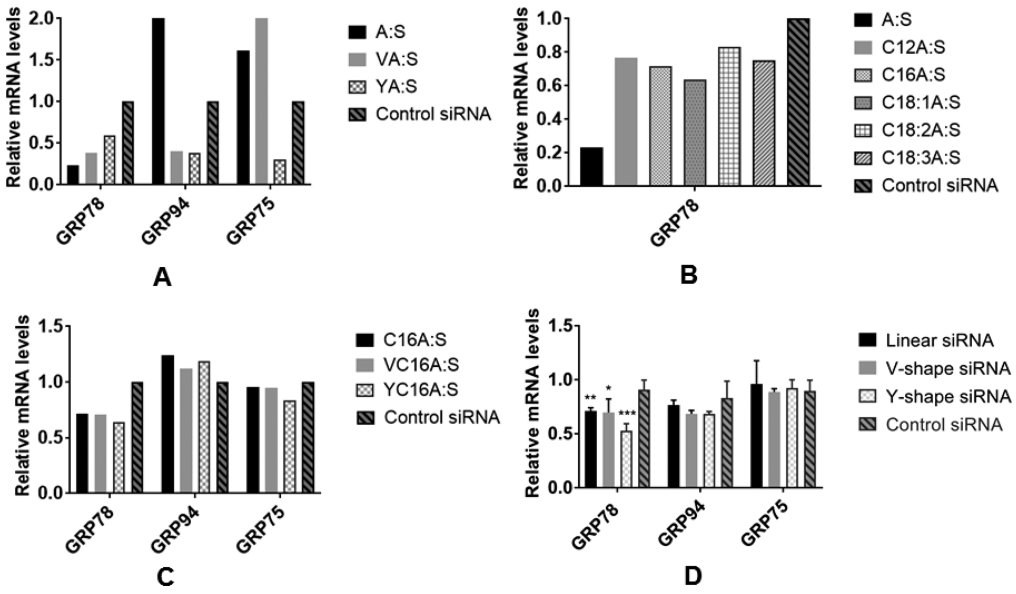

Figure 3.12 qRT-PCR analysis of GRP mRNA levels in PC-3 cells following (A) transfection of linear, V-, and Y-shaped siRNAs with the Trans-IT X2 dynamic delivery system, (B) direct transfection of saturated, unsaturated and polyunsaturated fatty acid-siRNA bioconjugates, (C) direct transfection of palmitamide conjugated linear, V-, and Y-shaped siRNA bioconjugates, (D) direct transfection of linear, V-, and Y-shaped siRNA bioconjugates, respectively, containing a single, double, and triple palmitamides. Target mRNA levels are relative to a control siRNA and represented as the mean fold change ± SD of 3 separate trials. *P < 0.05 and ***P < 0.001 in PC3 cells for GRP78 KD.

The direct transfections of the various linear FA-siRNAs into our model PC-3 cell line yielded mild knockdown (20-40%) of the GRP78 mRNA levels, when compared to a control siRNA hybrid transfected with the Trans-IT X2 dynamic delivery system (80%) according to qRT-PCR. Direct transfection of the V- and Y-shape hybrids containing a single palmitamide elicited modest knockdown of GRP78 (~40%) without any effect on the other GRP mRNA targets, GRP94 and GRP75. Direct transfection of the multi-palmitamide siRNA hybrids improved the GRP78 knockdown efficiency (5-65%) compared to the siRNA constructs containing a single palmitamide (20-40%); albeit to a lesser extent when compared to the Trans-IT X2 dynamic delivery system (80%).

3.4.9. Cell Uptake of the FA-siRNAs by Flow Cytometry

FACS analysis was used to gain a better understanding of the knockdown effects observed by qRT-PCR. In this assay, the FA-siRNA bioconjugates were additionally labeled with FITC (FL) to produce the bifunctional FA-FL-siRNA bioconjugates which were hypothesized to enable tracking of cell uptake in PC-3 cells. Linear, V-, and Y-shape FA-FL-siRNA bioconjugates (50 nM) containing either a single or double FA appendages and a single FITC probe were treated directly within PC-3 cells and tracked by flow cytometry at 3, 6, and 24 hrs (**Figure 3.13)**. The control FITC-siRNA transfected with the Trans-IT X2 dynamic delivery system resulted in a fluorescent spike at 6hrs which persisted into the next day (**Figure 3.13, A-C**). Conversely, the FA-FL siRNA bioconjugates exhibited a fluorescent spike at 6 hrs and then complete loss in fluorescent intensity by 24 hrs. We hypothesize that the FA-containing siRNA may be interacting with the cells during that period, but are unable to completely penetrate into the cytosol. However, this analysis was set to only show the effects on the bulk population of cells and not smaller subsets wherein cell penetration may be occurring and subsequent mild knockdown seen by qRT-PCR.

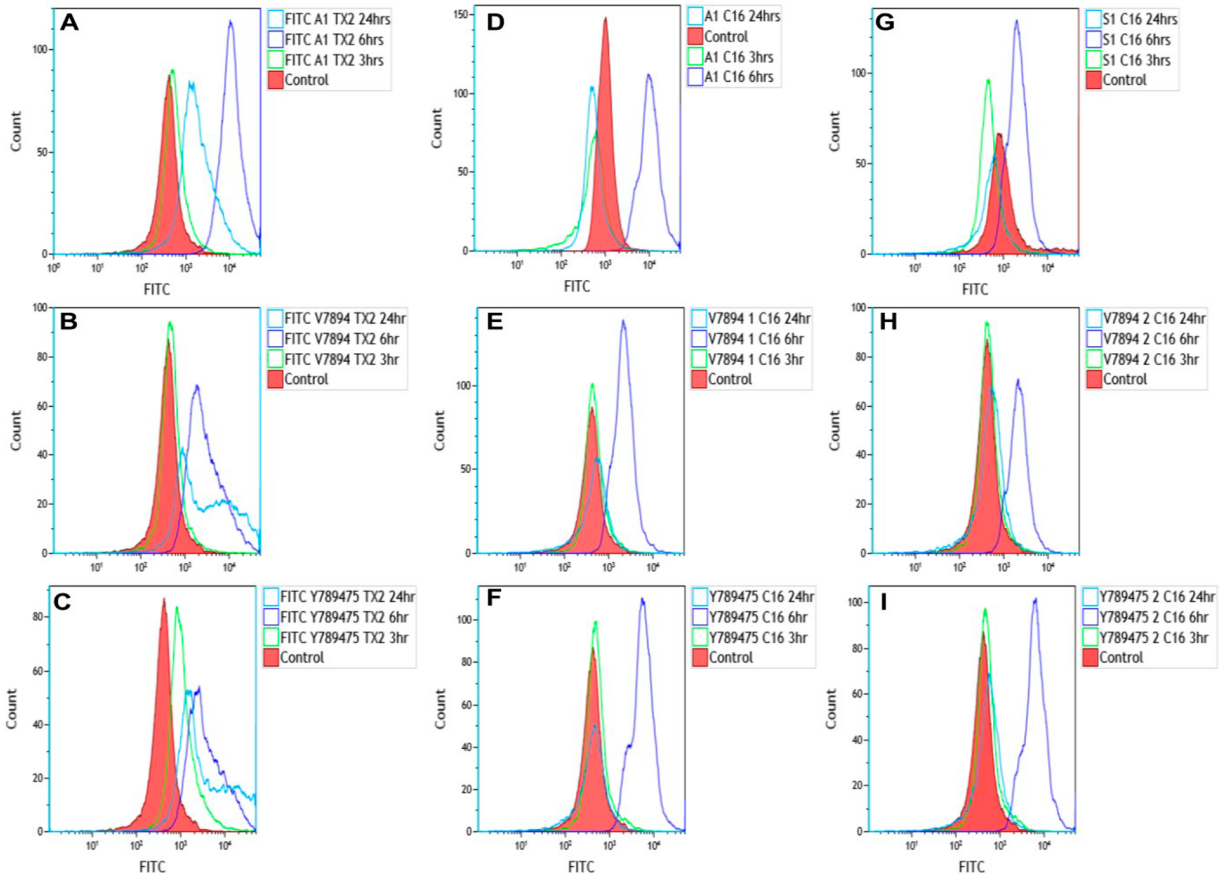

Figure 3.13 Time dependent (6−24 h) flow cytometry analysis of linear, V-, and Y-shaped FITC labeled siRNAs transfected with the Trans-IT X2 dynamic delivery system (A-C). Direct transfection of linear, V-, and Y-shape FITC-labeled siRNA containing single (D-F) and multiple (G-I) palmitamides within the PC-3 prostate cancer cell line.

3.4.10. Size and Morphology Characterization by DLS and TEM

To fully characterize the dynamics of the FA-siRNA bioconjugates, we analyzed their size and morphological properties by dynamic light scattering (DLS) and transmission electron microscopy (TEM). Given the spike in fluorescence intensity observed only within 6 hrs for the FA-FL-siRNA, we reasoned that the lack of cell penetration may be due to the aggregation of the lipid tails and formation of large, amorphous aggregates.

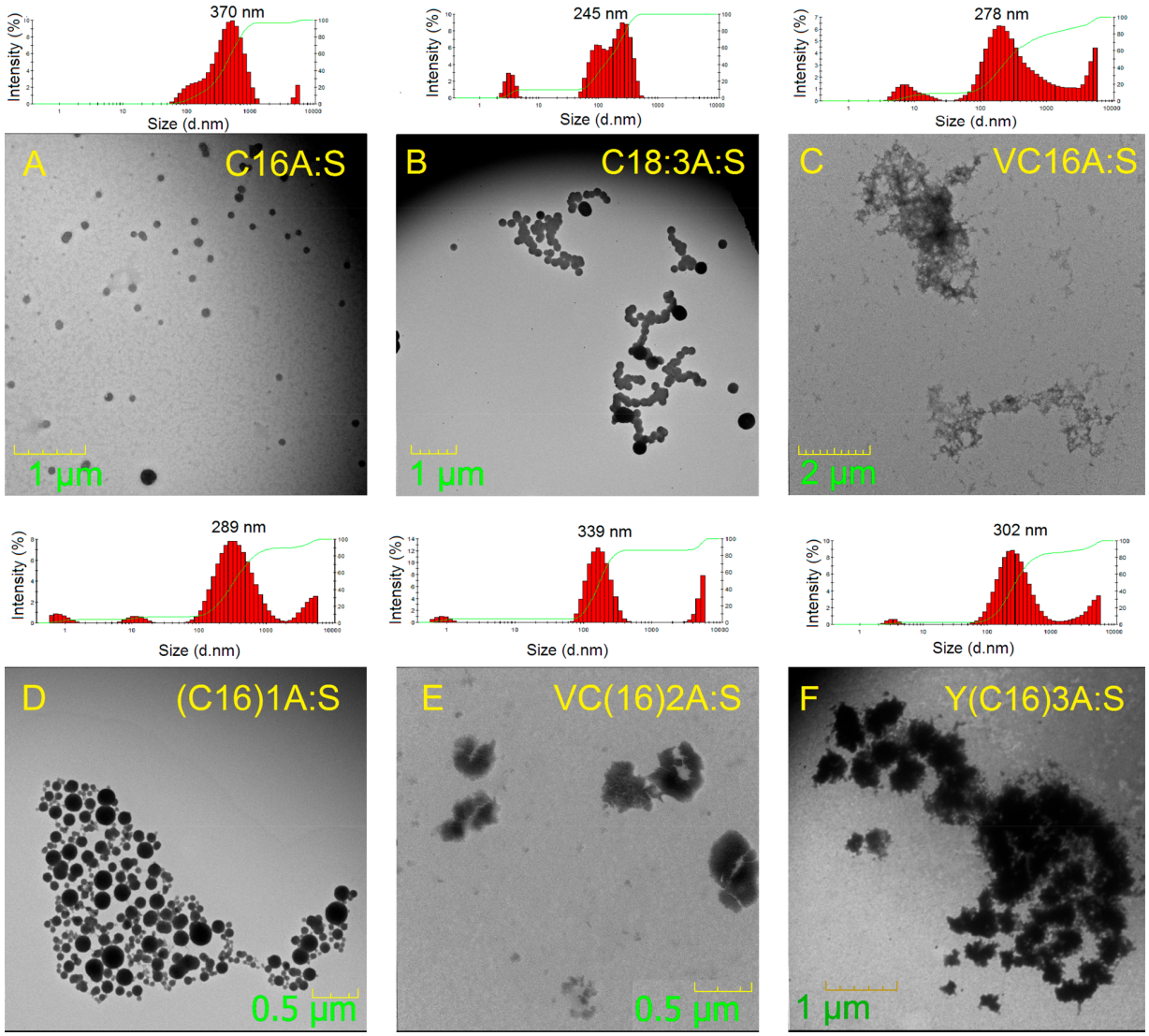

Figure 3.14 Figure 3. Representative DLS derived size distribution and corresponding TEM images of (A) saturated (C_{16}), (B) unsaturated ($C_{18:3}$), and (C) palmitic acid (C_{16}) conjugated V shaped siRNA bioconjugates. Palmitic acid (C_{16}) conjugated sense strands were used to generate the multifunctionalized Linear, V-, and Y-shaped RNA bioconjugates (D−F).

As expected, the TEM analysis showed large aggregates, especially with the V- and Y-shape templates containing 2 or 3 FA-siRNAs despite the average individual particle sizes ranging only from ~250-350 nm (**Figure 3.14**). Interestingly, the linear palmitamide-siRNA bioconjugate showed the least amount of aggregation and most uniformity which translated into a bioconjugate that was able to elicit GRP knockdown. Therefore, future derivatives of these compounds must be

designed to limit size and aggregation potential while allowing for an amphiphilic FA-siRNA complex to interact and penetrate efficiently the cell membrane for RNAi activity.

3.5 Conclusions

In this chapter the design and biological activity of unique RNA templates and their siRNA nanostructure formulations as well as the multi-functional siRNA bioconjugates have been described. The novel V-, and Y-shape RNA templates were capable of self-assembly with complementary RNA strands into nanostructure formulations that elicited potent knockdown of multiple GRP gene targets while also facilitating the incorporation of functional probes (FL and FA) that can track and trigger RNAi activity in cells. The siRNA nanostructure formulations were found to be active in a variety of cancer cell lines including breast, endometrial, and cervical which highlights their broad scope. Moreover, a covalent bioconjugation approach was designed and developed to attach fluorophores or various fatty acids to impart theranostic or self-delivering capabilities. This approach was then expanded to allow for the incorporation of multiple bio-active moieties on the V- and Y-shape siRNAs. This drastically improved the diagnostic capabilities of the FL-siRNAs as the Y-shape hybrids containing 3 FITC molecules provided the most intense and persistent fluorescent signal while maintaining gene silencing activity within a model prostate cancer cell line. Conversely, the FA-siRNAs did not produce as significant knockdown effects, presumably due to the limited cell permeability detected by flow cytometry. TEM and DLS analyses revealed large, amorphous aggregates which likely limited cell uptake of the FA-siRNA biconjugates. Despite this, the V- and Y-shape siRNAs have been shown to be a unique and potent class of synthetic siRNAs that can be expanded further into a myriad of biochemical probes for a wide scope of biomedical applications.

3.6 Materials and Methods

3.6.1 siRNA Hybridization

Purified complementary RNA strands were mixed in equimolar concentrations (10 uM) in annealing buffer (10-30 μL, 10 mM Tris, 50nM NaCl, 1 mM EDTA, pH 7.5-8.0). The solution was heated at 95°C for 5 minutes and left on a heating block to slowly cool to room temperature (25°C) over 40 minutes to afford the RNA hybrids. The hybrid mixture was subsequently used immediately or stored at 4°C overnight.

3.6.2 Dynamic Light Scattering (DLS) Analysis of the FA-siRNA Bioconjugates

A Malvern Zetasizer, Nano-ZS (Malvern Instruments, UK) employing a 173° scattering angle and a 4 mW incident He−Ne laser (633 nm) was used to measure the particle sizes (hydrodynamic diameter), size distributions, and zeta potentials of the siRNA hybrid control and siRNA-fatty acid bioconjugates. Samples were measured in triplicate at 25 °C. All samples were loaded into folded capillary cells (DTS1070) equipped with electrodes on both sides to allow measurement of their zeta potentials and by extension, the stability and degree of aggregation. Particle suspensions with highly positive or highly negative zeta potentials were considered stable because the electrical repulsion between the particles tends to counter the van der Waals forces that would otherwise result in aggregation and precipitation.

3.6.3 Transmission Electron Microscopy (TEM) Imaging of the FA-siRNA Bioconjugates

TEM analyses of the linear, V-, and Y-shaped siRNA bioconjugates were performed with a JEOL 1200EX Transmission Electron Microscope (JEOL Ltd., Japan) at an accelerating voltage of 80 kV. A mixture of 1:1 volume ratio 1% uranyl acetate and sample suspension was prepared and 10 μL of this solution placed on a TEM carbon-film-coated copper grid of 300 mesh (Electron Microscopy Sciences Inc., Hatfield, PA). Each sample was allowed to sit for 5 min on the grid before wicking the excess liquid followed by storage of 1 week to allow the samples to dry. Images were taken with a SIA-L3C CCD camera (Scientific Instruments and Applications, Inc.) using the software Maxim DL5 (Diffraction Limited, Ottawa, Canada).

3.6.4 Cell Culture

The MRC5 (ATCC® CCL-171™) normal lung cell line, AN3CA (ATCC® HTB-111™) endometrial cancer, MDA-MB-231(ATCC® HTB-26™) breast cancer, HeLa (ATCC® CCL-2™) cervical cancer, and PC3 (ATCC® CRL-1435™) prostate cancer cell lines were all purchased from ATCC. The MDA-MB-231, HeLA, and MRC5 cells were cultured in Dulbecco's Modified Eagle Medium (DMEM), the AN3CA cells in Minimum Essential Medium (MEM), and the PC3 cells in RPM1 1640 complete growth media. All media was supplemented with 10% (v/v) fetal bovine serum (FBS) and 1% (v/v) penicillin/streptomycin. The cells were cultured at 37°C in a CO_2 incubator set to 5% CO_2. The cells were subcultured using 0.25% trypsin and resuspended in fresh complete growth media.

3.6.5 siRNA Transfection in AN3CA, MDA-MB-231, HeLa, and MRC5 Cell Lines

Briefly, the cell lines were plated in separate 6-well culture plates containing complete growth media at a density of $1x10^5$ per well. Cells were then cultured for 48 h to a confluency ~60-80% prior to transfection. On the day of transfection, the siRNA hybrids (5-12.5 μL) were diluted in 250 μL of complete growth media and mixed with the Lipofectamine RNAiMAX transfecting reagent (2.5-7 uL, Thermo Fischer) according the manufacturer's protocol. The solutions were incubated at room temperature for 10min before being added to the cell cultures. The cells were then cultured in 5% CO_2 at 37°C.

3.6.6 siRNA Transfection in the PC3 Cell Line

The PC3 cell line was transfected using a modified reverse transfection protocol.[46] Briefly, on the day of transfection, the cells were suspended in complete growth media, counted, and plated in 24-well culture plates at a density of $9x10^5$ cells per well. Simultaneously, the siRNA hybrids (25-50 pmol) were diluted in 50 μL of Opti-MEM reduced serum media and mixed with the Mirus TransIT-X2® dynamic delivery system transfecting reagent (3 μL, MirusBio) according the manufacturer's protocol. The samples were incubated at room temperature for 15 minutes before being added to the PC3 cell culture. The cells were then incubated in 5% CO_2 at 37°C.

3.6.7 Cell Cytotoxicity

The cytotoxicity of the siRNA hybrids in the AN3CA, MDA-MB-231, and HeLA cancer cell lines were assayed using the Cytotoxicity Detection Kit (ThermoFisher). Following transfection of the GRP specific siRNAs, the rate of cell death was monitored by the release of LDH into the medium and quantified spectroscopically at 492 nm by the detection of the resultant

chromophore, red formazan. The cytotoxicity of the siRNA hybrids in the PC3 cancer cell lines were assayed using a Propidium Iodide (PI) assay. Following siRNA transfection, the cells were isolated and stained with PI according to the manufacturer's protocol and incubated for 15 min in the dark. The stained cells were diluted in PBS containing 1% BSA and then analyzed by flow cytometry. The data was processed using the Kaluza, Flow Cytometry Analysis Software (Beckman Coulter).

3.6.8 Cell Uptake by Flow Cytometry

Following transfection of the FL-siRNA and FA-siRNA into the PC3 cells, the cells were detached from the wells using 0.25% trypsin, isolated, and resuspended in 300μL of RPMI 1640 complete growth media. The samples were then analyzed on a Cytomics FC 500 flow cytometer (Beckman Coulter). Time dependent cell uptake studies of the FL-siRNA bioconjugates containing 1, 2, or 3 FITC probes over 72 hrs with data points being measured in triplicate at 2, 4, 8, 24, 48, and 72 hrs. Similarly the time dependent uptake study of the FL-FA-siRNA bioconjugates containing 1 or 2 fatty acid moieties and the FITC fluorophore (FL) over a 24 hr time span with data points being measured in triplicate at 3, 6, and 24 hrs. The data was processed using the Kaluza, Flow Cytometry Analysis Software (Beckman Coulter).

3.6.9 Cell Imaging

Following transfection of the FL-siRNA bioconjugates, the cells were imaged directly in the culture plate using a CellInsight™ High Content Screening (HCS) Platform (ThermoFisher). 5 random field of views from 3 separate wells were imaged under brightfield and then again after the cells were excited by a 480 nm LED filter within the platform at time points of 2, 4, 8, 24, 48,

and 72 hrs. The images were analyzed using Thermo Scientific™ HCS Studio™ Cell Analysis Software.

3.6.10 qRT-PCR

Total mRNA was isolated following transfection (48 hrs) from TriZol (Ambion) preserved cells using a TriRNA Pure Kit (Geneaid), following the manufacturer's instructions. The collected mRNA was then quantitated on a Qubit 3.0 fluorimeter using the Qubit Broad Range (BR) assay kit (Thermo Fisher Scientific), mRNA (200 ng) was reversed transcribed into cDNA using a high capacity cDNA kit (Applied Biosystems). RT-PCR was performed using pre-developed TaqManTM gene expression primer-probes for GRP78 (assay ID Hs99999174_m1), GRP94 (assay ID Hs00437665_g1), GRP75 (Hs00269818_m1), and GAPDH (Hs99999905_m1) and TaqManTM fast advanced master mix. qPCR fast assay was carried out on a StepOnePlus (Applied Biosystems). Fold changes were calculated with the ΔΔCt method using GAPDH as endogenous control and the negative siRNA as the control sample.

3.6.11 Western Blot

Total protein was isolated from the cell cultures following transfection (78 h). Protein lysates were prepared by lysing the cells in ice-cold RIPA buffer (G-Biosciences) supplemented with protease and phosphatase inhibitors (Millipore Sigma) which were diluted 1:10 as per the manufacturer's recommendations. Cell debris was removed by centrifugation at 16,000g at 4°C and protein concentrations were determined using a PierceTM BCA kit (Thermo Fisher Scientific). A sample (20-35 mg) of the supernatant protein was mixed with LDS buffer and DTT, incubated at 70 °C for 10 min and resolved on a 4-12% Bis-Tris PAGE gradient gel before being transferred

to a PVDF membrane. Following transfer, the membrane was blocked in 5% skim milk for 1 h, washed and incubated at 4 °C overnight with a rabbit 1° mAb against human GRP78, GRP94, GRP75 or GAPDH (all purchased from Cell Signaling Technology) at a 1:1000 dilution. The membrane was subsequently washed and incubated with an anti-rabbit HRP-conjugated 2° Ab (Cell Signaling Technology) for 1 h at room temperature at 1:2000 dilution. The bands were visualized using a SignalFireTM ECL reagent (Cell signaling Technology) on a ProteinSimple FluorChem E imager.

3.7 References

1. Cultrara, C. N.; Shah, S.; Kozuch, S. D.; Patel, M. R.; Sabatino, D. *Chem Bio Drug Des.* **2018**, 1-12.
2. Kozuch, S. D.; Cultrara, C. N.; Beck, A. E.; Heller, C. J.; Shah, S.; Patel, M. R.; Zilberberg, J.; Sabatino, D. *ACS Omega* **2018,** *3*, 12975-12984.
3. Patel, M. R.; Kozuch, S. D.; Cultrara, C. N.; Yadav, R.; Huang, S.; Samuni, U.; Koren, J. I.; Chiosis, G.; Sabatino, D. *Nano Lett.* **2016**, *16*, 6099-6108.
4. Shah, S.; Cultrara, C. N.; Kozuch, S. D.; Patel, M. R.; Ramos, J.; Samuni, U.; Zilberberg, J.; Sabatino, D. *Bioconj Chem.* **2018,** *29*, 3638-3648.
5. Ryther, R. C. C.; Flynt, A. S.; Phillips, J. A. I.; Patton, J. G. *Gene Ther.* **2005,** *12*, 5-11.
6. Shankar, P.; Manjunath, N.; Lierberman, J. *JAMA.* **2005,** *293*, 1367-1373.
7. Titze-de-Almeida, R.; David, C.; Titze-de-Almeida, S. S. *Pharm Res.* **2017,** *34*, 1339-1363.
8. Chiu, Y. L.; Rana, T. M. *Mol. Cell.* **2002,** *10*, 549-561.
9 . Elbashir, S. M.; Harborth, J.; Lendeckel, W.; Yalcin, A.; Weber, K.; Tushcl, T. *Nature.* **2001,** *411*, 494-498.
10. Kurreck, J. *J Biomed Biotechnol.* **2006,** 2006(4), *83757*.
11. Macrae, I.J.; Zhou, K.; Li, F.; Repic, A.; Brooks, A.N.; Cande, W.Z.; Adams, P.D.; Doudna, J.A.; *Science.* **2006,** *311*, 195-198.
12. Zamore, P. D.; Tushcl, T.; Sharp, P. A.; Bartel, D. P. *Cell* **2000,** *101*, 25-33.
13. Chiu, Y. L.; Rana, T. M. *RNA.* **2003,** *9*, 1034-1048.
14. Lima, W. F.; Wu, H.; Nichols, J. G.; Sun, H.; Murray, H. M.; Crooke, S. T. *J Biol Chem.* **2009,** *284*, 26017-26028.
15. Bumcrot, D.; Manoharan, M.; Koteliansky, V.; Sah, D. W. *Nat Chem Biol.* **2007,** *2*, 711-719.
16. Wang, S.; Shi, Z.; Liu, W.; Jules, J.; Feng, X. *BMC Biotechnology.* **2006,** *6*, 1-7.
17. Sajeesh, S.; Lee, T. Y.; Kim, J. K.; Son, D. S.; Hong, S. W.; Kim, S.; Yun, W. S.; Kim, S.; Chang, C.; Li, C.; Lee, D. K. *J Control Release.* **2014,** *196*, 28-36.
18. Guo, P. *Nat Nanotechnol.* **2010,** *5*, 833-842.

19. Shukla, G. C.; Haque, F.; Tor, Y.; Wilhelmsson, L. M.; Toulmé, J. J.; Isambert, H.; Guo, P.; Rossi, J. J.; Tenenbaum, S. A.; Shapiro, B. A. *ACS Nano.* **2011,** *5*, 3405-3418.
20. Afonin, K. A.; Viard, M.; Kagiampakis, I.; Case, C. L.; Dobrovolskaia, M. A.; Hofmann, J.; Vrzak, A.; Kireeva, M.; Kasprzak, W. K.; KewalRamani, V. N.; Shapiro, B. A. *ACS Nano.* **2015,** *9*, 251-259.
21. Nakashima, Y.; Abe, H.; Abe, N.; Aikawa, K.; Ito, Y. *Chem Comm..* **2011,** 47, 8367-8369.
22. Zuckerman, J. E.; Gritli, I.; Tolcher, A.; Heidel, J. D.; Lim, D.; Morgan, R.; Chmielowski, B.; Ribas, A.; Davis, M. E.; Yen, Y. *Proc Natl Acad Sci U S A.* **2014,** *111*, 11449-11454.
23. Patel, P. L.; Rana, N. K.; Patel, M. R.; Kozuch, S. D.; Sabatino, D. *ChemMedChem.* **2016,** *11*, 252-269.
24. Musacchio, T.; Vaze, O.; D'Souza, G.; Torchilin, V. P. *Bioconj Chem.* **2010,** *21*, 1530-1536.
25. Kubo, T.; Takai, Y.; Mihara, K.; Yanagihara, K.; Seyama, T. *Bioconj Chem.* **2012,** *23*, 164-173.
26. Kubo, T.; Yanagihara, K.; Sato, Y.; Nishimura, Y.; Kondo, S.; Seyama, T. *Bioconj Chem.* **2013,** *24*, 2045-2057.
27. Kubo, T.; Yanagihara, K.; Takei, Y.; Mihara, K.; Morita, Y.; Seyema, T. *Mol Pharm.* **2011,** *8*, 2193-2203.
28. Jeong, J. H. M., H.; Oh, Y.K.; Park, T.G. *Bioconj Chem.* **2009,** *20*, 5-14.
29. Sumer, B.; Gao, J. *Nanomedicine.* **2008,** *3,* 137-140.
30. Zhao, J.; Mi, Y.; Feng, S. S. *Nanomedicine.* **2013,** *8*, 859-862.
31. Liu, Y.; Gunda, V.; Zhu, X.; Xu, X.; Wu, J.; Askhatova, D.; Farokhzad, O. C.; Parangi, S.; Shi, J. *Proc Natl Acad Sci U S A.* **2016,** *113*, 7750-7755.
32. Maina, A.; Blackman, B. A.; Parronchi, C. J.; Morozko, E.; Bender, M. E.; Blake, A. D.; Sabatino, D. *Bioorg Med Chem Lett.* **2013,** *23*, 5270-5274.
33. Boulares AH, Yakovlev AG, Ivanova V, Stoica BA, Wang G, Iyer S, Smulson M. *J Biol Chem.* **1999**, *274*, 22932-22940.
34. Tsai YL, Zhang Y, Tseng CC, Stanciauskas R, Pinaud F, Lee AS. *J Biol Chem.* **2015**, *290*, 8049-8064.
35. Nami, B.; Ghasemi-Dizgah, A.; Vaseghi, A. *Bioimpacts.* **2016**, *6*, 105–110.
36. Dadey DYA, Kapoor V, Hoye K, Khudanyan A, Collins A, Thotala D, Hallahan DE. *Clin Cancer Res.* **2017**, *23*, 2556-2564.
37. Kapulkin, V.; Hiester, B. G.; Link, C. D. *FEBS letters.* **2005,** *579*, 3063-3068.
38. Cultrara CN, Kozuch SD, Ramasundaram P, Heller CJ, Shah S, Beck AE, Sabatino D, Zilberberg J. BMC Cancer. **2018**, *18*, 1263.
39. Leuschner, P.; Ameres, S.; Kueng, S.; Martinez, J. *EmBO Rep.* **2006,** *7*, 314-320.
40. Pham, J. W.; Sontheimer, E. J. *J Biol Chem.* **2005,** *280*, 39278-39283.
41. Maier, T.; Guell, M.; Serrano, L. *FEBS letters.* **2009,** *583*, 3966-3973.
42. Lecoeur, H. *Exp Cell Res.* **2002,** *277*, 1-14.
43. Rietwyk, S.; Peer D. *ACS Nano.* **2017**, *11*, 7572-7586.
44. Jackson, A. L.; Burchard, J.; Schelter, J.; Chau, B. N.; Cleary, M.; Lim, L.; Linsley, P. S. *RNA.* **2006,** *12*, 1179-1187.
45. Judge, A. D.; Sood, V.; Shaw, J. R.; Fang, D.; McClintock, K.; MacLachlan, I. *Nature Biotechnol.* **2005,** *23*, 457-462.

46. Lu, Y. et al. *Oncogene.* **2011,** *30* (45), 4567-4577.

Chapter 4: Targeting the Prostate Specific Membrane Antigen Receptor for Targeted siRNA Delivery

4.1 Abstract

In this study, oligoarginine peptides are conjugated to a short cancer-targeting peptide (CTP) selective for the prostate-specific membrane antigen (PSMA) receptor. The PSMA receptor is present on the cell surface of metastatic and castrate resistant prostate cancer (PCa) cells and functions as a clinically relevant biomarker for cancer-targeting strategies. In our cancer-targeting gene therapy approach, the PSMA-R_n (n= 6 and 9) peptides were synthesized by solid phase peptide synthesis (SPPS), isolated and characterized by LCMS and condensed with the Glucose Regulated Protein (GRP) silencing siRNAs. Native gels revealed formation of stable CTP:siRNA ionic complexes at low mole ratios (1:25). Furthermore, siRNA release was affected by heparin competition, underscoring the capabilities for the peptides to act as effective condensing and releasing agents. DLS and TEM studies revealed the importance of size and shape of the CTP:siRNA particles for cell biology applications. The CTP:siRNA formed large anionic complexes which were prone to aggregation and limited cell uptake for RNAi activity when compared to the control siRNA complex formed with the commercial Trans-IT dynamic delivery system. Therefore, the development of efficient peptide based siRNA delivery systems is contingent on the formulation of discrete, neutral nanoparticles that can effectively condense, and release siRNA across the cell membrane for RNAi action.

4.2 Introduction

4.2.1 Targeted Delivery Ligands

A major limitation in the development of siRNA-based drugs is the non-specificity of the various delivery methods. Not only can this lead to off-target silencing of genes, but also widespread distribution in healthy tissues potentially resulting in cytotoxicity.[1] Conversely, selective delivery systems can increase the specificity and potency of siRNA therapies.[2-4] Ligands that can target cell surface receptors have been functionalized to condense siRNAs and facilitate their selective delivery across cell membranes for RNAi activity. These ligands encompass both small and large molecules that have binding affinity and selectivity for their target receptors. They are typically functionalized with a cell penetrating domain, that can effectively condense siRNA cargo and facilitate its translocation across cell membranes, typically by receptor mediated endocytosis (**Figure 4.1**). Once internalized, the siRNA is released in the cytosol of the cell and recruits the RISC complex for gene silencing activity.

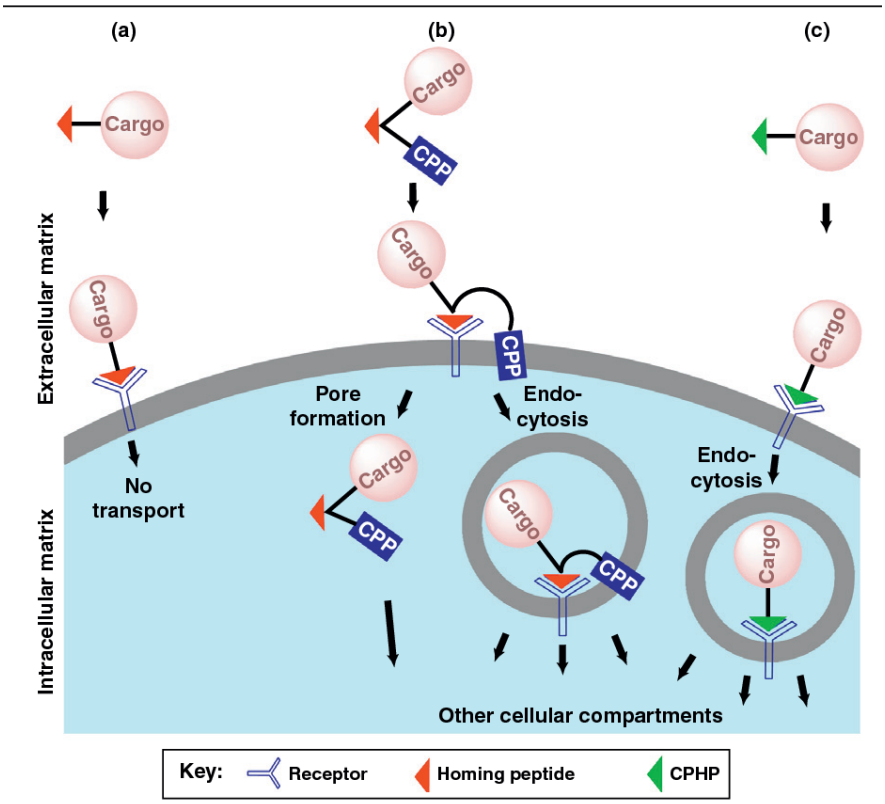

Figure 4.1 Illustration of ligand targeted delivery of cargo into cells. Image reprinted with permission from Elsevier: Svensen, N.; Walton, J.G.; Bradley, M. *Trends Pharmacol Sci.* **2012,** *33*(4):186-92[5]

The folate and cholesterol receptors are common targets whose ligands, folate and cholesterol (or cholesterol analogs) respectively, are readily available and conjugate easily to siRNA based delivery systems (i.e. transfection reagents). The folate receptor is highly expressed among a variety of cancer types yet has minimal expression in healthy tissues except the kidneys. One study has shown molecular folate conjugated to polycationic polymers polyethylenamine and polylysine (PEI/PLL) formed siRNA carrier formulations for transfection into nasopharyngeal carcinoma cells which resulted in potent gene silencing.[2,6,7] Similarly, cholesterol conjugated siRNA was introduced intrasystemically in an *in vivo* mouse model. The cholesterol-siRNA bioconjugate was found to accumulate only lightly in the kidneys and heart, but highly into target hepatocytes where the cholesterol receptors present on these cells helped endocytose the ligand.

Moreover, the naked siRNA was not found to localize or accumulate in any specific tissue and the siRNA-cholesterol bioconjugate was able to elicit upwards of 60% knockdown of the target protein, apoB.[8]

The larger macromolecular targeting ligand class is typically represented by peptides, proteins, and antibodies. Antibodies, in particular, are particularly interesting as they are among the most selective receptor targeting ligands, including representative examples of antibody-based siRNA delivery *in vivo.* For example, siRNA targeting ku70 mRNA has been complexed to a fusion protein that contains the antibody binding domain for the ErbB2 receptor and successfully delivered siRNA into $ErbB2^{+}$ breast cancer.[9] Likewise, an antibody conjugated cationic liposome was able to deliver siRNA targeting Cyclin D1 as a treatment against inflammatory bowel disease.[10] Yet, antibodies are not without their drawbacks as they are large molecules that are not readily cell permeable, susceptible to denaturation and proteolytic degradation which greatly reduces their therapeutic effect, while raising toxicity concerns by stimulating immune responses.

Peptide based ligands are also highly favorable as targeting ligands due to their flexibility in size and composition as well as ease in synthesis. One of the most highly studied and useful peptide ligands for targeted delivery is the RGD sequence. This peptide can bind to transmembrane integrins which are commonly overexpressed receptors on the surface of cancer cells.[11] This peptide has been conjugated to various delivery system, such as PEI based formulations, which facilitate the selective accumulation of siRNA into integrin presenting cancerous cells ultimately leading to targeted cytotoxicity.[12] Another example is the use of a homing peptide to target the VEGF receptor – another commonly targeted cellular receptor overexpressed on the surface of a panel of cancer cell lines.[13] In a representative application, a 6-mer homing peptide, A1, (WFLLTM) was conjugated to the TAT cell penetrating peptide (RKKRRQRRR) to effectively

condense and internalize siRNA selectively into the targeted VEGF receptor 1 overexpressing cancer cells in a co-culture model.[14] Furthermore, these cancer-targeting peptides (CTPs) are also applicable *in vivo.* For example, a short 29-mer peptide derived from the rabies virus glycoprotein conjugated to a nona-D-arginine sequence was used to target the acetylcholine receptor, and deliver siRNA targeting Cyclophilin B and HMGB1selectively into dendrites and macrophages to help suppress an overactive immune system in the blood and brain.[15, 16] These examples highlight peptides as a highly interesting and promising siRNA delivery ligands.

4.2.2 Cell Penetrating Peptides

Cell penetrating peptides (CPPs) have also been used to facilitate intracellular delivery of siRNA. There are three conventional designs for CPPs : 1) poly-cationic in which the sequence contains dense regions of basic amino acids such as lysine or arginine, 2) amphiphatic which contains alternating sequences of polar and hydrophobic amino acids, such as arginine and tryptophan and 3) completely hydrophobic sequences such as poly(histidine) peptides. These peptides have been used in many cell uptake studies, however, their mechanism of uptake can vary depending on CPP type and sequence.[17] Moreover, these peptide motifs are important for siRNA encapsulation and release based on a combination of competing ionic and aromatic interactions. Therefore, CPPs are bifunctional in their ability to condense and deliver siRNA across cell membranes. Furthermore, CPPs have been functionalized with targeting ligands (small molecules, peptides and antibodies) to facilitate selective cell uptake of siRNA and other payloads (**Table 4.1**).

Table 1
siRNA delivery by CPPs.

Peptide	Subgroup	Sequence
Hydrophilic CPPs		
Tat	–	RKKRRQRRR
Arginine oligomer	–	Rn; 6 < n < 16
Amphiphilic CPPs		
$MPG^{\Delta NLS}$	Bipartite peptide	GALFLGFLGAAGSTMGAWSQPKSKRKV
MPG-8	Bipartite peptide	bAFLGWLGAWGTMGWSPKKKRK-Cya
MPGα	Bipartite peptide	Ac-GALFLAFLAAALSLMGLWSQPKKKRKV-Cya
BPrPp	Bipartite peptide	MVKSKIGSWILVLFVAMWSDVGLCKKRPKP-amide
Pep-1	Bipartite peptide	Ac-KETWWETWWTEWSQPKKKRKV
Penetratin	α-Helical peptide	RQIKIWFQNRRMKWKK-amide
CADY	α-Helical peptide	Ac-GLWRALWRLLRSLWRLLWRA-cysteamide
KALA	α-Helical peptide	WEAKLAKALAKALAKHLAKALAKALKACEA
Targeting ligand–CPP conjugates		
Fab-protamine	Antibody-based	Fab-ARYRCCRSQSRSRYYRQRQRSRRRRRRSCQTRRRAMRCCRPRYRPRCRRH
scFv-dR9	Antibody-based	scFv-dRdRdRdRdRdRdRdR
mAb-R9	Antibody-based	mAb-RRRRRRRRR
A1-Tat	Homing peptide-based	WFLLTM-RKKRRQRRR
RVG-R9	Homing peptide-based	YTIWMPENPRPGTPCDIFTNSRGKRASNGGGG-RRRRRRRRR
Activatable CPPs		
ACPP	Enzyme activated	EEEEEEE-GALGLP-RRRRRRRRKKR

Table 4.1 List of various CPPs used to deliver siRNA into cells and ranging in size and composition. Image adapted with permission from Elsevier: Tai, W.; Gao, X., *Adv. Drug Del. Rev.* **2017,** *11*, 157-168.[17]

The first CPP was derived from the short transduction region of the HIV-1 TAT protein. This 9-mer peptide sequence (RKKRRQRRR) can rapidly translocate across the cell membrane and is considered a universal carrier for cellular delivery.[14] In particular, this peptide has been covalently conjugated to a fluorescently labeled siRNA which tracked localization within cellular endosomes and transport into the perinuclear space for release, RISC assembly and RNAi activity.[18, 19] However, direct conjugation of TAT peptides to the siRNA may hinder assembly within the RISC complex, reducing the overall effectiveness of the RNAi response.[17] Therefore, the CPP:siRNA based delivery systems are typically formulated as reversible ionic complexes for more effective cell biology applications.

The oligoarginine and polyarginine peptides are another important class of CPPs capable of siRNA delivery. This type of CPP is a short 6 to 16-mer sequence comprised solely of arginine. Oligoarginine peptides are hydrophilic cationic CPPs with a high polycationic charge density and

have a higher cell penetrating potential due to the strong affinity of the guanidinium group for the phospholipids in the cell membrane. The charged side chains can infiltrate into the lipid bilayer and essentially create a pore within the membrane through which the CPP and its cargo can penetrate into the cell.[20, 21] The R_9 -siRNA complexes have been used to silence eGFP expression in human gastric carcinoma cells.[22] Moreover, an *in vivo* application of an R_{12} CPP – siRNA complex was found to reduce subcutaneous tumor growth in a mouse xenograft model via the silencing of the Her2 protein.[23] Furthermore, substituting L/D-R_n has been found to improve peptide stability and the siRNA silencing effect. However, these peptides are not without their limitations, as the oligoarginine CPPs can be difficult to use as they need to be used in large excess compared to their siRNA cargo. While this may not affect all tissue models, the large excess can elicit nonspecific interactions with other anionic components in the cellular microenvironment and circulatory system. This can lead to a loss in stability of the formulation as well as off target silencing or inefficient *in vivo* circulation. Often, these hydrophilic cationic peptides are combined with a targeting ligand to offset this limitation.[17]

4.2.3 Targeting the PSMA Receptor with anti-PSMA Peptides

The prostate specific membrane antigen, PSMA, is a type-II transmembrane protein which functions as a surface carboxypeptidase enzyme, an exopeptidase with folate hydrolase activity because it progressively liberates glutamates from glutamate rich sources.[24] Moreover, this receptor has been shown to have an internalization signal which, once activated, allows for the internalization of the enzyme from the membrane into the cell via an endosome formed from clathrin dependent endocytosis.[25] In cancer, PSMA is expressed in all prostatic tissues including primary prostate adenocarcinomas, prostate tumors metastatic to bone and in the tumor

neovasculature of many solid cancers but not normal tissues.[26,27] In prostate cancer, PCa, PSMA is highly expressed in poorly differentiated, highly metastatic prostatic cells and in castrate-resistant models.[28] In fact, PSMA-based PET and CT imaging is an emerging field in the diagnosis and treatment of advanced and resistant PCa, rendering PSMA a valuable biomarker for targeted forms of therapies.[28]

The phage display selection of PSMA binding peptides has resulted in the identification of three peptide sequences: GDHSPFT, SHFSVGS and EVPRLSLLAVFL, capable of targeting, binding and internalizing within PSMA expressing PCa cells.[29] The selected lead PSMA binding peptides were based on the consensus sequences, SHSFSVGSGDHSPFT and GRFLTGGTGRLLRIS. These peptides were labeled with the 5-FAM fluorophore and were shown to bind selectively to PSMA expressing PCa cells, and accumulated intracellular by the observation of disperse fluorescent punctuate regions found within the cells. Similarly, a separate phage display study was used to identify another PSMA binding peptide. This 12-mer peptide, GTIQPYPFSWGY, was shown to have good binding affinities (8-9 μM) to $PSMA^+$ LNCaP and C4-2 PCa cell lines and attachment of a fluorophore allowed for the surface staining of these cells for microscopy.[30] Moreover, this peptide was capable of delivering the D-$(KLAKLAK)_2$ cytotoxic peptide to LNCaP cells and induce cell death. This peptide also had favorable *in vivo* distribution where it selectively accumulated in a C4-2 mouse xenograft with minimal uptake in any other major organ. These key lead peptides highlight the potential in targeting this receptor as a potential diagnostic and for the specific delivery of therapeutics against PCa.

Recently, a folate targeted cyclodextrin-based nanoparticle formulation had been developed to selectively deliver siRNA targeting the RelA gene in $PSMA^+$ cell lines, LNCaP and VCaP. The formulation silenced mRNA levels by 22% and 44%, respectively, while no significant

knockdown was observed with complexes absent of the folate ligand.[31] Moreover, gold nanoparticle (AuNPs) containing a folate ligand selectively delivered RelA siRNA into $PSMA^+$ LNCaP resulting in a moderate 35% decrease in transcript levels.[32] While these examples highlight the interest in targeting the PSMA receptor as a means of selective siRNA delivery, they are limited in only using small molecule ligands as the targeting agent. As described, there are multiple examples of PSMA-specific peptide ligands for cell delivery, yet none describe their use in siRNA uptake in PCa cells. Therefore, the generation of peptide-based delivery systems targeting PSMA may enhance the uptake and gene silencing of siRNA therapies.

4.3 Chapter Objectives

This chapter will focus on the design and development of a novel targeted delivery siRNA vector based on the PSMA receptor. In this application, oligoarginine CPPs (R_6 and R_9) and a model PSMA cancer targeting peptide (CTP), GRFLTGGTGRLLRIS, were combined to afford an amphiphilic peptide with two main functional domain: a PSMA targeting domain with the potential to trigger receptor mediated endocytosis, and a poly-cationic domain which functions to complex siRNA facilitate translocation into the cell (**Figure 4.2**). The peptides will be synthesized by Fmoc-solid phase peptide synthesis (Fmoc-SPPS) with and without an N-terminal FITC label to track peptide cell biology. The crude peptides will be purified by RP-IP HPLC and identity confirmed by ESI-MS. The siRNA condensation and release studies will be optimized by native PAGE analysis while the size, shape and charge distributions of the CTP:siRNA formulation will be evaluated by DLS and TEM. Cell biology will be next accomplished in $PSMA^{+/-}$ cell lines to determine binding and knockdown efficiency by flow cytometry, qRT-PCR, and western blot.

Taken together, this study is expected to yield a new peptide based siRNA delivery system in PSMA+ PCa cells for targeted gene therapy applications.

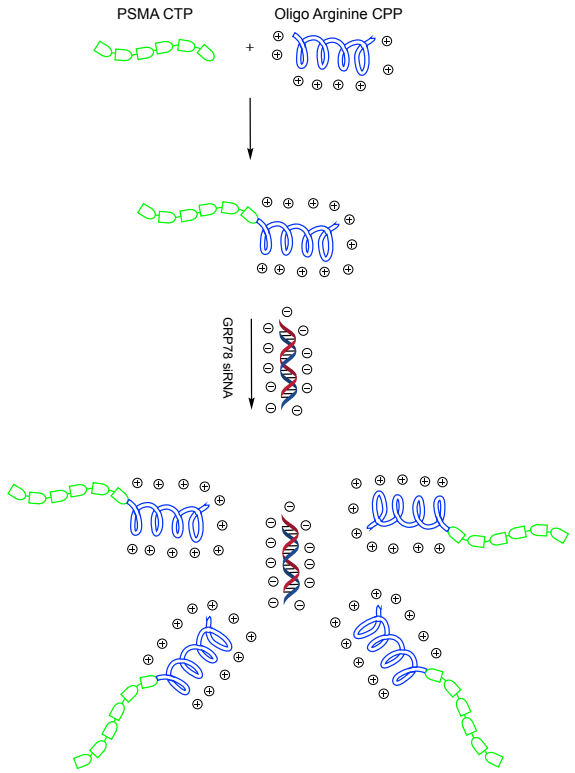

Figure 4.2 Representation of the PSMA-R_n siRNA delivery system. Drawn in ChemBioDraw.

4.4 Results and Discussion

4.4.1 Rational Design and Synthesis of PMSA-R_n Peptides

The PSMA binding peptide chosen for this work was based on the phage display selection reported by Shen, et. al.[29] Among the PSMA binding peptides reported in this study, the sequence GRFLTGGTGRLLRIS (PSMA-1) was selected for our work due to its potential synthesis efficiency and aqueous solubility given its amphiphilic nature for cell biology. To the PSMA-1 sequence, a hexa-arginine peptide, R_6, was incorporated at the *C*-terminus to generate the CTP, PSMA-1-R_6. The R_6 sequence was selected to complex siRNA and facilitate cell delivery as

polyarginine peptides have been classified as cell penetrating peptides (CPPs) for cell based and *in vivo* studies.[22,23] Furthermore, PSMA-1 does exhibit some cell permeability, potentially via a receptor-mediated endocytotic mechanism which should also contribute to cell penetration.

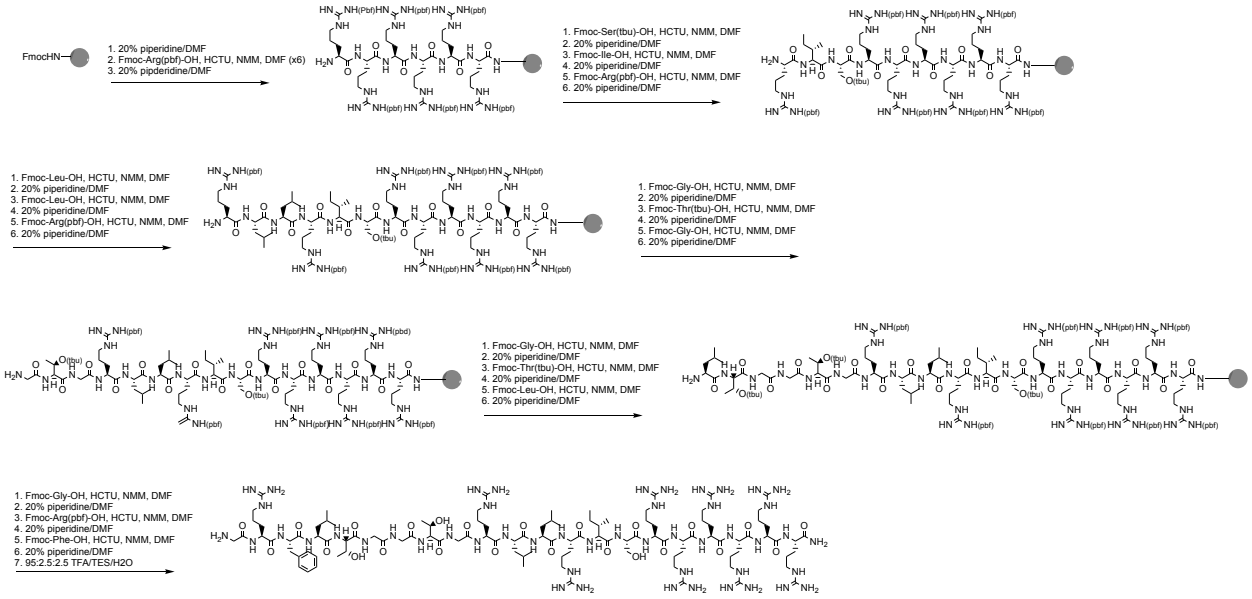

Scheme 4.1 Synthesis of the lead PSMA-1 -R_6 CTP. Drawn in ChemBioDraw,

Peptide synthesis of the lead CTP, PSMA-1-R_6 (**Scheme 4.1**) was accomplished using classical Fmoc-SPPS conditions.[33] The hydrophilic poly(ethylene glycol) PEG resin was selected for making the polar PSMA-1-R_6 sequence and its related controls, FITC-PSMA-1, to track PSMA binding on PCa cells and FITC-PSMA-1-R9 to track the influence of the nona-arginine sequence on siRNA delivery in PCa cells. Fmoc-protected amino acids were efficiently coupled using HCTU as activator followed by Fmoc deprotections with basic piperidine conditions. For FITC labeling, the peptide N-terminus was functionalized with an aminohexanoic acid (Ahx) linker followed by direct couple of FITC in the dark. Following synthesis, the peptides were cleaved and deprotected from the solid support and subjected to RP-IP HPLC purification (>90%) and characterization by ESI-MS (**Table 4.2**)

Peptide	Isolated Purity[a]	Expected Mass (g/mol)	Found Mass (g/mol)	M/Z[b]
FITC-PSMA$_1$	>95%	2106	702.7	+3
PSMA$_1$-R$_6$	90%	2541	509	+5
FITC-PSMA$_1$-R9	95%	3510	461.7	+8 (+22)

Table 4.2 Purity and MS characterization of the isolated PSMA-1 peptides. [a] Purity as determined by RP-HPLC. 20-80% MeCN gradient over 18min.[b] Denotes charge state of the mass fragments found. +22 indicates a sodium adduct for that fragment

4.4.2 PSMA-1-R$_6$ Can Efficiently Complex siRNA

The poly(arginine) domain of the peptides have the capability of interacting with and complexing to RNA electrostatically through the negatively charged phosphate backbone of the RNA and the positively charged side chain guanidium groups of the arginines. Native PAGE shift assays were used to determine the extent of CTP:siRNA complexation by optmization of the stoichiometric mol ratios. **Figure 4.3** highlights the optimization conditions of the CTP:siRNA complexes. The PSMA-1-R$_6$ CTP was used to probe the extent of siRNA complexation as the R$_9$ variant was rationalized to interact with the siRNA in similar fashion. In order to optimize the stoichiometric ratios of the CTP:siRNA complexes, excess CTP (1-100 eq.) was added to the hybrid siRNA (250pmol) in (describe annealing buffer conditions), followed by incubation at 37°C for 30 min prior to addition of the gel loading sucrose buffer for native PAGE analysis (**Figure 4.3 B**). CTP:siRNA complex formation was identified by a shift to more retained bands on the gel with a decrease in intensity when compared to the untreated siRNA controls. In this case, it is expected that the CTP:siRNA formulation moves to a more retained higher-order complex with

much slower electrophoretic mobility due to RNA charge masking and with limited signal detection due to the limited capabilities of the staining dye to stain RNA in the CTP:siRNA complex form. These trends were also observed in the time and temperature optimization studies (**Figure 4.3, A**) which indicates CTP:siRNA complex formation within 15 min at 25ºC and 37ºC. At 50 eq of CTP, incubated at 37 °C for 30 min, the most efficient CTP:siRNA complex was detected for the linear and V-shape siRNA (**Figure 4.3, D**). Furthermore, the CTP:siRNA complex at these optimized conditions was challenged by a heparin release assay to validate the bifunctional siRNA complex and release capabilities of the CTP. In this assay (**Figure 4.3, C**), a concentration dependent study (0.1-10 eq.) of heparin was used to determine the extent of CTP:siRNA complex stability and the optimal heparin concentration for siRNA displacement. PAGE analysis revealed that at 10 eq heparin, siRNA (250pmol) was displaced from the CTP (12.5nmol) and stained as a dark violet band by the Stains-All dye solution. This result confirmed to important reversibility of the CTP:siRNA complex formulation for cell uptake and RNAi activity.

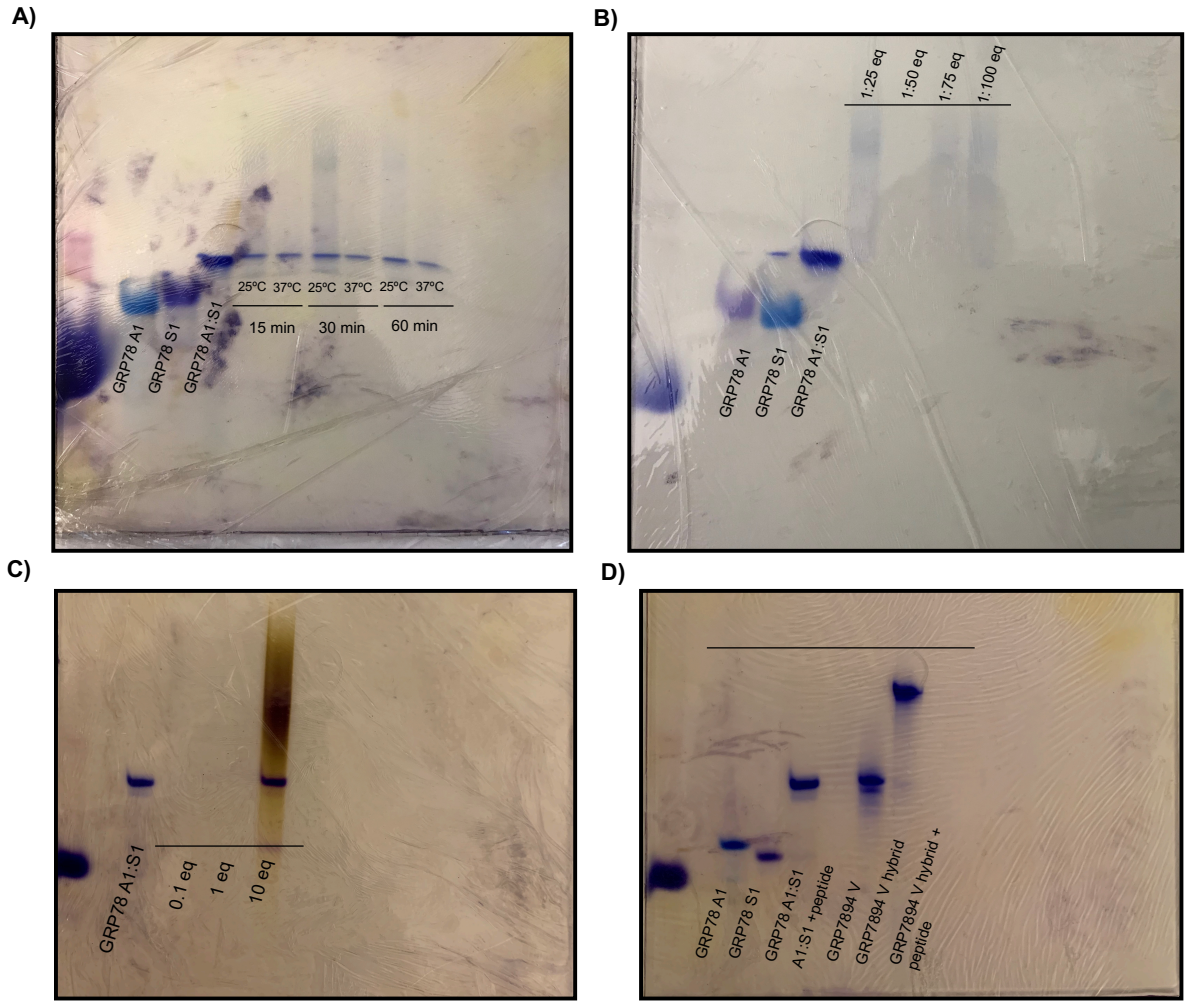

Figure 4.3. Optimization conditions of the CTP:siRNA complexes. A) Time (0-60 min) and temperature (25 and 37 °C) dependence. B) siRNA:CTP stoichiometric mol ratios (1:25-100 eq.). C) Concentration dependent (0.0163-1.63 mg/mL) heparin release assay at 37 °C for 30 min. D) CTP:siRNA complexes with linear and V-shape siRNA (250pmol) in combination with PSMA-1-R_6 (12.5nmol)

4.4.3 The PSMA-1 Peptide Binds to PSMA$^+$ PCa cells via Flow Cytometry

The PSMA-1 peptide's ability to bind to PSMA$^+$ PCa cells was next investigated. An FITC labeled version of the PSMA-1 peptide was used for this assay to ensure applicability to flow cytometric cell surface detection of PSMA$^+$ PCa cells. The PSMA-1-R_6 peptide was not analyzed in this study due to its expected cell permeability which would restrict cell surface PSMA detection

on the PCa cells. Two PCa ($PSMA^+$ LNCaP and a $PSMA^-$ PC3) cell lines were tested for FITC-PSMA-1 binding by flow cytometry (**Figure 4.4**). Surface expression of the PSMA receptor was confirmed on the LNCaP cells using a PE-conjugated PSMA mAb. No mAb binding was observed on the PC3 cells, validating that this cell line is $PSMA^-$. A distinct increase in the fluorescent intensity for the FITC-PSMA-1 peptide was detected on the LNCaP cells (**Figure 4.4 C**) relative to the PC3 cells (**Figure 4.4. F**) indicating PSMA binding on the LNCap cells with some small degree of nonspecific binding detected on the PC3 cells. Of note, the peptide was used in higher concentrations (~1 mg/mL) when compared to the anti-PSM mAb (~10-100 ug/mL) which may account for the observed non-specific binding to the PC3 cells.

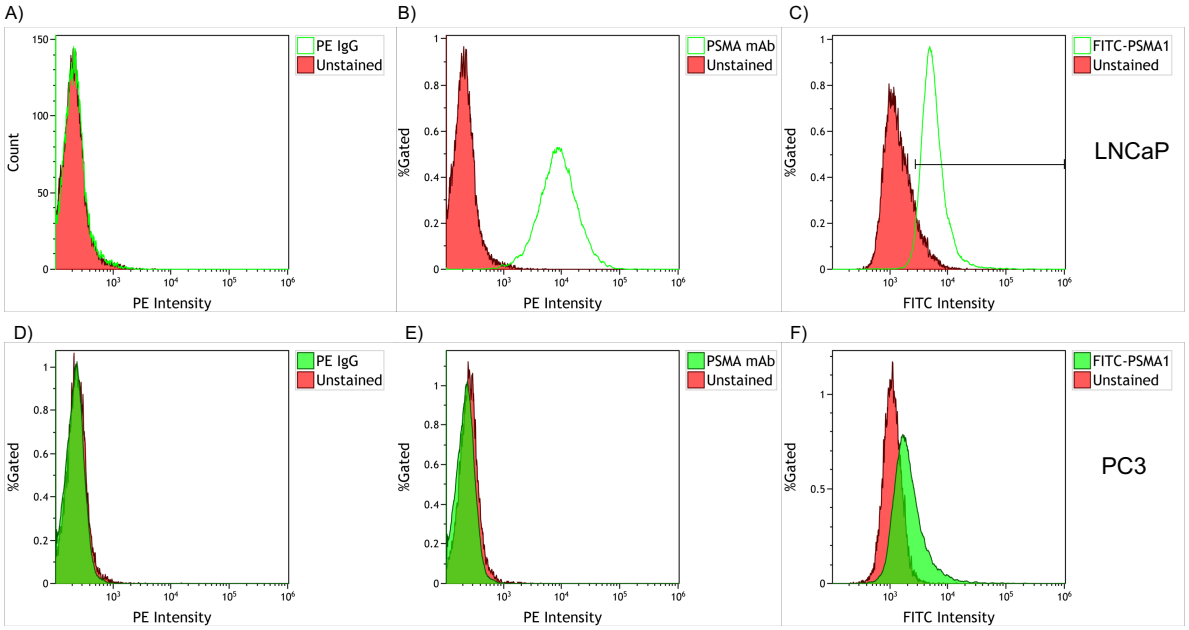

Figure 4.4. Flow cytometric analysis of FITC-PSMA-1 binding to LNCaP and PC3 PCa cell lines. Binding was measured after 15 minutes for the PSMA mAb (**B and E**) or 60 minutes for the peptide (**C and f**).

4.4.4 Cell Uptake of the FITC-PSMA-1-R_9 by Fluorescent Imaging

The FITC-PSMA-1-R_9 was first assayed to determine whether the peptide would effectively condense and deliver siRNA in LNCaP cells. The peptide (1.25 uM) was incubated with siRNA (25 nM) and introduced to a monolayer of LNCaP cells at ~60-70% confluency and imaged over a 24 h. Little to no fluorescence was observed at any time points along the surface of the cells or intracellularly indicating a lack of binding and uptake as detected by flow cytometry (**Figure 4.5**).

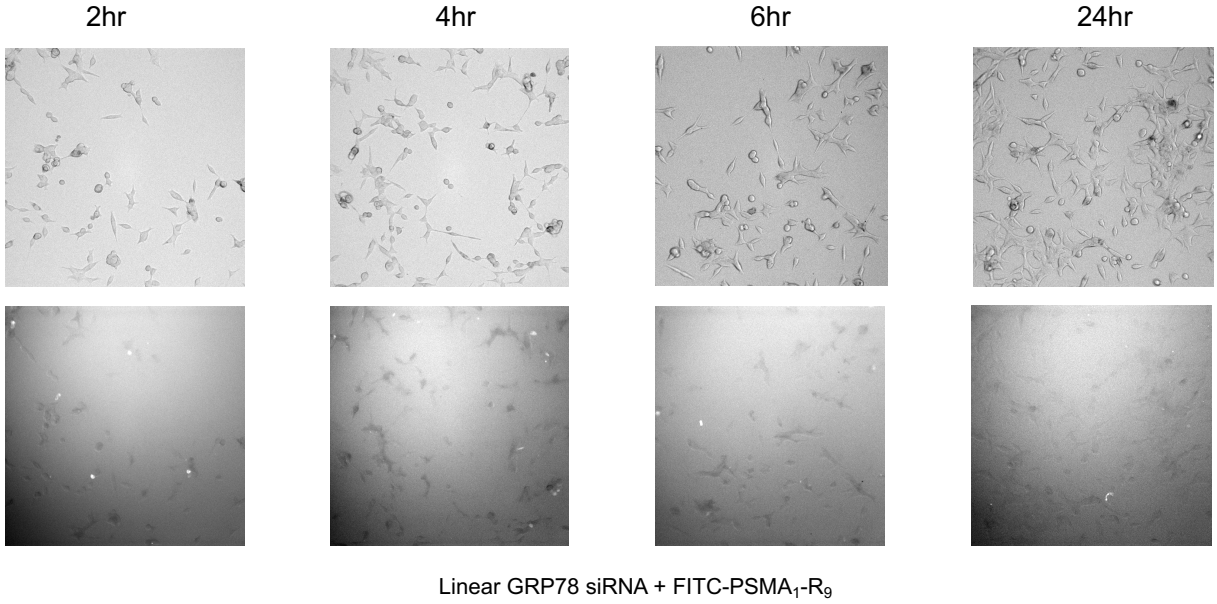

Figure 4.5 HCS imaging of LNCaP cells incubated with FITC-PSMA-1-R_9: siRNA complexes over time. Top: brightfield channel, Bottom: LED filter (485/520 ex/em).

4.4.5 GRP78 Knockdown in LNCaP and PC3 Cells

The initial lead peptide, PSMA-1-R_6 was also probed for its ability to potentially function as a selective transfection vector. The peptide (1.25 μM) was mixed with siRNA (25 nM) and incubated with a monolayer of either LNCaP or PC3 cells at ~60-70% confluent. Likewise, the siRNA was complexed with the Trans-IT X2 transfection reagent and also transfected separately

into the cells. The knockdown efficiency was monitored by qRT-PCR and western blot at 48 hrs or 72 hrs post transfection, respectively.

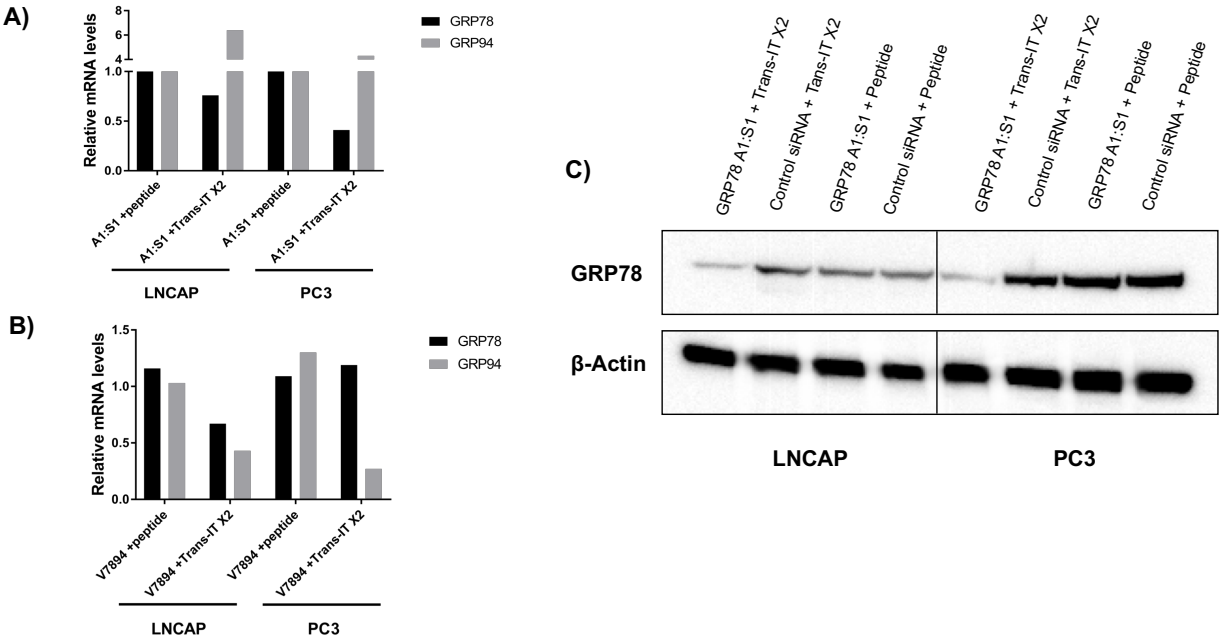

Figure 4.6 GRP knockdown in the LNCaP or PC3 cell lines using the PSMA-1-R_6 peptide or the Trans-IT X2 system as the transfection reagents. The cells were transfected with 25 nM siRNA with relative mRNA levels analyzed by qRT-PCR at 48 hrs and total protein levels analyzed at 72hrs. All knockdown levels were normalized against a negative siRNA control. mRNA knockdown comparison by qRT-PCR of the knockdown efficiency between the peptide or the trans-IT X2 reagent of A) linear siRNA against GRP78 and B) V-shape siRNA against GRP78 and GRP94. C) Protein expression change comparison between the peptide or the Trans-IT X2 reagent

No changes in the mRNA levels (**Figure 4.6, A**) or the protein expression levels (**Figure 4.6, B**) were observed when transfecting a linear siRNA against GRP78 into either cell line as compared to 30-70% knockdown when using the Trans-IT X2 reagent. Similarly, peptide-based transfection of higher order V-shape siRNA against GRP78 and GRP94 into the LNCaP cells resulted in no knockdown of the target genes compared to the Trans-IT X2 control.

4.4.6 DLS and TEM Analysis of the CTP:siRNA Complexes

One advantage of using transfection reagents to shuttle siRNA into cells is their ability to condense the siRNA molecules into small discrete particles of similar size and shape. DLS analysis and TEM imaging were used to determine if the PSMA-1-R_n peptides were capable of effecting siRNA condensation. The R_6 and an R_9 variant of the PSMA-1 peptide were assayed to determine whether the length of arginine had an effect on the peptide's ability to condense the siRNA. These were compared to the size and morphology of the complexes generated when mixing the siRNA with the Trans-IT X2 transfection reagent. **Table 4.3** summarizes the relative sizes of the complexes along with their effective net charge determined as its zeta potential. The siRNA:Trans-IT X2 complexes had a uniform size ~400nm with a net charge hovering around neutral. This was in stark contrast to that observed with the PSMA-1- R_n peptide complexes.

Sample	Effective Diameter (nm)	Zeta Potential (mV)
siRNA : Trans-IT X2	411.8 ± 55.8 456 ± 60.6	0.768 ± 1.24
siRNA: PSMA-1-R6	1450 ± 332.3 878 ± 40.23	-2.16 ± 0.387
siRNA: PSMA-1-R9	2135 ± 357.1 1041 ± 222.2	-5.88 ± 0.251

Table 4.3 Size and Zeta potential analysis by DLS of the siRNA: PSMA-1 complexes compared to that of an siRNA: Trans-IT X2 transfection reagent complex. The top diameter represents the relative aggregate sizes while the bottom represents individual particle sizes.

Both the R_6 and R_9 PSMA-1 variants showed individual particle sizes ranging from ~800-1000 nm with slightly negative net charges, (-5mV – -2mV). However, the relative sizes of the complexes ranged from 1.5-2 μm in diameter, roughly 4-5x larger than the complexes generated with the transfection reagent. This indicates that the complexation observed by native SDS-PAGE were simply an ionic interaction that does not result in a condensation of the siRNA into sizes amenable for cellular uptake regardless of the mechanism of uptake. The TEM images (**Figure 4.7**) confirm these results and give an indication of the extent of aggregation and the resulting morphology. Interestingly, the more amphiphilic peptide sequence, PSMA-1-R_9 was the least efficient in condensing the siRNA and, in fact, generated large porous networks of peptide bound siRNA. Conversely, the R_6 variant was able to produce particles of similar morphology which were, on average, 200-300 nm larger than those of the siRNA: Trans-IT X2 complexes. Interestingly, the aggregation is proportional to the arginine sequence length which may be related to the overall amphiphilicity of the peptide sequence and its behavior in solution. Moreover, as the CTP-siRNA complex becomes more neutral in charge, their relative hydrophobicity may play a more pronounced effect as both the siRNA and peptides' aqueous solubility come from their ability to be charged in solution. As the charge is reduced and the system becomes more organic in nature, the complexes may then be aggregating through hydrophobic interactions to reduce the non-favorable solvating effects of the aqueous medium. Nevertheless, this data confirmed that the peptides ability to complex siRNA, albeit with limited capabilities of forming small, discrete nanoparticles for targeted cell delivery.

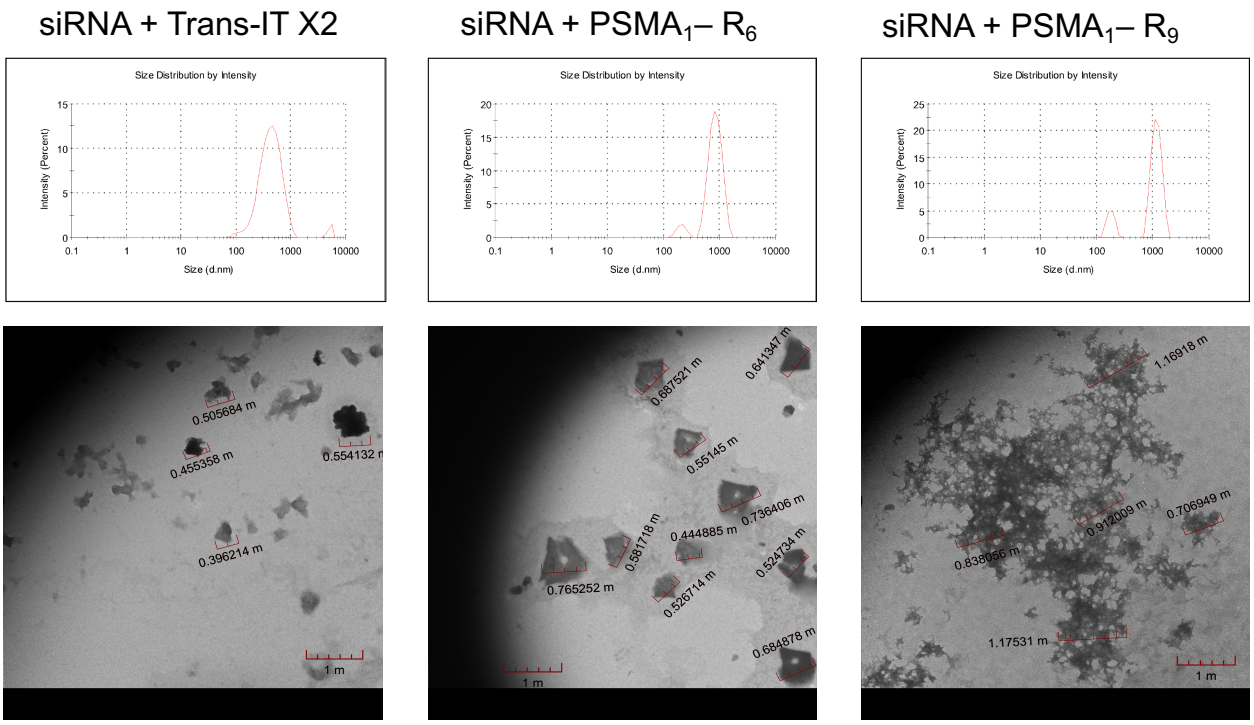

Figure 4.7 DLS and TEM analysis of the siRNA: PSMA-1 complexes as compared to an siRNA: transfection reagent complex.

4.5 Conclusions

This chapter highlights a method of creating unique cell targeting and cell penetrating peptides for the delivery of siRNA. Native PAGE of the R_6 and R_9 -PSMA-1 peptide hybrids, they were not efficient in condensing the siRNA complexes into discreet particles. The large particles and aggregates were not suitable for cell uptake and no downstream gene silencing was observed at either the transcript or protein levels. Complex aggregation likely sterically inhibited the PSMA peptide from binding to its receptor and triggering an endocytosis for siRNA uptake in the cells. Moreover, they were too large to passively diffuse through the membrane as is typical with oligoarginine delivery systems. However, our approach in developing these multifunctional peptide hybrids can expand the scope of peptides for the delivery of siRNA to include targeting peptides that have not previously been suitable for targeted siRNA-based cancer gene therapy.

4.6 Materials and Methods

4.6.1 Materials

Amino acids for the synthesis of all peptides, were purchased from Novabiochem (San Diego, CA, USA). Peptide syntheses were conducted on a Rink Amide ChemMatrix (0.47 mmol/g) (Biotage Inc., Charlotte NC, USA). 2-(6-chloro-1H-benzotriazole-1-yl)-1,1,3,3-tetramethylaminium hexafluorophosphate, HCTU, was purchased from Advanced ChemTech (Louisville, KY, USA). Fluorescein isothiocyanate, FITC, was purchased from ThermoScientific (Rockford, IL, USA) as a single isomer and used in the dark to fluorescently label all peptides. Trifluoroacetic acid (Biograde) was purchased from VWR (Radnor, PA, USA); *N*-*N*-dimethylformamide, acetonitrile, methanol, and dichloromethane were all purchased from MACRON (Center Valley, PA, USA). Piperidine, triethylsilane (98+%) and pyridine (ACS, 99%) were purchased form Alfa Aesar (Ward Hill, MA, USA). *N*-methylmorpholine (99%) was purchased from Acros Organics (Pittsburg, PA, USA). Diethyl ether (99%, ACS), Et_2O, used to precipitate peptides was purchased from Sigma Aldrich (St. Louis, MO, USA). All chemicals were used directly as received.

4.6.2 Peptide Synthesis

All peptides were synthesized by stepwise manual solid phase peptide synthesis using Fmoc-chemistry. Fmoc-amino acids (3eq, 0.3 mmol) were coupled on a Rink amide linker poly(ethylene glycol) solid support (0.47 mmol/g, 0.1 mmols) for 1 h using [HCTU (3eq 0.3 mmol), NMM (6eq, 0.6 mmol) in DMF (3.5 mL). Fmoc deprotection was done with a 20% piperidine in DMF solution (3 mL, 2x10 min). Amino acid couplings and Fmoc deprotections were

repeated until the desired sequences were completed. Upon completion of the PSMA-1 and PSMA-1-R_9 sequences, solid support was subjected to FITC labeling. A slurry of FITC (1.1 equiv., 0.33 mmol) in pyridine/DMF/DCM (12:7:5 v/v) was prepared and added to the reaction cartridge and left on a shaker for 16-18hrs. After FITC-labeling was completed, the resin was washed with DMF (3 x 3 mL), MeOH (3 x 3 mL), and DCM (3 x 3 mL). Peptide cleavage and deprotection from the solid support was accomplished using a mixture of TFA:TES:H_2O, (95:2.5:2.5 v/v/v) for 4hrs. Peptide samples were concentrated under nitrogen to a viscous oil, precipitated with cold Et_2O, and centrifuged to a white pellet. The supernatant was decanted and the peptide pellets were dissolved in MeCN/H_2O for LCMS analyses.

4.6.3 RP IP HPLC and ESI-MS

Sample analyses were performed on an Agilent 1100 series ESI-LCMS with single quadrupole mass analyzer and LC conditions which used an isocratic binary solvent system (85% MeOH/H_2O, 0.1% FA, 2min) in positive mode. Analytical RP-HPLC was performed using a Waters 2695 Symmetry® C18 column (3.9 x 150 mm, 5 μm particle size) using a gradient of 20-80% MeCN/H_2O, 0.1% TFA, over 18 min at 25°C, with a 1 mL/min flow rate and detection at 220 nm or 480nm for FITC labeled samples. Purified peptides were lyophilized to a fine powder before being dissolved in TE buffer (10 mM Tris, 50 nM NaCl, 1 mM EDTA, pH 7.5-8.0) to confirm purity.

4.6.4 Native PAGE Shift Assay

Linear GRP78 siRNA (250pmol) was incubated with the PSMA-1-R_6 peptide (25-100 eq, 6.25-25 nmol) over 60 minutes at either 25°C or 37°C. Aliquots were taken at 15-minute intervals,

mixed with a 30% sucrose buffer, and loaded into wells of an 18% polyacrylamide gel. V-shape siRNA were incubated separately with 50 eq of peptide for 30 min at 37°C before being loaded into the gel. The assay was run at 300V, 100mA, 12W for 5 hours following subsequent staining with a Stains-All solution. For the heparin titration assay, the linear siRNA were incubated with 50 eq. of peptide for 30min at 37°C and let cool to room temperature. Heparin (0.1-10eq) was titrated into the siRNA: peptide complexes and incubated for 30min at 37°C before being loaded into a separate 18% polyacrylamide gel and run at 300V, 100mA, 12W for 5 hours following subsequent staining with a Stains-All solution.

4.6.5 Dynamic Light Scattering

A Malvern Zetasizer, Nano-ZS (Malvern Instruments, UK) employing a 173° scattering angle and a 4 mW incident He−Ne laser (633 nm) was used to measure the particle sizes (hydrodynamic diameter), size distributions, and zeta potentials of the siRNA hybrid control and siRNA-fatty acid bioconjugates. Samples were measured in triplicate at 25 °C. All samples were loaded into folded capillary cells (DTS1070) equipped with electrodes on both sides to allow measurement of their zeta potentials and by extension, the stability and degree of aggregation. Particle suspensions with highly positive or highly negative zeta potentials are considered stable because the electrical repulsion between the particles tends to counter the van der Waals forces that would otherwise result in aggregation and precipitation.

4.6.6 TEM Imaging

TEM analyses of the linear, V-, and Y-shaped siRNA bioconjugates were performed with a JEOL 1200EX Transmission Electron Microscope (JEOL Ltd., Japan) at an accelerating voltage of 80 kV. A mixture of 1:1 volume ratio 1% uranyl acetate and sample suspension was prepared

and 10 μL of this solution placed on a TEM carbon-film-coated copper grid of 300 mesh (Electron Microscopy Sciences Inc., Hatfield, PA). Each sample was allowed to sit for 5 min on the grid before wicking the excess liquid followed by storage of 1 week to allow the samples to dry. Images were taken with a SIA-L3C CCD camera (Scientific Instruments and Applications, Inc.) using the software Maxim DL5 (Diffraction Limited, Ottawa, Canada)

4.6.7 Cell Culture

PC3 (bone metastatic PCa cell line, ATCC®-CRL-1435) LNCaP (Clone FGC ATCC®-CRL-1740) were purchased from ATCC. Both cells were cultured in RPMI-1640 medium containing 10% FBS, 2.5mM of L-glutamine and 1% penicillin/streptomycin at 37˚C in a humidified tissue culture incubator containing 5% CO_2.

4.6.8 Flow Cytometry

PSMA mAb (GCP-05) and PE conjugated IgG control were purchased from Thermo Fisher and used according to the manufacturer's protocol. PC3 and LNCaP cells were dissociated mildly using TryplE, harvested, and resuspended in 1X PBS at a density of $5.0x10^5$/mL. The antibodies were used at a 1:10 dilution and incubated in the dark for 15 minutes. The FITC-PSMA-1 peptide was used at a concentration of 1mg/mL and incubated in the dark at 37°C for 1hr. The samples were then analyzed on a Cytomics FC 500 flow cytometer (Beckman Coulter) and the data was processed using the Kaluza, Flow Cytometry Analysis Software (Beckman Coulter).

4.6.9 siRNA Transfection

A monolayer of PC3 or LNCaP cells were grown in a 24-well culture plate in complete growth media until 60-70% confluent to ensure expression of the PSMA receptor. Linear GRP78

siRNA (12.5 pmol) was incubated with either the PSMA-1-R_6 or the FITC-PSMA-1-R_9 peptides (625 pmol) for 30min at 37°C in Opti-MEM before being added to the cells and diluted to a final siRNA concentration of 25nM. siRNA was also complexed with the Trans-IT X2 transfection reagent in Opti-MEM according to the manufacturer's protocol and added to the cells at a final concentration of 25 nM. The cells were then incubated at 37°C in a humidified tissue culture incubator containing 5% CO_2.

4.6.10 siRNA Uptake via Fluorescent Imaging

The uptake of the siRNA complexed with the FITC-PSMA-1-R_9 peptide was monitored at 2, 4, 6, and 24hrs post transfection. The cells were imaged directly in the culture plate using a CellInsight™ High Content Screening (HCS) Platform (Thermo Fischer). Five random field of views from 3 separate wells were imaged under brightfield and then again after the cells were excited by a 480nm LED filter within the platform. The images were analyzed using Thermo Scientific™ HCS Studio™ Cell Analysis Software.

4.6.11 qRT-PCR

Total mRNA was isolated following transfection (48 hrs) from TriZol (Ambion) preserved cells using a TriRNA Pure Kit (Geneaid), following the manufacturer's instructions. The collected mRNA was then quantitated on a Qubit 3.0 fluorimeter using the Qubit Broad Range (BR) assay kit (Thermo Fisher Scientific), mRNA (200 ng) was reversed transcribed into cDNA using a high capacity cDNA kit (Applied Biosystems). RT-PCR was performed using pre- developed TaqManTM gene expression primer-probes for GRP78 (assay ID Hs99999174_m1), GRP94 (assay ID Hs00437665_g1), and GAPDH (Hs99999905_m1) and TaqManTM fast advanced

master mix. qPCR fast assay was carried out on a StepOnePlus (Applied Biosystems). Fold changes were calculated with the ΔΔCt method using GAPDH as endogenous control and the negative siRNA as the control sample.

4.6.12 Western Blot

Total protein was isolated from the cell cultures following transfection (78 h). Protein lysates were prepared by lysing the cells in ice-cold RIPA buffer (G-Biosciences) supplemented with protease and phosphatase inhibitors (Millipore Sigma) which were diluted 1:10 as per the manufacturer's recommendations. Cell debris was removed by centrifugation at 16,000g at 4°C and protein concentrations were determined using a PierceTM BCA kit (Thermo Fisher Scientific). A sample (20-35 mg) of the supernatant protein was mixed with LDS buffer and DTT, incubated at 70 °C for 10 min and resolved on a 4-12% Bis-Tris PAGE gradient gel before being transferred to a PVDF membrane. Following transfer, the membrane was blocked in 5% skim milk for 1 h, washed and incubated at 4 °C overnight with a rabbit 1° mAb against human GRP78, GRP94, GRP75 or β-Actin (all purchased from Cell Signaling Technology) at a 1:1000 dilution. The membrane was subsequently washed and incubated with an anti-rabbit HRP-conjugated 2° Ab (Cell Signaling Technology) for 1 h at room temperature at 1:2000 dilution. The bands were visualized using a SignalFireTM ECL reagent (Cell signaling Technology) on a ProteinSimple FluorChem E imager.

4.7 References

1. Tatiparti, K.; Sau, S.; Kashaw, S. K.; Iyer, A. K., *Nanomaterials* **2017,** *7*, 77.
2. Guo, P.; Coban, O.; Snead, N.; Trebley, J.; Hoeprich, S.; Guo, S.; Shu, Y., *Adv Drug Deliv Rev* **2010,** *62*, 650-666.
3. Shim, M.S.; Kwon, Y.J. *FEBS J.* **2010**, 277, 4814-4827.
4. Pirollo, K. F.; Chang, E. H., *Cancer Res* **2008,** *6*, 1247-1250.
5. Svensen, N.; Walton, J. G.; Bradley, M., *Trends Pharmacol Sci* **2012,** *33*, 186-192.
6. Lee, R. J.; Low, P. S., *J Biol Chem* **1994,** *269* (5), 3198-3204.
7. Mathias, C. J.; S.;, W.; R.J.;, L.; Waters, D. J.; Low, P. S.; Green, M. A., *J Nucl Med* **1996,** *37* , 1003-1008.
8. Wolfrum, C.; Shi, S.; Jayaprakash, K. N.; Jayaraman, M.; Wang, G.; Pandey, R. K.; Rajeev, K. G.; Nakayama, T.; Charrise, K.; Ndungo, E. M.; Zimmermann, T.; Koteliansky, V.; Manoharan, M.; Stoffel, M., *Nature Biotechnol.* **2007,** *25*, 1149-1157.
9. Song, E.; Zhu, P.; Lee, S. K.; Chowdhury, D.; Kussman, S.; Dykxhoorn, D. M.; Feng, Y.; Palliser, D.; Weiner, D. B.; Shankar, P.; Marasco, W. A.; Lieberman, J., *Nature Biotechnol.* **2005,** *23*, 709-717.
10. Peer, D.; Park, E. J.; Morishita, Y.; Carman, C. V.; Shimaoka, M., *Science* **2008,** *319*, 627-630.
11. Kapp, T.; et al. *Scientific Reports*. **2017**, 7, 39805
12. Schiffelers, R. M.; Ansari, A.; Xu, J.; Zhou, Q.; Tang, Q.; Storm, G.; Molema, G.; Lu, P. Y.; Scaria, P. V.; Woodle, M. C., *Nucleic Acids Res* **2004,** *32*, e149.
13. Murukesh, N.; Dive, C.; Jayon, G.C. *Br J Cancer*. **2010**, 102(1), 8-18
14. Fang, B.; Jiang, L.; Zhang, M.; Ren, F. Z., *Biochimie* **2013,** *95*, 251-257.
15. Kim, S. S.; Ye, C.; Kumar, P.; Chiu, I.; Subramanya, S.; Wu, H.; Shankar, P.; Manjunath, N., *Mol. Ther.* **2010,** *18*, 993-1001.
16. Ye, C.; Choi, J. G.; Abraham, S.; Wu, H.; Diaz, D.; Terreros, D.; Shankar, P.; Manjunath, N., *Proc Natl Acad Sci U S A* **2012,** *109*, 21052-21057.
17. Tai, W.; Gao, X., *Adv Drug Deliv Rev.* **2017,** *110*, 157-168.
18. Vives, C.; Brodin, P.; Lebleu, B., *J Biol Chem* **1997,** *272*, 16010-16017.
19. Chiu, Y. L.; Ali, A.; Chu, C. Y.; Cao, H.; Rana, T. M., *Chem Biol* **2004,** *11*, 1165-1175.
20. Tunnemann, G.; Ter-Avetisyan, G.; Martin, R. M.; Stockl, M.; Herrmann, A.; Cardoso, M. C., *J Pept Sci.* **2008,** *14*, 469-476.
21. Futaki, S.; Suzuki, T.; Ohashi, W.; Yagami, T.; Tanaka, S.; Ueda, K.; Sugiura, Y., *J Biol Chem* **2001,** *276*, 5836-5840.
22. Wang, Y. H.; Hou, Y. W.; Lee, H. J., *J Biochem Biophys Methods* **2007,** *70*, 579-586.
23. Kim, S. W.; Kim, N. Y.; Choi, Y. B.; Park, S. H.; Yang, J. M.; Shin, S. J., *J Control. Rel* **2010,** *143*, 335-343.
24. Pinto, J. T.; Suffoletto, B. P.; Berzin, T. M.; et al. *Clin Cancer Res* **1996,** *2*, 1445-1451.
25. Rajasekaran, S. A.; Anilkumar, G.; Oshima, E.; et al. *Molecular biology of the cell* **2003,** *14*, 4835-4845
26. Ross, J.S.; Sheehand, C.E.; Fisher, H.A.G.; et al. *Clin Cancer Res.* **2009**, 9, 6357-6362
27. Silver, D. A.; Pellicer, I.; Fair, W. R.; et al. *Clin Cancer Res* **1997,** *3*, 81-85.
28. Von Eyben, F. E.; Baumann, G. S.; Baum, R. P., *Clin Transl Imaging* **2018,** *6*, 145-148.
29. Shen, D.; Xie, F.; Edwards, B., *PLoS One* **2013,** *8* (7), e68339.

30. Jin, W.; Qin, B.; Zhijin, C.; Liu, H.; Barve, A.; Cheng, K., *Int J Pharmaceutics* **2016,** *513* (1-2), 138-147.
31. Evans, J.C.; et al. *Nanomedicine*. **2016**, *12*(8), 2341-2351.
32. Guo, J.; O'Driscoll, C.M.; Holmes, J.D.; Rahme, K. *Int J Pharm.* **2016**, 509(1-2), 16-27
33. Cho, H.J.; Lee, T.K.; Kim, J.W.; Lee, S.M.; Lee, Y.S. *J Org Chem*. **2012**, 77(20), 9156-9162

Chapter 5: Conclusions and Contributions to Knowledge

5.1 Conclusions and Contributions to Knowledge Made in this Thesis

5.1.1 Investigating the Role of GRP78 in Cell Adhesion

RNAi is a powerful tool that has found wide applicability in disease gene therapies as well as in basic research to investigate the role of specific genes in complex molecular pathways. The main research objectives of this thesis revolve around improving the utility of synthetic siRNAs in cancer gene therapy by targeting and silencing the Glucose Regulated Proteins (GRPs) that play key roles in the development, progression and spread of cancer. Chapter 2 highlights a novel role that GRP78 has in cell-cell adhesion and its implication in tumors (multiple myeloma, MM and prostate cancer, PCa) that target the bone as a primary metastatic site. By silencing GRP78 via siRNA, a concomitant downregulation of a mesenchymal cell-adhesion marker, N-cadherin, was observed in multiple myeloma and prostate cancer cell lines (**Figure 2.1**). N-cadherin, and its epithelial counterpart E-cadherin, are two major adhesion proteins involved in the EMT pathway, for epithelial tumors to transition to mesenchymal form during a metastatic event which leads to adhesion to a secondary tumor site. Upon further investigation with an epithelial prostate cancer cell line, PC3, it was noted that the GRP78 silencing led to concomitant downregulation of E-cadherin and subsequent upregulation of TGF-β1 and Snail-2 (**Figure 2.5**). Interestingly, TGF-β1 expression has been correlated with EMT and the upregulation of N-cadherin, suggesting that our findings indicate a novel function of GRP78 in which it can modulate the expression of adhesion molecules in a manner that supersedes the natural pathways that regulate their expression in PCa. We also show that this action is not related to the other GRPs, GRP94 and GRP75, as their expression levels remained unchanged after GRP78KD despite a known compensatory mechanism that alters the expression of one GRP in response to another (**Figure 2.4, A**). Furthermore, the PC3

cells treated with GRP78 siRNA produced drastic changes in their morphology from their normal elongated shape to a more rounded shape (**Figure 2.6**). This change in cell phenotype is important because cells tend to be less adhesive in a rounded shape. This resulted in a reduction in their adhesion to an osteoblast (bone cell) monolayer in an N-cadherin dependent manner (**Figure 2.7**). These results help establish a novel correlation between GRP78 and N-cad in MM and PCa cells and present GRP78 as an ancillary regulator of markers associated with the EMT pathway and its implications in the adhesion properties of PCa to the bone. Aside from the extensively described roles in tumor progression, our data suggest that downregulation of GRP78 may represent a suitable therapeutic intervention strategy for modulating tumor-microenvironment adhesive interactions leading to tumor progression.

5.1.2 Development of Higher Order siRNA hybrids and their Bioconjugates for RNAi Activity in Cancer

Chapter 3 discussed the application of a synthetic methodology that led to the production of linear, V-shape and Y-shape RNA templates, the latter two by the incorporation of a unique branchpoint ribouridine synthon. In this application, the RNA templates were used to hybridize complementary RNA strands that self-assembled into higher order nanostructure formulations. These formulations were designed to adopt genetically encoded shapes that resulted in siRNA hybrids that targeted multiple GRPs (**Figure 3.4**). The first generation of these siRNA nanoparticles targeted multiple regions of the GRP78 mRNA and produced a much more pronounced knockdown effect and induction of apoptosis in an endometrial AN3CA cancer cell line when compared to the control transfection with linear siRNAs targeting the same GRP78 mRNA sites (**Figure 3.4**). The second generation lead Y-shape siRNA targeted all three GRPs, GRP78,94,75, and was capable of inducing a synergistic knockdown of the GRPs in multiple

tumor types (endometrial, breast, cervical) yet proved relatively inert in a non-cancerous lung cell line (**Figure 3.5**). This established that the self-assembled siRNA nanostructures as a more potent anti-cancer gene therapy tool as compared to a cocktail of linear siRNAs, administered separately. These results highlight the novelty of these siRNAs in enhancing their gene therapy potential and also allows flexibility in screening the effects silencing multiple oncogenes on tumor progression and viability.

siRNA bioconjugates based on the V- and Y-shape RNA templates were designed to incorporate multi-functionality to the siRNA constructs and improve their scope. Theranostic agents, tools that combine therapy with diagnostics, are rapidly emerging in their utility and applications, including those involving siRNAs. In this chapter, a solid phase synthetic strategy was developed to covalently attach a fluorophore, FITC, onto chemically synthesized RNA templates. A self-assembly strategy was also developed for incorporating multiple FITCs within single molecular V- and Y-shape siRNA constructs. These siRNAs provided a unique opportunity to track cell uptake, localization, and mechanism of action with greater sensitivity (up to 72 hrs post transfection) due to the enhanced signaling effect of the multi-FITC containing siRNAs within the PC3 PCa model (**Figures 3.7, 3.8**). Sense strand functionalization provided the most potent GRP KD effects (50-95%) which translated to the most significant cell death effects (20-95%) within a model PC3 PCa cell line (**Figures 3.9, B and 3.11**).

A similar approach was used to conjugate fatty acids to the RNA templates on solid phase to generate amphiphilic siRNA bioconjugates that may have the potential to diffuse across the cell membrane without the need of a transfection vector, ultimately improving their clinical utility. Long and short chain fatty acids (C12-C18) as well as C18 unsaturated fatty acids (ω-3,6,9) were conjugated to the linear anti and sense sequences, yet only the C16 and C18 conjugated siRNAs

were able to elicit GRP78 knockdown, albeit a moderate one (~30-40%) (**Figure 3.12, B**). To potentially improve this modest effect, the sense strands were conjugated with palmitic acid (C16) and hybridized to the corresponding linear, V-, and Y-shape antisense RNA templates. This self-assembly approach provided the opportunity to incorporate a single, double or triple palmitamides within the linear, V- and Y-shape siRNAs, respectively. However, this did not result in improved GRP KD effects (**Figure 3.12, D**). Cell uptake studies performed by flow cytometry with a chimeric fluorophore – fatty acid siRNA bioconjugate revealed that there is an interaction of the siRNA with the cells, which rapidly dissipates within 24hrs post transfection (**Figure 3.13**). Furthermore, DLS and TEM analysis revealed large aggregate particles with sizes upwards of 1 μm (**Figure 3.14**). Taken together, these results suggest that the amphiphilic lipidated siRNAs may contribute to transient cell membrane binding affinity, which rapidly dissipates due to formation of large molecular aggregates which impede cell binding and uptake altogether. This effect may be applicable to other gene delivery strategies, making this discovery an important one. Furthermore, the siRNA bioconjugates effectively expand the scope and utility of the synthetic siRNAs, making them more effective therapeutic agents in cancer gene therapy applications.

5.1.3 Development of Cancer Targeting and Cell Penetrating Chimeric Peptides for the Targeted Delivery of siRNA in PCa cells

A major limitation of siRNA therapies is their lack of cell selectivity, especially when delivered with a conventional transfection reagent into non-targeted cells leading to potentially deleterious off-target side effects. Chapter 4 of this thesis illustrates a unique method for targeting cells for siRNA delivery. The use of cell targeting peptides (CTPs) function to target and bind to a cell surface receptor, in this case PSMA, found on PCa cells. Moreover, the incorporation of

poly(cationic) cell penetrating peptides (CPPs), such as poly(arginine), can have dual functionality in condensing siRNA by favorable electrostatic interactions and facilitating cell uptake within the target cell lines. The PSMA receptor is a surface bound enzyme expressed in metastatic PCa, linked with poor prognosis and, most importantly, found on castrate-resistant PCa tumors. Recently, peptides were discovered from phage display to target and bind to the PSMA receptor on selected PCa cells leading to cell penetration by receptor mediated endocytosis. A lead model peptide sequence, PSMA-1, was functionalized with short oligo(arginine) sequences (R_6 and R_9). The peptides were synthesized on solid phase, purified by RP-HPLC, and characterized by ESI-MS. (**Scheme 4.1, Table 4.1**). Furthermore, an FITC tag was included on the parent PSMA-1 peptide as well as the PSMA-1-R_9 peptide in order to track cell binding and uptake. The PSMA-1 peptide was able to effectively bind to $PSMA^+$ LNCaP cells with a limited amount of nonspecific binding to a $PSMA^-$ PC3 cell line (**Figure 4.4**). The R_6 variant was shown to efficiently complex and release siRNA according to a gel shift assay (**Figure 4.3**), yet no GRP78 KD was detected at the mRNA and protein levels of expression within the PC3 or LNCaP cells (**Figure 4.7**). Cell uptake studies by flow cytometry revealed that the FITC-PSMA-1-R_9 peptide showed limited uptake into the cells when bound with siRNA (**Figure 4.5**). DLS and TEM analysis showed large particle sizes (1-2 μm), polydisperse particle distributions, negative surface charge densities and aggregation which prevented cell uptake of the CTP:siRNA complexes when compared to siRNA complexed with a commercial transfection reagent. This suggests that although the peptides are capable of complexing and releasing siRNA, they do no efficiently condense the siRNA into small, monodisperse, neutral particles that can easily penetrate the cell membrane. Future work is aimed at improving the design and delivery characteristics of the peptide-based transfection reagent.

5.2 Future Work

While the results in this thesis highlight important accomplishments in the field of siRNA-based gene silencing, there is still progress to be made. The V- and Y-shape siRNAs, to date, have been used to target only the GRPs. An important variation would be to generate siRNAs that target other oncogenes and investigate their activity. For instance, designing an siRNA to targets both GRP78 and N-cad may have an even more pronounced effect on E-cad and other EMT markers. Similarly, the bioconjugation strategies could be expanded to include different fluorophores and amphiphilic or cationic lipids. Different fluorophores would allow the siRNAs to be used in differential imaging and co-localization experiments particularly when being used to deduce molecular pathways or protein mechanism of actions. The addition of cationic or amphiphilic lipids to the siRNA would mimic the formulations used by many commercial transfection reagents and may allow for improved siRNA nanoparticle formulations for cell delivery.

Moreover, the CTP-CPP chimeras need to be designed to improve siRNA condensation in order for cell uptake to proceed efficiently. One design approach could be to create dendrimeric peptides in which the PSMA targeting peptide displays multiple oligo(arginine) sequences. In doing so, the chimeric peptide may be able to encapsulate the siRNA. Another approach would be to introduce linkers, such as polyethylene glycol (PEG), between the CTP domain and the oligoarginine domain. This may help to restore the ligand binding properties by reducing aggregation and steric block of receptor mediated endocytosis. Regardless of the variations, we envision that the future iterations of the formulations presented in this thesis will significantly help to further enhance the functionality of siRNA in cancer gene therapy applications.

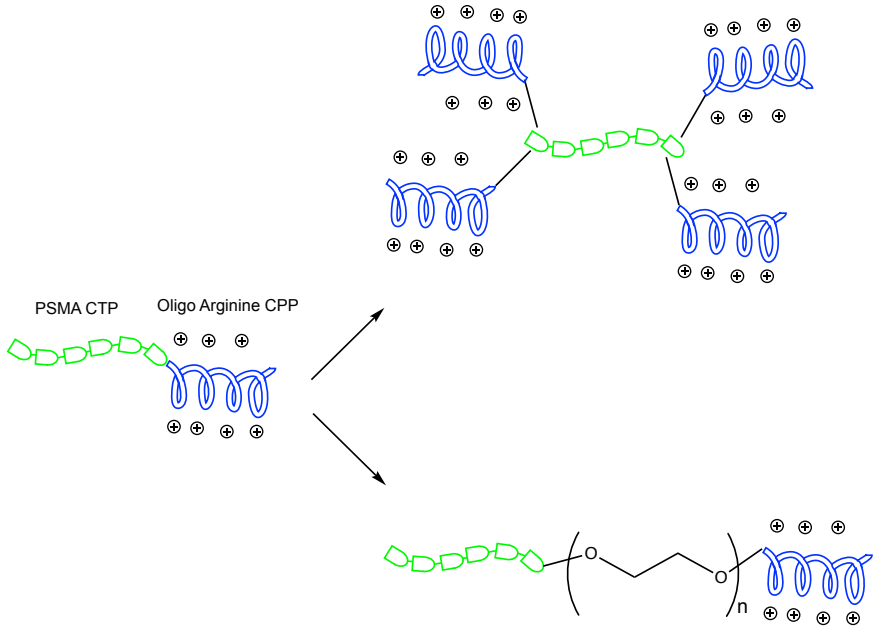

Figure 5.1 Future CTP-CPP variations. Top: dendrimeric peptides containing multiple oligo-arginine moieties branching from a single PSMA CTP. Bottom: A linear peptide with a PEG linker separating the CTP and CPP domains.

5.3 Publications, Awards, Invention Disclosures and Conference Presentations

5.3.1 Publications

- Cultrara, C. N.; Kozuch, S. D.; Ramasundaram, P.; Heller, C. J.; Shah, S.; Beck, A. E.; Sabatino, D.; Zilberberg, J., *BMC Cancer* **2018,** *18* (1), 1263.
- Cultrara, C. N.; Shah, S.; Kozuch, S. D.; Patel, M. R.; Sabatino, D. *Chem Bio Drug Des.* **2018**, 1-12.
- Kozuch, S. D.; Cultrara, C. N.; Beck, A. E.; Heller, C. J.; Shah, S.; Patel, M. R.; Zilberberg, J.; Sabatino, D. *ACS Omega* **2018,** *3*, 12975-12984.
- Shah, S.; Cultrara, C. N.; Kozuch, S. D.; Patel, M. R.; Ramos, J.; Samuni, U.; Zilberberg, J.; Sabatino, D. *Bioconj Chem.* **2018,** *29*, 3638-3648.
- Rana, N.; Cultrara, C.N.; Phillips, M.; Sabatino, D. *Bioorg Med Chem Lett*. **2017**, 27(17), 4019-4023
- Patel, M. R.; Kozuch, S. D.; Cultrara, C. N.; Yadav, R.; Huang, S.; Samuni, U.; Koren, J. I.; Chiosis, G.; Sabatino, D. *Nano Lett.* **2016**, *16*, 6099-6108.

5.3.2 Manuscripts in Preparation

- Cultrara, C.N.; Shah, S.; Heller, C.J.; Beck, A.E.; Zilberberg, J.; Sabatino, D. Evaluation of an Oligo-arginine derived PSMA Targeting Peptide for the Selective Delivery of siRNA to Prostate Cancer Cell Lines. *Manuscript in Preparation*

5.3.3 Awards

- Dr. John D. Bogden Fellowship
- Dr. Robert DeSimone Fellowship

5.3.2 Poster Presentations

- Kozuch, SD; Cultrara, CN; Shah, S; Beck, AE; Heller, CJ; Zilberberg, J; Sabatino, D. **Cancer Gene Therapy using siRNA Nanotechnology and Bioconjugation.** *New York Academy of Sciences Meeting*, New York, NY. May 2018. (**Poster Presentation**)

- Kozuch, SD; Cultrara, C.N.; Shah, S; Beck, AE; Heller, CJ; Zilberberg, J; Sabatino, D. **Cancer Gene Therapy using siRNA Nanotechnology and Bioconjugation.** *Petersheim Academic Exposition*, Seton Hall University, April 2018. (**Poster Presentation**)

- Montel, R.; Cultrara, C.N.; Peña, G.; Donelly, R.; Sabatino, D.; Zilberberg, J. **Identification of Mutational Variants in the *HSPA5* Gene as a Biomarker in the Development and Progression of Multiple Myeloma**. *Annual Clinical Genetics Meeting,* Charlotte, NC. April 2018. (**Poster Presentation**)

- Montel, R.; Cultrara, C.N.; Peña, G.; Donelly, R.; Sabatino, D.; Zilberberg, J. **Identification of Mutational Variants in the *HSPA5* Gene as a Biomarker in the Development and Progression of Multiple Myeloma**. *Petersheim Academic Exposition*, Seton Hall University, April 2018. (**Poster Presentation**)

- Kozuch, SD; Cultrara, C.N.; Shah, S; Zilberberg, J; Sabatino, D. **Cancer Gene Therapy using siRNA Nanotechnology and Bioconjugation.** *New York Academy of Sciences Meeting*, New York, NY. May 2017. (**Poster Presentation**)

- Kozuch, SD; Cultrara, C.N.; Shah, S; Zilberberg, J; Sabatino, D. **Cancer Gene Therapy using siRNA Nanotechnology and Bioconjugation.** *Petersheim Academic Exposition*, Seton Hall University, April 2017. (**Poster Presentation**)

APPENDIX

TABLE OF CONTENTS

A. SUPPLEMENTAL IP-RP-HPLC AND ESI-MS CHROMATOGRAMS

Figure A1 Western Blot Analysis of Basal GRP78 and N-cad expression in PC3 and MM.1S

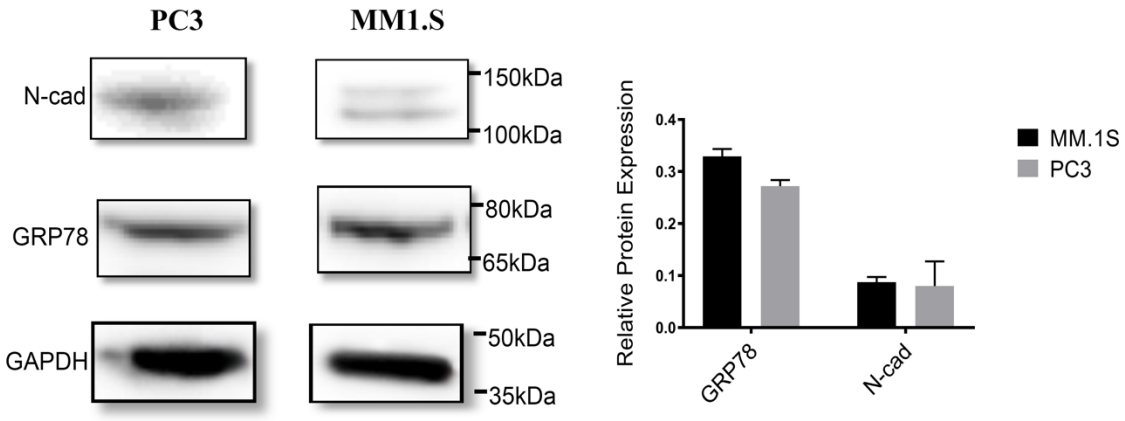

Figure A2 RP IP HPLC Analysis of FITC-PSMA-1 (220nm)

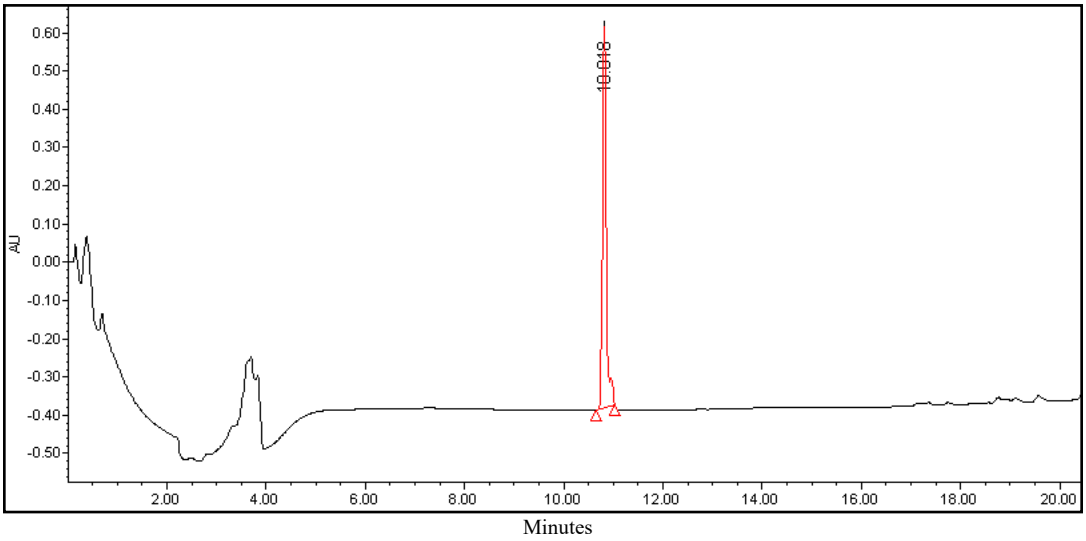

	RT	% Area	Area (µV*sec)
1	10.018	100	979467

Figure A3 RP IP HPLC Analysis of FITC-PSMA-1 (480nm)

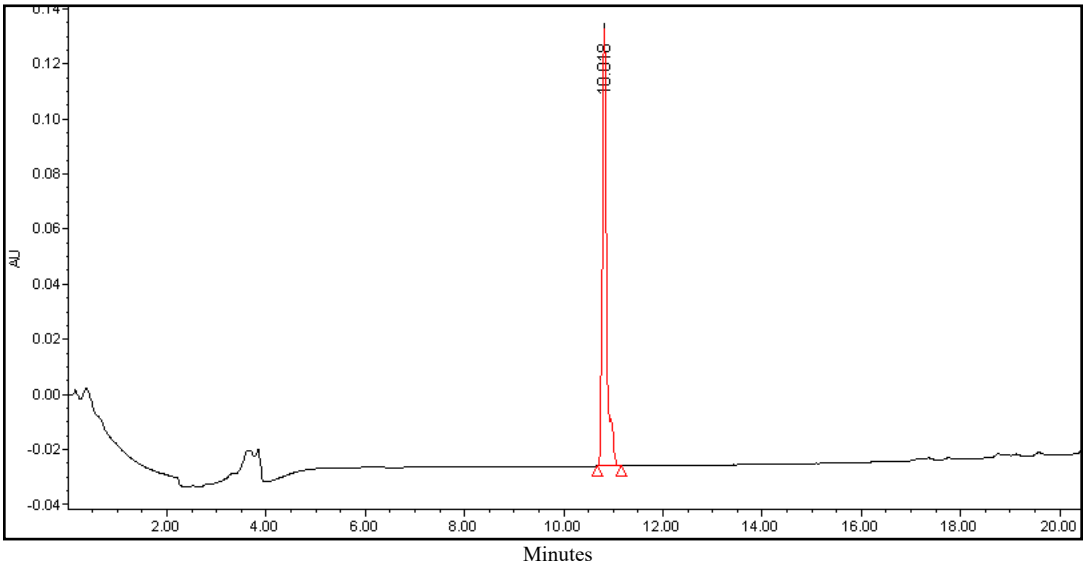

	RT	% Area	Area (µV*sec)
1	10.018	100	156568

Figure A4 ESI-MS Analysis of FITC-PSMA-1

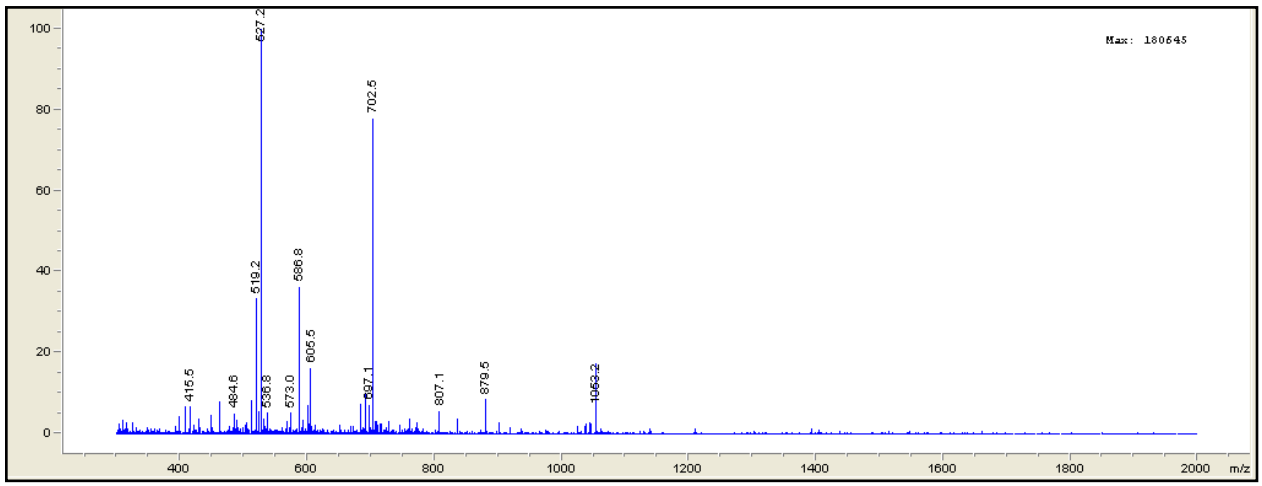

Figure A5 RP IP HPLC Analysis of PSMA-1-R_6 (220nm)

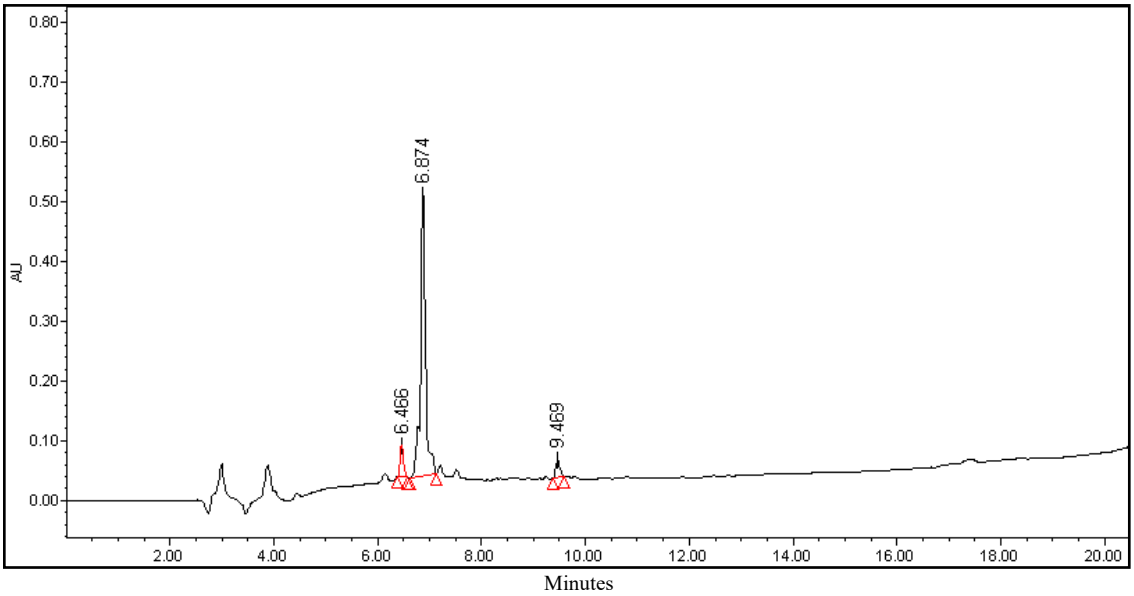

	RT	% Area	Area (µV*sec)
1	6.466	6.88	53173
2	6.874	88.09	473200
3	9.469	5.03	38875

Figure A6 ESI-MS Analysis of PSMA-1-R_6

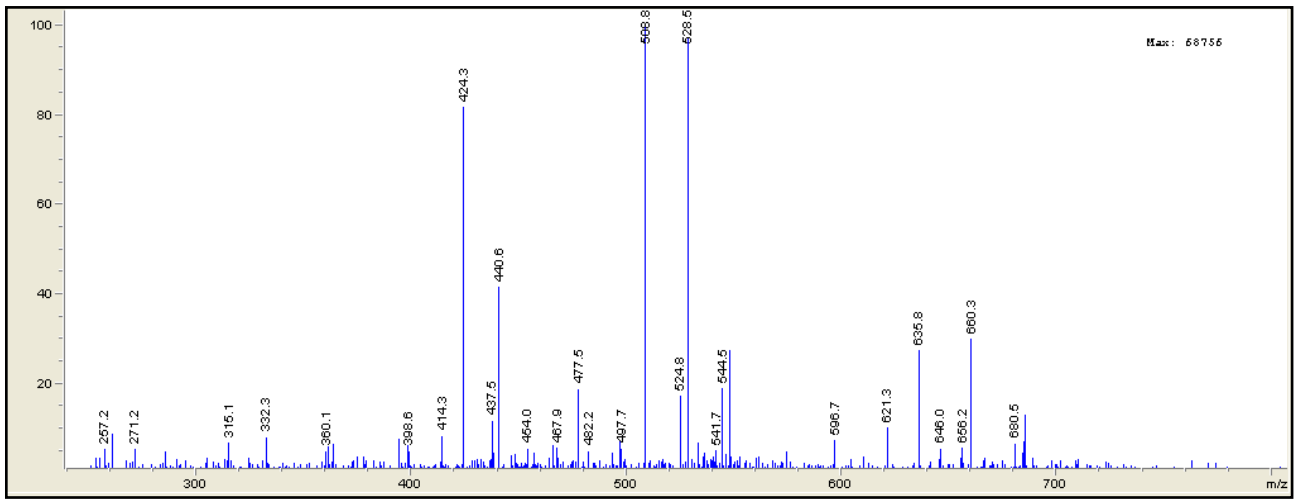

Figure A7 RP IP HPLC Analysis of FITC-PSMA-1-R_9 (220nm)

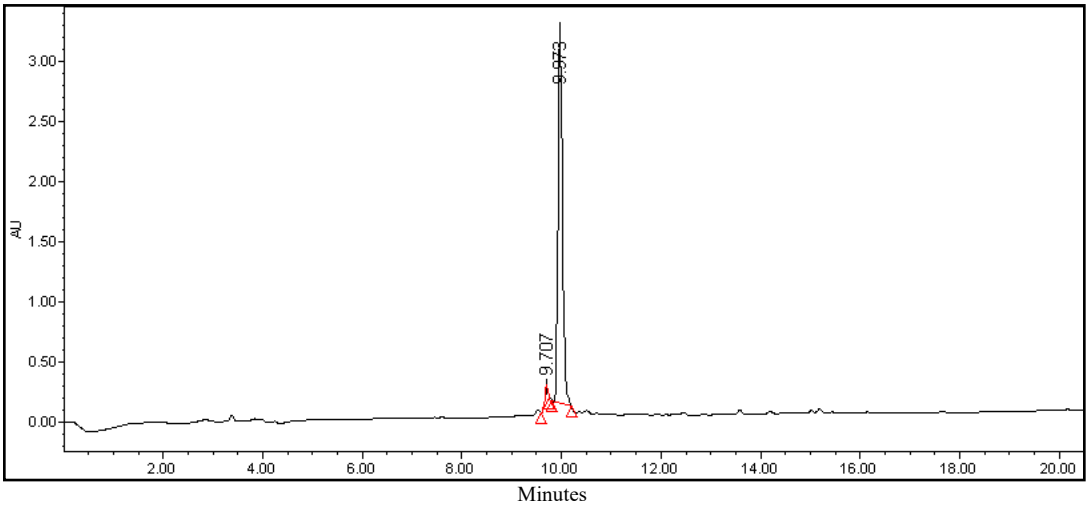

	RT	% Area	Area (μV*sec)
1	9.707	3.18	149571
2	9.973	96.82	3153448

Figure A8 RP IP HPLC Analysis of FITC-PSMA-1-R_9 (480nm)

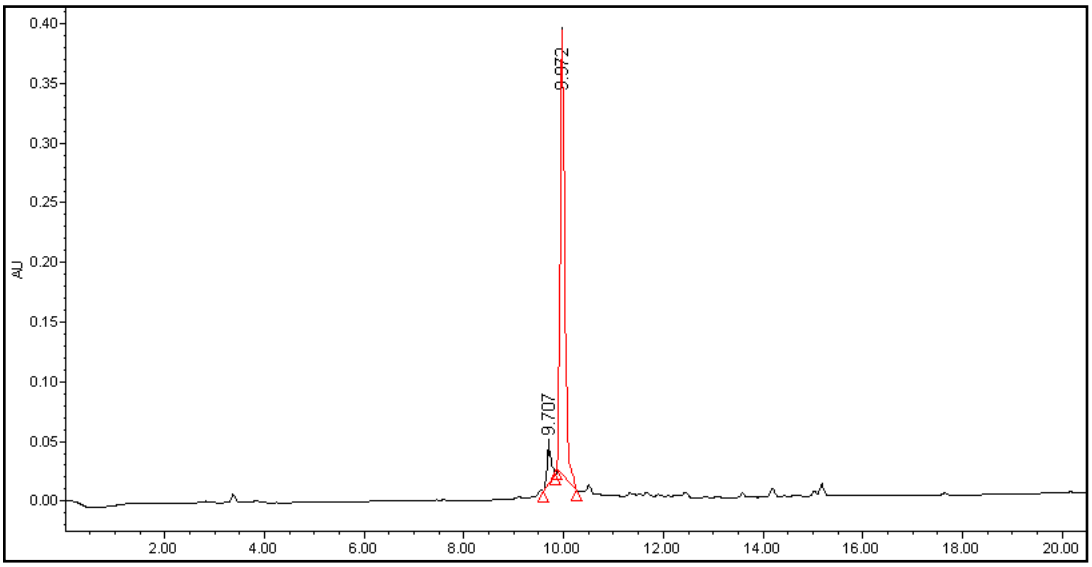

	RT	% Area	Area (µV*sec)
1	9.707	7.22	28945
2	9.973	92.78	371957

Figure A9 ESI-MS Analysis of FITC-PSMA-1-R_9